DESIGN AND CALIBRATION OF A PRECISE ION ENERGY CONTROL SYSTEM FOR A VAN DE GRAAFF ELECTROSTATIC ACCELERATOR AND ITS USE IN THE STUDY OF RESONANT REACTIONS IN SOME LIGHT ELEMENTS.

by

David Andrew Aaronson

A THESIS SUBMITTED IN PARTIAL FULFILMENT OF
THE REQUIREMENTS FOR THE DEGREE OF
DOCTOR OF PHILOSOPHY

in

PHYSICS

We accept this thesis as conforming to the standard required from candidates for the degree of Doctor of Philosophy in Physics.

Members of the Department of Physics

THE UNIVERSITY OF BRITISH COLUMBIA

December, 1952.

ABSTRACT.

A precise energy control system has been constructed for the U.B.C. electrostatic accelerator. Over the past six months it has provided analyzed beams of protons as large as 4½ microamperes on a target with an energy homogeneity of 0.1%.

In the system adopted, the accelerated positive ions are analyzed by a 90° deflection magnet provided with entrance and exit slits to define the beam path. The magnetic field is stabilized to a few parts in 100,000, and controlled by a nuclear magnetic resonance method. A fraction of the emergent beam falls on two insulated slits, "sniffers", connected to a differential amplifier, the output of which varies as the beam impinges more on one than the other. Thus an error signal is obtained according to the shift in energy and hence position of the beam, which is used to modulate a reverse beam of electrons sent up the differential pumping tube of the generator. This beam loads the generator so as to maintain its voltage, and hence the energy of the ions, constant. The main central part of the beam passes through the slits onto the target mounted beyond. One-dial control over a range of 20 KeV is achieved by simply tuning the oscillator controlling the frequency of the nuclear magnetic resonance fluxmeter head. The energy of the ions can be varied in steps as fine as 0.2 KeV

in 1,000 KeV.

The generator's voltage scale (the generating voltmeter) and energy scale (the magnetic field of the analyzing magnet) have been calibrated relative to the currently accepted standard value of Herb, Snowdon, and Sala of 0.8735 MeV for the strong $F^{19}(p, \alpha\gamma)O^{16}$ resonance and checked with the 0.3404 MeV resonance occurring in the same reaction. Additional calibration points were obtained using mass 2 and 3 beams.

The complete gamma ray excitation curve for the reactions from F^{19} bombarded with protons has been taken up to 2 MeV and new resonances found at 1.62 and 1.84 MeV. The 1.355, 1.381 MeV doublet was resolved with a peak to trough value of 9/1 which is excellent confirmation of the homogeneity of the proton beam.

The resonances in the $N^{15}(p, \alpha\gamma)C^{12}$ reaction have also been investigated and background yields from various target backing materials measured up to 2 MeV.

THE UNIVERSITY OF BRITISH COLUMBIA

Faculty of Graduate Studies

PROGRAMME OF THE FINAL ORAL EXAMINATION FOR THE DEGREE OF DOCTOR OF PHILOSOPHY

of

DAVID ANDREW AARONSON

B.Sc. (Western Ontario) 1949
M.A. (Brit. Col.) 1950

TUESDAY, DECEMBER 16th, 1952, at 3:00 P.M.
IN ROOM 301, PHYSICS BUILDING

COMMITTEE IN CHARGE

Dean H. F. Angus, *Chairman*

Professor J. B. Warren	Professor E. Leimanis
Professor C. A. Barnes	Professor F. Noakes
Professor W. B. Coulthard	Professor J. Halpern
Professor G. M. Shrum	Professor E. Signori

GRADUATE STUDIES

Field of Study: Physics.

X-Rays and Crystal Structure -- Professor J. B. Warren
Nuclear Physics -- Professor K. C. Mann
Quantum Mechanics -- Professor G. M. Volkoff
Electromagnetic Theory -- Professor W. Opechowski
Special Relativity -- Professor W. Opechowski
Advanced Quantum Mechanics -- Professor W. Opechowski
Electronics -- Professor A. van der Ziel
Advanced Electronics -- Professor A. van der Ziel
Theory of Measurements -- Professor A. M. Crooker
Statistical Theory of Matter -- Professor A. J. Dekker
Chemical Physics -- Professor A. J. Dekker

Other Studies:

Differential Equations -- Professor T. E. Hull
Advanced Differential Equations -- Professor T. E. Hull
Design of Electrical Machinery -- Dean H. J. MacLeod
Operational Methods in Engineering -- Professor W. B. Coulthard
Advanced Circuit Analysis -- Professor W. B. Coulthard

THESIS

DESIGN AND CALIBRATION OF A PRECISE ION ENERGY CONTROL SYSTEM FOR A VAN DE GRAAFF ELECTROSTATIC ACCELERATOR AND ITS USE IN THE STUDY OF RESONANT REACTIONS IN SOME LIGHT ELEMENTS

A precise energy control system has been constructed for the U.B.C. electrostatic accelerator. Over the past six months, it has provided analyzed beams of protons as large as 4½ microamperes on a target with an energy homogeneity of 0.1%.

In the system adopted, the accelerated positive ions are analyzed by a 90° deflection magnet provided with entrance and exit slits to define the beam path. The magnetic field is stabilized to a few parts in 100,000, and controlled by a nuclear magnetic resonance method. A fraction of the emergent beam falls on two insulated slits, "sniffers," connected to a differential amplifier, the output of which varies as the beam impinges more on one than the other. Thus an error signal is obtained according to the shift in energy and hence position of the beam, which is used to modulate a reverse beam of electrons sent up the differential pumping tube of the generator. This beam loads the generator so as to maintain its voltage, and hence the energy of the ions, constant. The main central part of the beam passes through the slits onto the target mounted beyond. One-dial control over a range of 20 KeV is achieved by simply tuning the oscillator controlling the frequency of the nuclear magnetic resonance fluxmeter head. The energy of the ions can be varied in steps as fine as 0.2 KeV in 1,000 KeV.

The generator's voltage scale (the generating voltmeter) and energy scale (the magnetic field of the analyzing magnet) have been calibrated relative to the currently accepted standard value of Herb, Snowdon, and Sala of 0.8735 MeV for the strong F^{19} $(p,\alpha\gamma)O^{16}$ resonance and checked with the 0.3404 MeV resonance occurring in the same reaction. Additional calibration points were obtained using mass 2 and 3 beams.

The complete gamma ray excitation curve for the reactions from F^{19} bombarded with protons has been taken up to 2 MeV and new resonances found at 1.62 and 1.84 MeV. The 1.355, 1.381 MeV doublet was resolved with a peak to trough value of 9/1, which is excellent confirmation of the homogeneity of the proton beam.

The resonances in the N^{15} $(p,\alpha\gamma)C^{12}$ reaction have also been investigated and background yields from various target backing materials measured up to 2 MeV.

PAPERS PRESENTED BEFORE LEARNED SOCIETIES

1. Crystal Controlled Frequency Divider from 150 kc/s to 60 c/s. Presented before the Institute of Radio Engineers, London, Ontario, chapter, 1949.

MEMBERSHIP IN LEARNED SOCIETIES

1. Student member, Canadian Association of Physicists, 1947/52.
2. Student member, Institute of Radio Engineers, 1946-52.
3. Engineering pupil, Association of Professional Engineers, 1947-52.

ACKNOWLEDGEMENT.

The author wishes to express his sincere thanks to Prof. J.B. Warren who has constantly guided and encouraged him in all his work at the University of British Columbia. Thanks are also due to Dr. C.A. Barnes for invaluable help in nuclear physics and to Prof. W.B. Coulthard for the many helpful discussions on regulator systems.

He is very grateful to the members of the Van de Graaff group of the University of British Columbia, both staff and research students, without whose generous help, this work could not have been done.

The author would like to express his appreciation of the awards of a Bursary and Studentships made to him by the National Research Council without which it would have been impossible for him to pursue his scientific carreer to this stage. Thanks are due to the Defence Research Board for their financial aid in carrying out this research work.

Table of Contents.

Part II

Voltage and Energy Calibration

Part III

Determination of Some Nuclear Excitation Functions

LIST OF ILLUSTRATIONS.

Introduction.

The Electrostatic Generator in Nuclear Physics.

The Van de Graaff electrostatic generator[1] is a machine for providing a constant source of d-c potential of several million volts which is free from ripple and stable to better than 1%. An important precise tool for Nuclear Physics research is obtained by fitting a suitable vacuum tube to the generator for acceleration of positive ions or negative electrons for use as bombarding particles. The whole assembly of d-c generator, vacuum accelerating tube, and the auxilliary apparatus needed to provide the source of ions as well as a selection and control of their energy, is called the "electrostatic accelerator".

The electrostatic accelerator is the most suitable machine available at present for investigating the energy levels in the light elements for it alone can provide a very constant but readily variable accelerating potential. It is the object of this thesis to describe how the electrostatic accelerator of the University of British Columbia was stabilized to $\pm$ 0.1%, calibrated with respect to an absolute voltage and energy scale, and then used in the investigation of $(p, \alpha\gamma)$ resonances in some light nuclei.

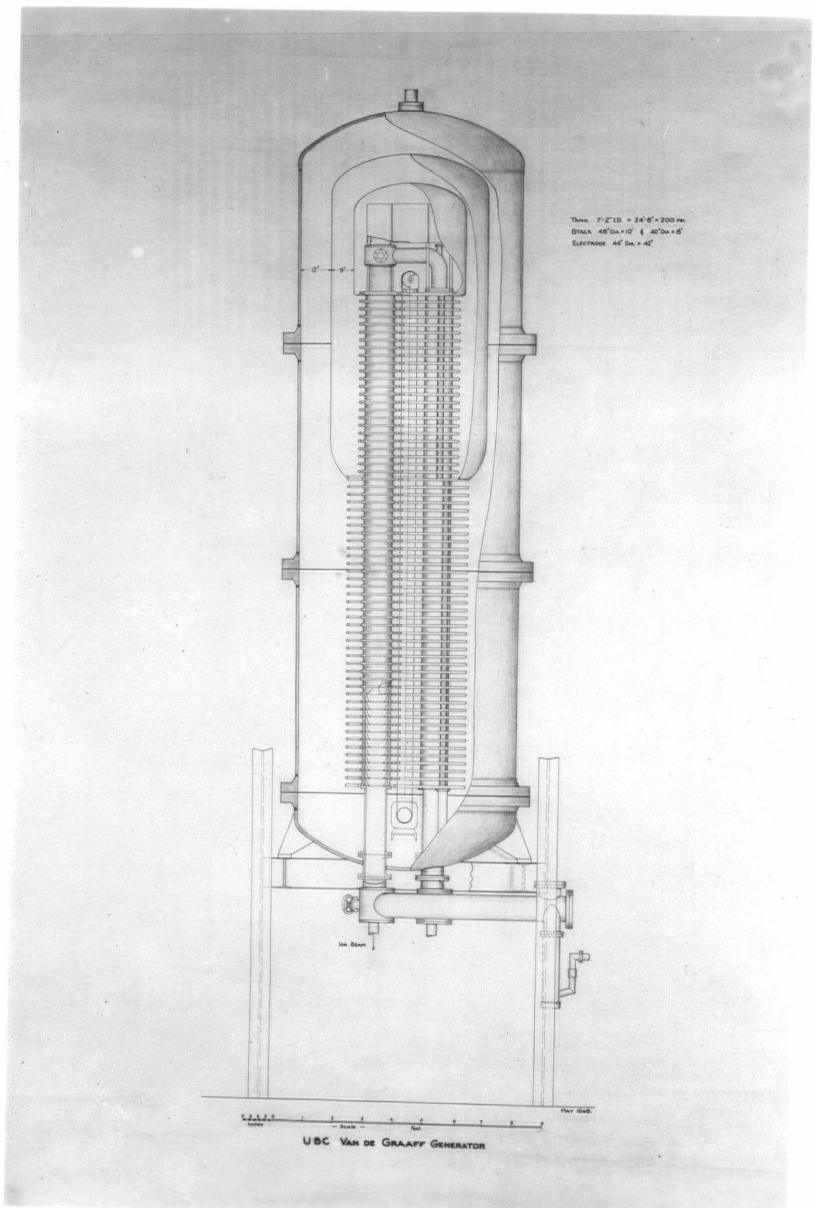

Figure 1.

Prototype of U.B.C. Van de Graaff Generator

to face page 1.

Part I

The Van de Graaff Accelerator and Stabilizing Equipment

I. Acceleration of a Beam of Positive Ions

The Van de Graaff generator provides a high voltage for the acceleration of ions. Figure 1, shows a cut-away view of the prototype of the U.B.C. machine. Positive charge, which is sprayed from a high voltage set on to a long endless insulating belt, is carried up into the inside of a large hollow metal electrode where it is removed. This charge, which spreads to the outside surface of the electrode, raises it to a very high potential of equilibrium value determined by the balance of charge carried up and the load on the generator. A long vacuum tube, fitted with an ion source and focussing system at the top end, reaches from inside the hollow metal electrode to ground where it connects with a vacuum box containing a target. The ions are injected into the vacuum tube, are focussed and accelerated by the high potential with respect to ground and strike the target with a high velocity. The generator voltage is coarsely adjusted by varying the spray current from the high voltage set.

The University of British Columbia Van de Graaff is a vertical pressurized machine designed for a potential of four million volts. It uses an electrodeless, radio frequency type of ion source[2] which provides a source of al-

most monoenergetic atomic ions (up to 75% of H^+ in a total current of up to 50 μ amps, homogeneous in energy within 100 electron volts, (eV)), with low gas consumption (about 0.15 c.c. per minute at 760 mm. of mercury) and good focussing. The ion source, together with pressure bottles of hydrogen and deuterium, palladium thimbles, power supplies, controls and monitoring meters ise fitted in the confining space of the polished top terminal (about $3\frac{1}{2}$ feet diameter and $3\frac{1}{2}$ feet high). There are two vacuum columns, 16 feet long, one of which is used for differential pumping while the other is the main accelerating tube used for the positive ion beam. Four large oil diffusion pumps maintain a vacuum of 2×10^{-5} mm. of mercury or less during normal operation with a beam of positive ions.

The insulating column supporting the top terminal and equipment is made up of 64 aluminum equipotential plates, each spaced by three 2 7/8 inch porcelain spacers. Sections of conducting rubber join each plate to the metal electrodes of the two vacuum tubes. In addition there is a 450 megohm resistor linking each pair of plates to provide a constant load of 2.84×10^4 megohms for the machine. The first equipotential plate up from ground is however returned to a negative potential of 1200 volts to suppress secondary electrons emitted from the grounded inner surfaces of the bottom of the vacuum tubes.

The main parts of the machine (figure 1.) are enclosed in a large steel pressure tank which is pumped up with

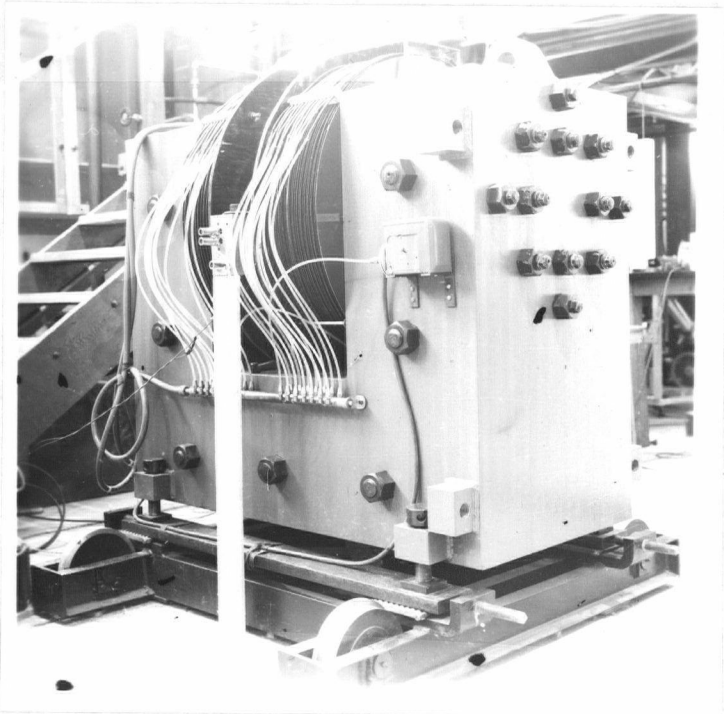

Figure 2.

Analyzing Magnet.

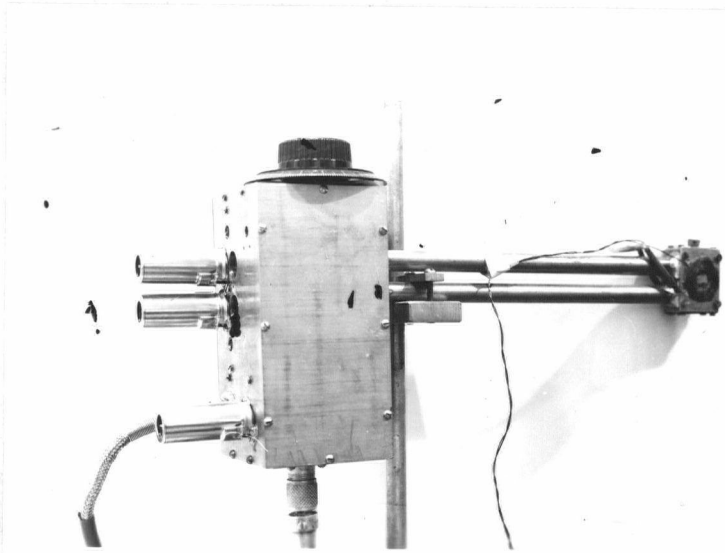

Figure 4.

Fluxmeter r-f Head.

to face p.3

dry nitrogen (plus freon 12) to a pressure of 75 to 100 pounds per square inch to inhibit corona. The pressure tank is provided with a number of glass viewing ports as well as a periscope for viewing meters in the top electrode.

The accelerator will of course accelerate any type of ions produced by the source, but for most investigations, atomic ions of hydrogen - protons - or of deuterium - deuterons - are required. For some purposes a source of helium ions would be useful but the r-f type source tends to produce He^+ ions, not alpha particles with two charges.

II. The Energy Selector and Analyzing Magnet.

1. Introduction.

The accelerated beam of ionized hydrogen contains the following ions:

H^+ - protons, (mass 1),

HH^+ - singly charged hydrogen molecules, (mass 2),

HHH^+ - (mass 3).

A large 90° analyzing magnet provided with a vacuum box between its pole faces was used to focus and separate the different mass components. This magnet, weighing over seven tons, required a current of about 45 amperes at 250 volts d-c to provide a field of about 20,000 gauss over its 16 inch square pole faces through its one inch air gap. A degenerative electronic current stabilizer, built

Figure 3

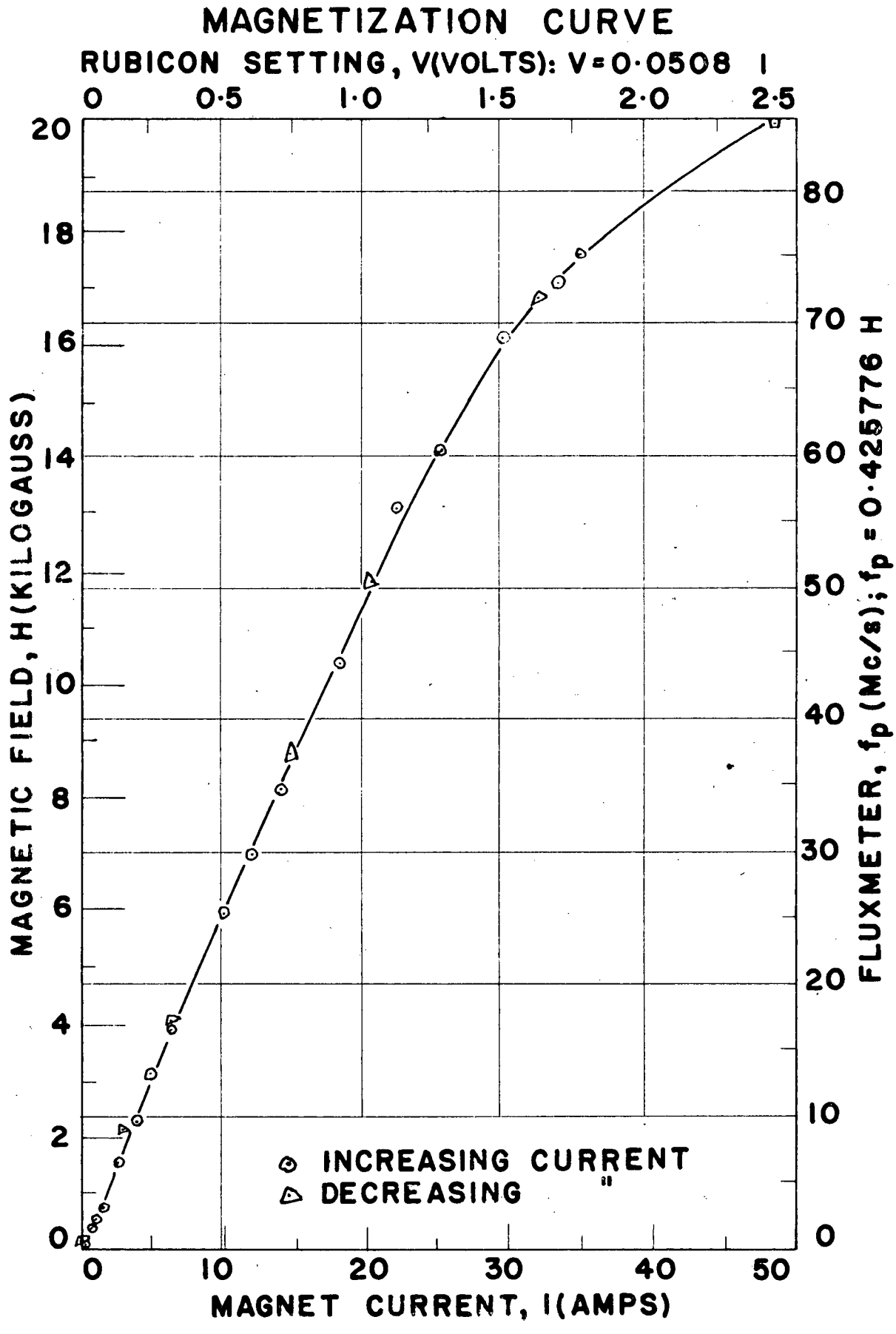
MAGNETIZATION CURVE
RUBICON SETTING, V(VOLTS): V = 0·0508 I
0
0·5
1·0
1·5
2·0
2·5
MAGNETIC FIELD, H(KILOGAUSS)
FLUXMETER, f_p (Mc/s); f_p = 0·425776 H
INCREASING CURRENT
DECREASING "
MAGNET CURRENT, I(AMPS)

by the author[3], held the field constant to a few parts in 10,000. Figure 2 is a photograph of the magnet. The magnetization curve is shown in figure 3. The hysteresis loop was too narrow to show up, about 0.2 amperes wide at 15 amperes and about 200 gauss high at 4 kilogauss.

The analyzing magnet separates ions of different charge to mass ratio and of different energy. Thus if a parallel beam of ions of energy

$$eV = \tfrac{1}{2} mv^2 \qquad \text{(II.1)}$$

are incident on the entrance slit, then they will be deflected through 90^o and pass through the exit slit if their radius of curvature is of value ρ fixed by the positions of the slits, where:

$$\frac{H e v}{c} = \frac{mv^2}{\rho}, \qquad \text{(II.2)}$$

and (using c.g.s. units)

H is the magnetic field strength between the pole faces in e.m.u.,

e is the charge of the ion in e.s.u.,

m is the mass of the ion,

v is the velocity of the ion,

c is the velocity of light,

ρ is the radius of the path of the ion,

V is the potential through which the ion was accelerated.

Combining equations (II.1) and (II.2) gives the relationship between the accelerating voltage, V, charge-to-mass ratio, e/m and the momentum of the particles, $H\rho$:

$$V = \frac{e}{2 m c^2} H^2 \rho^2 . \qquad (II.3)$$

In addition, the well known focussing properties of a 90° magnet[4] allow maximum beam on the target with exact definition of ρ and hence of beam energy.

Since e/m is constant for each mass component, and since ρ may be fixed by entrance and exit slits on the magnet box, ions of energy $eV = E$ only will be focussed at the exit slit in a field of constant H. However, from equation (II.3), it can be easily seen that for a given curvature,

$$\frac{\Delta E}{E} = \frac{\Delta V}{V} = \frac{2\Delta H}{H} \qquad (II.4)$$

so that a highly stabilized field is needed to maintain the emergent ion beam homogeneous in energy, E. For this purpose a proton magnetic resonance fluxmeter was built for field measurement, stabilization and control.

2. Proton Magnetic Resonance Absorption.[5]

As a consequence of quantum mechanics, all isolated nuclear systems possess a total angular momentum I quantized in integral or half-integral values, in units of $h/2\pi$ ($\hbar$). Experiment shows that for even mass number (A) nuclei, I is integral (0,1,2.....) and for odd A nuclei, I is half integral ($\frac{1}{2}$, 3/2,.....). It is also found that all nuclei having an even number of protons (Z) and an even number of neutrons (N) have $I = 0$. Associated with this total angular momentum, which may be loosely called nuclear spin, is a nuclear magnetic moment

$$\mu = \gamma I \hbar \qquad \text{(II.5)}$$

which is again of course, zero for even Z, even N nuclei. γ, the gyromagnetic ratio, the ratio of the magnetic moment to the angular momentum, has been measured quite accurately for a large number of nuclei.

When nuclei are placed in a strong magnetic field, H, they may orient themselves in different quantized directions with respect to the field because of their magnetic moment. Each position defines a quantum mechanical state possessing a certain energy and there are $(2I+1)$ possible states. The energy of these states is[*]

$$E = E_0 + M_I \frac{\mu H}{I} \qquad \text{(II.6)}$$

where M_I is the projection of the vector I on the axis of the magnetic field H. For transitions between adjacent levels, $\Delta M_I = \pm 1$ and no others are allowed by selection rules. Therefore the energy difference between these states is

$$\Delta E = \mu \frac{H}{I} = \hbar \gamma H . \qquad \text{(II.7)}$$

If, now an oscillating magnetic field, H_1, perpendicular to H is applied, transitions may be induced between neighboring states most strongly when the magnetic resonance relation holds true, ie.

$$\Delta E = \hbar \omega = \hbar \gamma H, \qquad \text{(II.8)}$$

where ω is the frequency of the applied field H_1 in the

---

[*] 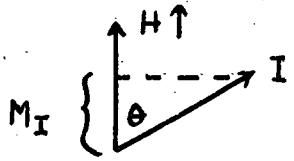

the work done to rotate the dipole μ against a field H from the past to the next possible position is $\mu H \cos\theta = \mu H \frac{M_I}{I}$

r-f range, and gives the Larmor precession frequency for the nuclear spin vector about H. These transitions will occur not only by absorbing energy from the r-f field applied but also in stimulated emission. Since the transition probability is the same for each direction no absorption of energy from the applied field would occur if this was the only factor to be considered. However the thermal motions within the sample of nuclei set up fluctuating magnetic fields which can act upon the aligned magnetic dipoles and sometimes change their orientation. This "spin-lattice" interaction does not affect states of higher and lower energy equally however; Boltzman statistics indicate that a slight preponderance of dipoles will exist in the lower states. Thus for protons for which $I = \frac{1}{2}$ there are two states, parallel and anti parallel having an energy difference $\Delta E = 2\mu_p H$ so that in equilibrium, which takes place with a time constant T_1, the "Relaxation Time", of from 10^{-4} to 100 seconds depending on the lattice conditions, the ratio of protons present in the two states is:

$$\frac{N_{higher}}{N_{lower}} \doteq e^{-\Delta E/kT}, \qquad \text{(II.9)}$$

where k is Boltzmann's constant and T is the absolute temperature. For room temperature with a field of 5,000 gauss, $\Delta E/kT \approx 3 \times 10^{-6}$ whence:

$$\frac{N_{lower} - N_{higher}}{N_{lower}} \approx \frac{\Delta E}{kT} \approx \frac{2\mu_p H}{kT}. \qquad \text{(II.10)}$$

Thus the slightly larger population of the lower state

will result in a higher absorption than stimulated emission from the upper state. The extra energy so absorbed appears as heat energy in the lattice vibrations and motions.

Consider protons in a sample of water. With no external magnetic field, the orientation of the protons will be quite random. When a field, H, is applied the protons will assume only two quantized positions with respect to the applied field; statistically about half will be aligned parallel to the field and about half anti-parallel. The thermal motion of the nuclei brings about changes in their spin orientations so that there is a slight excess of protons in the lower energy state (parallel) according to Boltzmann's statistics. There is a characteristic time associated with this re-orientation process, the spin-lattice time, T_1, which for protons in water (plus some $MnCl_2$) is of the order of 0.01 seconds. The excess of protons in the lower energy state is about 7 per million in a field of 10 kilogauss. The magnetic resonance condition (II.8) may be satisfied if the oscillating magnetic field, H_1, in the radio frequency (r-f) range (about 40 Mc/s) is supplied by a small coil surrounding the water sample. H_1, of the order of 5 gauss, may be obtained by applying about 0.5 volts from a suitable oscillator to the r-f coil. The magnetic resonance absorption signal observed under the above conditions varies from a few microvolts to a millivolt depending on H, the size of the sample, the value of T_1 and the homogeneity of H around the sample.

In practice, r-f power is supplied to a small coil containing the sample of protons. The strong magnetic field, H, applied to the sample is modulated by a small pair of Helmholtz coils so as to sweep through the resonance condition many times (up to 500) per second. The net absorption of power by the nuclei from the r-f coil is detected as a lowering of the Q of the oscillator coil (an increase in the effective series resistance of the coil) and may be displayed as a resonance signal after amplification on a cathode ray tube operated in synchronism with the modulation frequency.

By using the most recent value[6] of γ_p for protons and substituting in (II.8), the simple relation for measuring the magnetic field H in terms of the frequency f_p is obtained:

$$H \text{ (kilogauss)} = 0.234865\ f_p \text{ (Mc/s)} \pm 0.002\% \qquad \text{(II.11)}$$

A suitable r-f power source, set of modulation coils, amplifying and detecting equipment therefore constitutes a very precise fluxmeter. Fields as low as 11 gauss and as high as 12 kilogauss have been measured with this method using proton samples. The lower limit is set by the strength of the resonance signal obtained, which varies directly as the square of H and the size of the sample[7]. Since the signal strength decreases with inhomogeneity in H, size of the sample is also a limit although water samples as large as one liter have been used. The upper limit is set by the difficulty of obtaining the r-f field excitation over a sufficiently large sample of protons in the presence

Fig.5

BLOCK DIAGRAM OF COMPLETE PROTON RESONANCE FIELD CONTROL EQUIPMENT

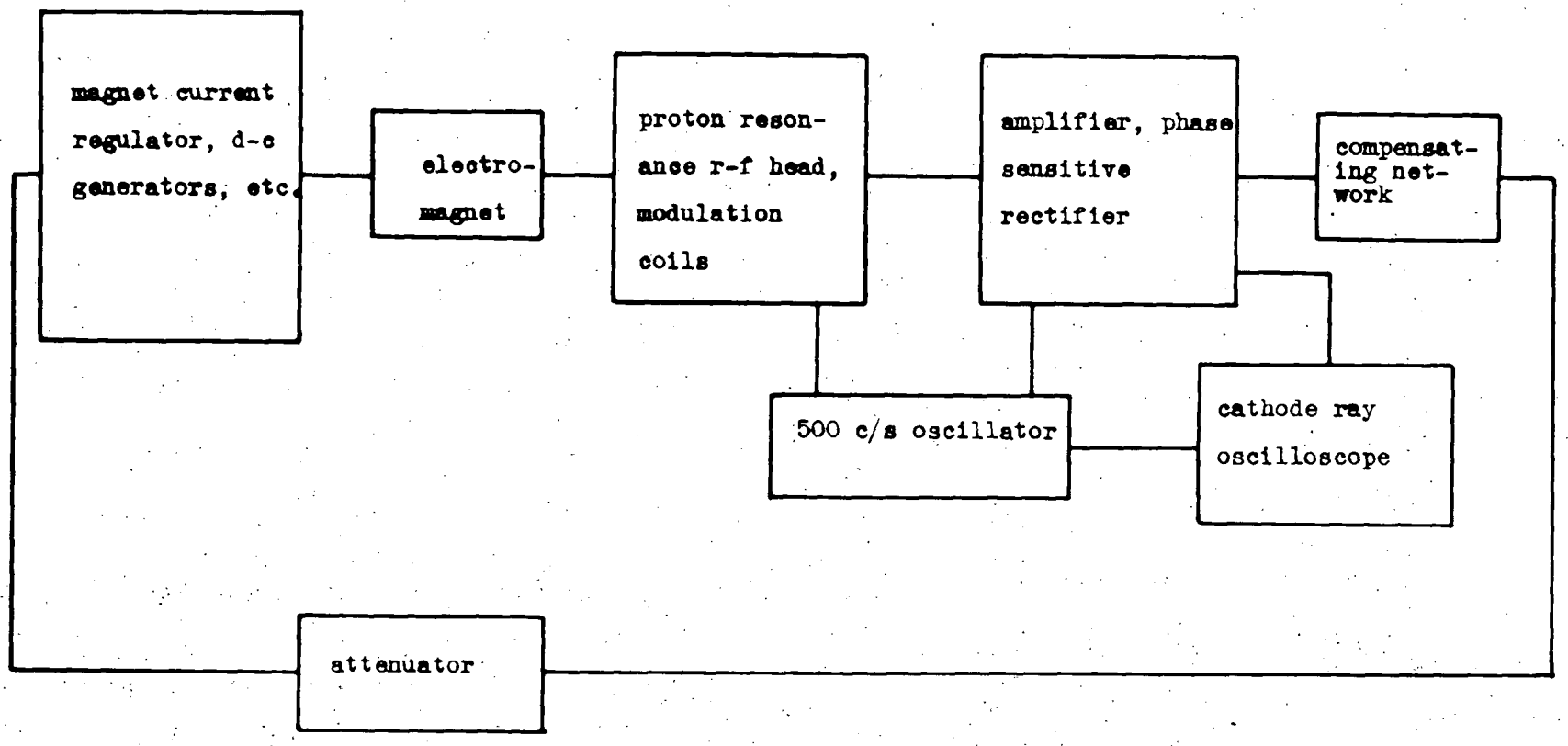

of a very strong magnetic field. The noise level is set by the tubes in the detector and the first stage in the amplifier. For protons, the S/N ratio is sufficiently large to give signals adequate for use in stabilizing systems without the need for low noise high gain amplifier[8]. This is not the case for other nuclei.

Higher magnetic fields may be measured at lower frequencies (than that for protons) by using a nucleus such as Li^7 which has a larger gyromagnetic ratio than the proton. For example, in the same magnetic field, H, the ratio;

$$\frac{f_{Li}}{f_p} = 0.388625 \qquad \text{(II.12)}$$

has been measured experimentally so that equation (II.11) becomes, when using a sample containing Li^7 nuclei:

$$H(\text{kilogauss}) = 0.6043486\ f_{Li}(\text{Mc/s}). \qquad \text{(II.13)}$$

This means that with suitable extra amplifying equipment, fields over 2½ times as great could be measured at the same frequencies shown in (II.11) for protons.

3. Proton Magnetic Resonance Fluxmeter and Field Stabilizer.

(a) Magnet Current Regulator.

Before the field of the magnet was stabilized, its current was controlled by a degenerative regulator circuit. A standard manganin resistor inserted in the magnet current leads produced a voltage drop which was compared to the voltage of a standard cell (through a Rubicon potentiometer) by means of a Brown converter chopper. An error signal derived from this after amplification and detection was used to control the field current of two

Figure 6

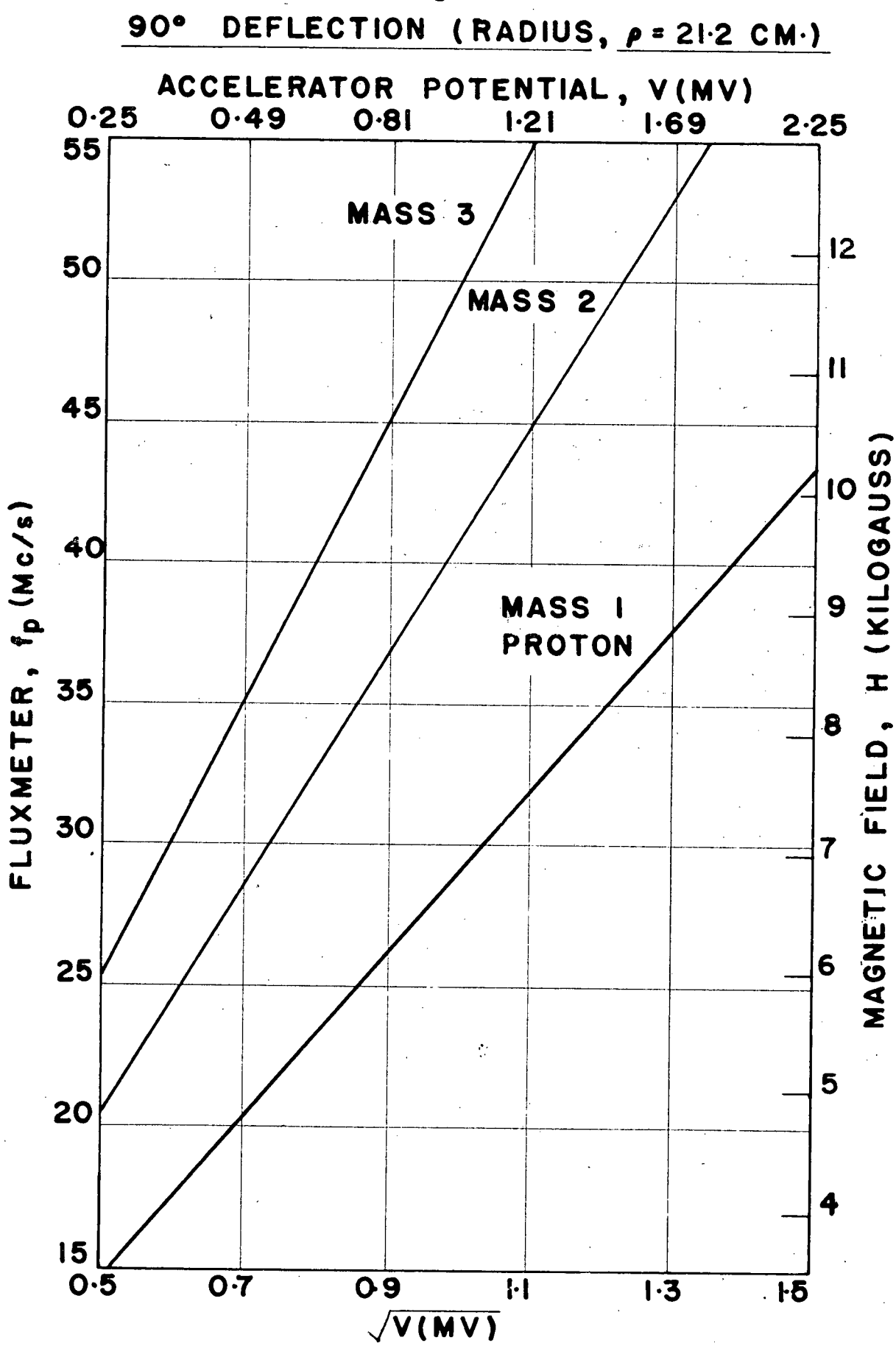
90° DEFLECTION (RADIUS, ρ = 21·2 CM·)
ACCELERATOR POTENTIAL, V(MV)
0·25
0·49
0·81
1·21
1·69
2·25
MASS 3
MASS 2
MASS 1
PROTON
FLUXMETER, fp (Mc/s)
MAGNETIC FIELD, H (KILOGAUSS)
55
50
45
40
35
30
25
20
15
12
11
10
9
8
7
6
5
4
0·5
0·7
0·9
1·1
1·3
1·5
√V(MV)

constant speed d-c generators supplying the magnet current. The resulting magnetic field, up to 16,000 gauss, was held to one part in 10,000 over short periods and to within a few parts in 10,000 over longer periods.

(b) Error Signal from the Proton Magnetic Resonance Equipment.

The proton resonance equipment provides a d-c error voltage proportional to the deviations of the magnetic field from the desired value H, as given above. The amplitude and polarity of this flux error voltage vary as the magnetic field is below, equal to, or above the value H within the few gauss range of the proton resonance. The flux error voltage is derived as follows. An a-c signal is first obtained by modulating the magnetic field by a small pair of coils so as to sweep across the proton resonance[9]. This a-c signal of a few hundred microvolts is then amplified and passed through a phase sensitive rectifier to give the required d-c error voltage (see figure 12). This flux error voltage, when added to the magnet current error voltage, provides the final control of the magnetic field.

Figure 4 is a close-up view of the fluxmeter r-f head. One of the modulating coils may be seen at the right, on the outside of the search coil box. The r-f coil and proton sample are inside the brass case, behind the modulating coil. A block diagram of the complete flux control

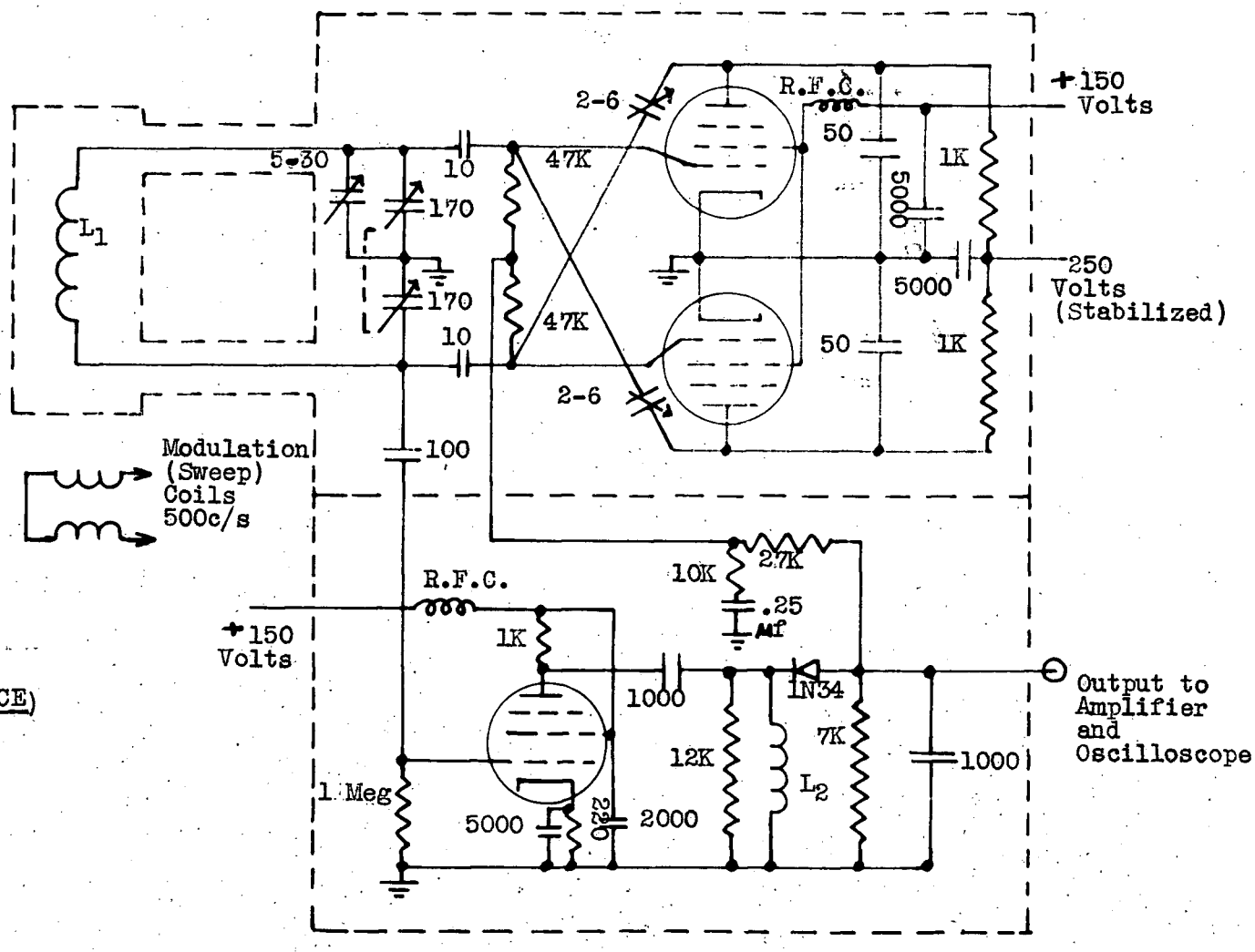

FLUXMETER

(PROTON RESONANCE)

R. F. HEAD

Figure 7

All tubes 6AG5; All condensers in $\mu\mu$f.
25-44 Mc/s - L_1 = 8 turns, L_2 = 3 μh.
K = Kilohm.

epuipment is shown in figure 5. The equipment built to control the flux directly consisted of the following units: r-f head and stabilized power supply, proton resonance signal amplifier and phase sensitive rectifier, 500 c/s oscillator, compensating network, cathode ray oscilloscope and power supply. Power for all these units was supplied by a Sola constant voltage transformer.

(c) Fluxmeter r-f head.

The circuit of the fluxmeter r-f head following the design of T. Collins[10] is shown in figure 7. The head contains a weakly oscillating detector consisting of a pair of 6AG5 tubes in a push-pull arrangement. The oscillations are kept small by the two by-pass condensers from plate to ground and feedback from the additional 6AG5 tube used as a low gain amplifier. Only one control, the two-gang variable air condenser, is needed to tune the oscillator over about a 2 to 1 frequency range. This condenser together with the search coil, inside of which is placed about 1 c.c. of a 0.1 molar solution $MnSO_4$, forms the tank circuit which is loosely coupled to the oscillator tubes.

The complete r-f head is rigidly mounted in a heavy brass box with the search coil protruding (figure 4). Two 40 turn double-pancake wound coils are cemented to the outside shield plates of the search coil for modulating the magnetic field.

Two r-f heads with additional coils were finally used

Figure 8

Proton Resonance Amplifier & Phase Sensitive Rectifier

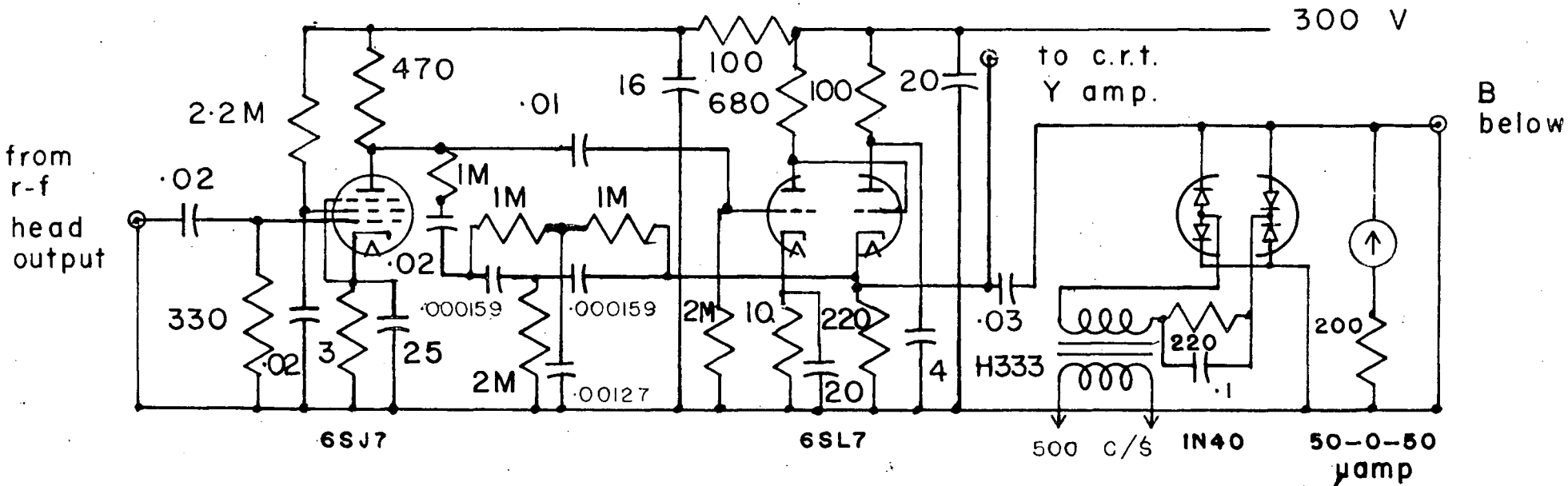

Figure 9

Compensating Network

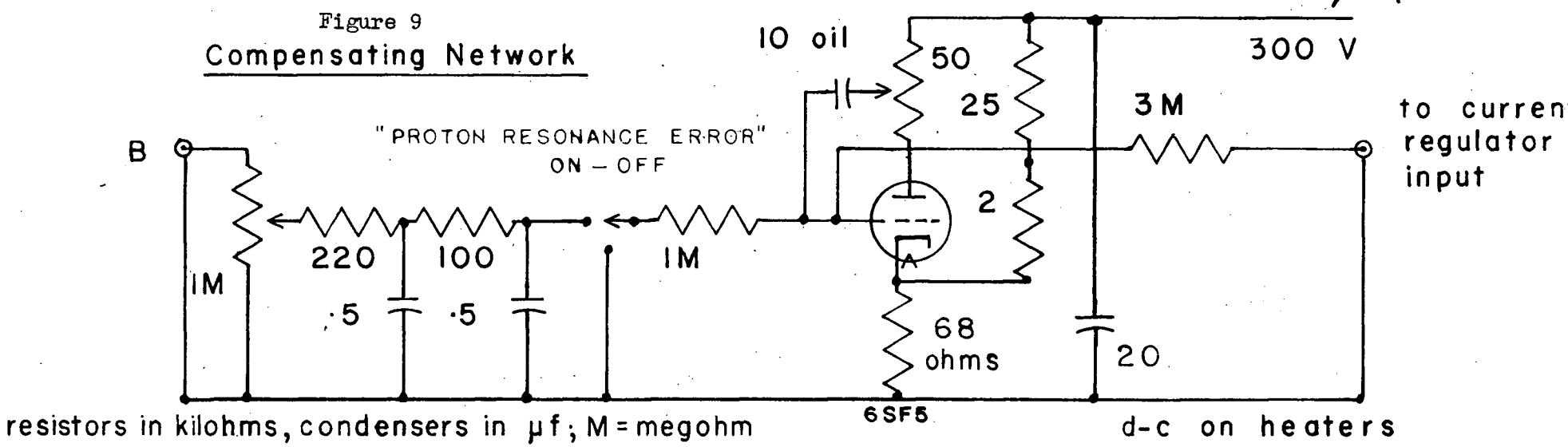

resistors in kilohms, condensers in μf; M = megohm

d-c on heaters

to cover the frequency range from 11 Mc/s to 55 Mc/s in four overlapping steps as shown in Table 1.

Table 1.

Fluxmeter Coil Ranges.

Head #	Coil #	Frequency Range Mc/s	Flux Range kilogauss
1	1	55 - 33	12.9 - 7.75
	2	44 - 25	10.3 - 5.9
2	3	27 - 18	6.3 - 4.25
	4	19 - 11	4.5 - 2.6

(d) r-f Head Power Supply.

An electronically stabilized power supply[11] (Elmore and Sands, p. 373) provided the r-f head with 250 volts and 150 volts (gaseous diode regulated). A 0-50 milliameter inserted in the 250 volt lead indicated the strength of oscillation in the r-f head (8 to 10 ma. indicated strong oscillation, 10 to 15 ma. or greater showed weak oscillations, while greater than 20 ma. meant no oscillations at all). This, together with a voltmeter, was completely enclosed in a steel cabinet and mounted near the magnet.

A 6 volt lead-and-acid storage battery supplied the heaters for the r-f head as well as those of the proton resonance signal amplifier.

(e) Fluxmeter Signal Amplifier and Phase Sensitive Rectifier.

This unit, figure 8, consisted of a conventional two stage r-c coupled amplifier with some negative feedback and a cathode follower output. The output was

coupled to a phase sensitive rectifier and output meter. The bandwidth of the amplifier was limited by a twin-T feedback network, antiresonant at the modulation frequency of 500 c/s. The overall voltage gain at 500 c/s was 10,000. The gain was down 15 db. at 120 c/s and 2,000 c/s; down 21 db. at 60 c/s and 5,000 c/s. This limited bandwidth kept the signal to noise ratio to about 50 to 1 for the proton signals at the output of this amplifier. The a-c flux-error signal was fed via 35 feet of coaxial cable to the regulator chassis, where it was displayed on a cathode ray tube.

A Sylvania 1N40 (which consists of 2 matched pairs of 1N34 germanium diodes) was used as a phase sensitive rectifier or switch demodulator[12]. The values of resistance and capacitance used as "bias"[10] (220 k and 0.1 uf) gave maximum d-c output for the 500 cycle input signals. The 500 c/s local signal for the phase sensitive rectifier, and the plate supply voltage were both fed via a shielded cable from the fluxmeter regulator chassis.

A centre-reading microammeter with multiplier, connected across the output of the phase sensitive rectifier, showed when the proton magnetic resonance was being detected. The meter needle, reading 20-0-20 volts full scale, indicated proton magnetic resonance field regulation by its small random motion about centre.

This unit was also completely enclosed in a shielded cabinet and mounted beside the magnet.

(f) Fluxmeter Regulator Chassis.

This chassis contained the 500 c/s modulat-

Figure 13

SPRAY CURRENT STABILIZER

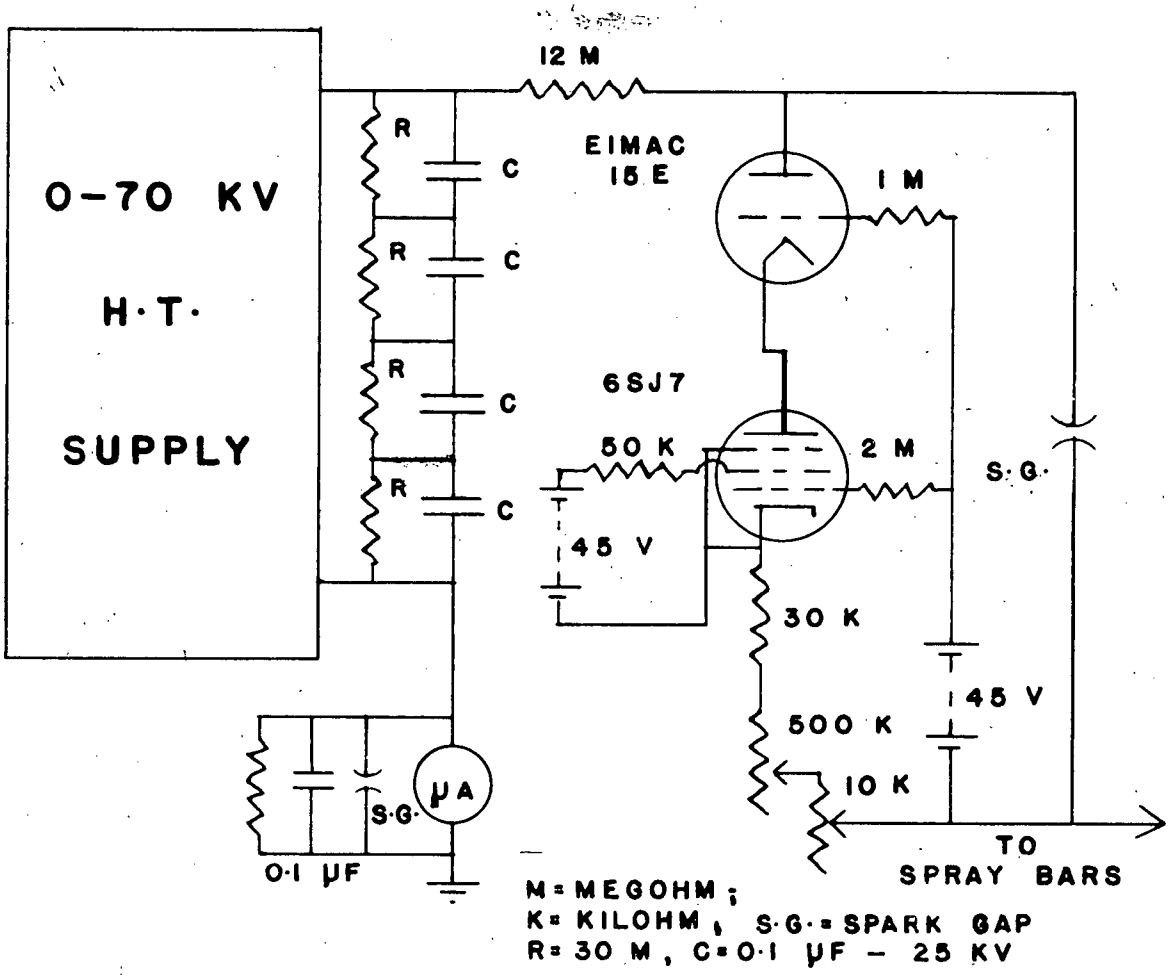

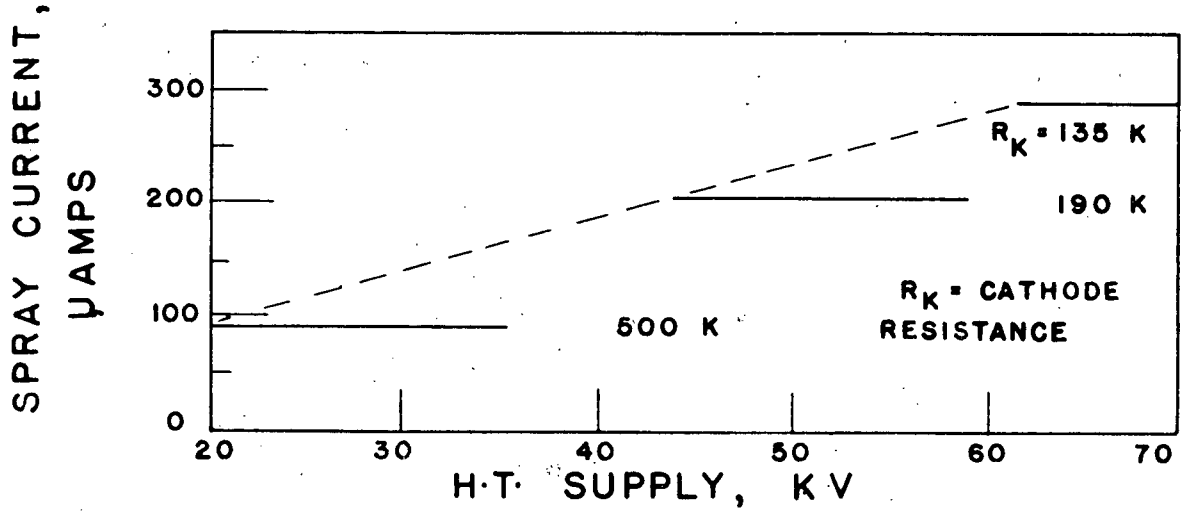

Fig. 10

500 C/S OSCILLATOR

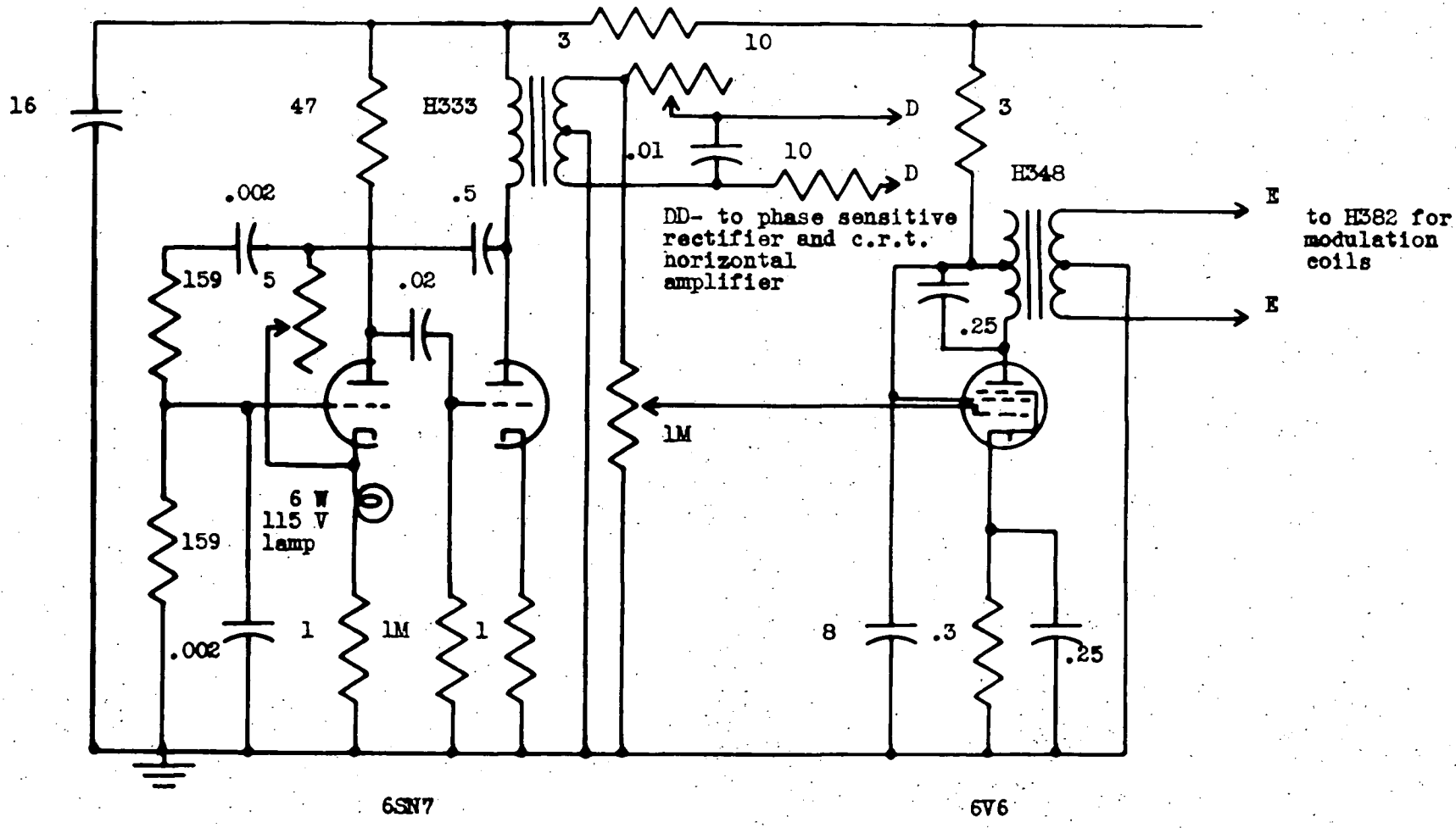

resistors in kilohms; condensers in uf; M megohm. a-c on heaters

ing oscillator, gain control, compensating network, a cathode ray oscilloscope, and a power supply for the above components.

The 500 c/s oscillator, figure 10, differed from the usual Wien Bridge oscillator only in the use of a transformer load (H333) in the second half of the 6SN7. The secondary of this transformer supplied about 20 volts to the phase sensitive rectifier and the 6V6 power amplifier as well as to the horizontal sweep amplifier tube of the cathode ray oscilloscope. A phase shifting network was inserted ahead of the phase sensitive rectifier and c.r.t. sweep amplifier to compensate for changes in phase that the modulating signal received in its path through the 6V6 tube, coupling transformers, fluxmeter head, and amplifier. The 6V6 tube supplied up to 100 ma. of current to the 80-turn modulation coils, allowing a few gauss sweep of the magnet's field.

The gain control, filter network, switch, and Miller integrating circuit are shown in figure 9 as the "compensating network". The two stage r-c filter smoothed the output pulses of the phase sensitive rectifier. The Miller integrating network provided a long time constant needed for stability of the flux control loop. The effective grid-to ground capacity is given by the formula

$$C = C_{\text{grid-to-plate}}(1 + K)$$

where K is the voltage gain of the stage ≈ 40

(g) Attenuator Interconnecting Network.

A simple resistive attenuator network was

Fig. 11

INTERCONNECTION of FLUX and CURRENT ERROR SIGNALS

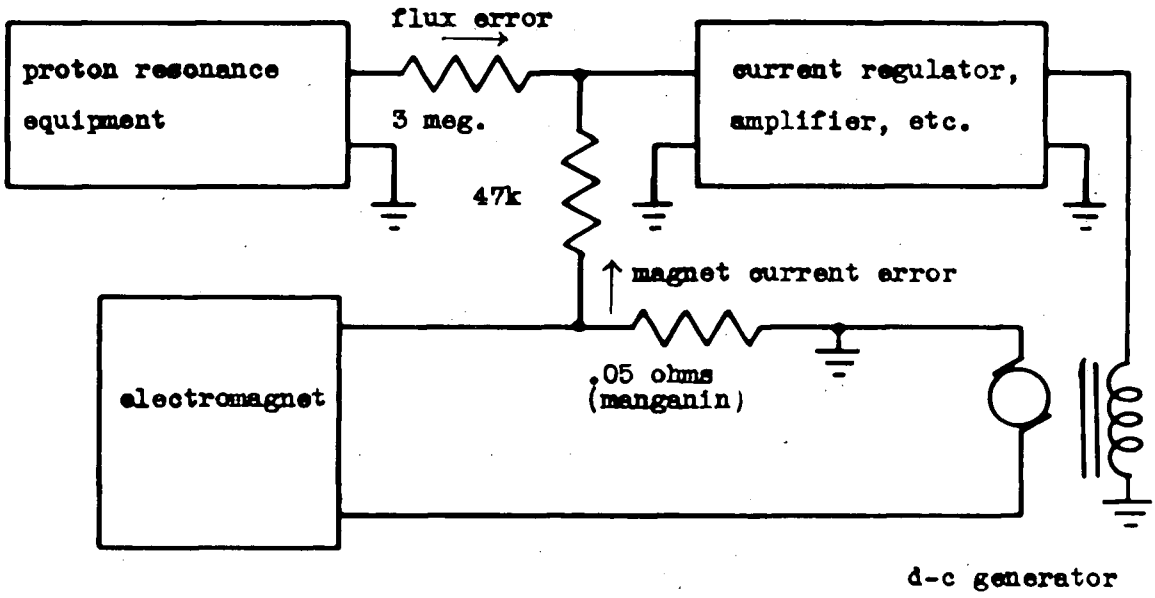

Fig. 12

TOTAL ERROR SIGNAL (flux plus current)

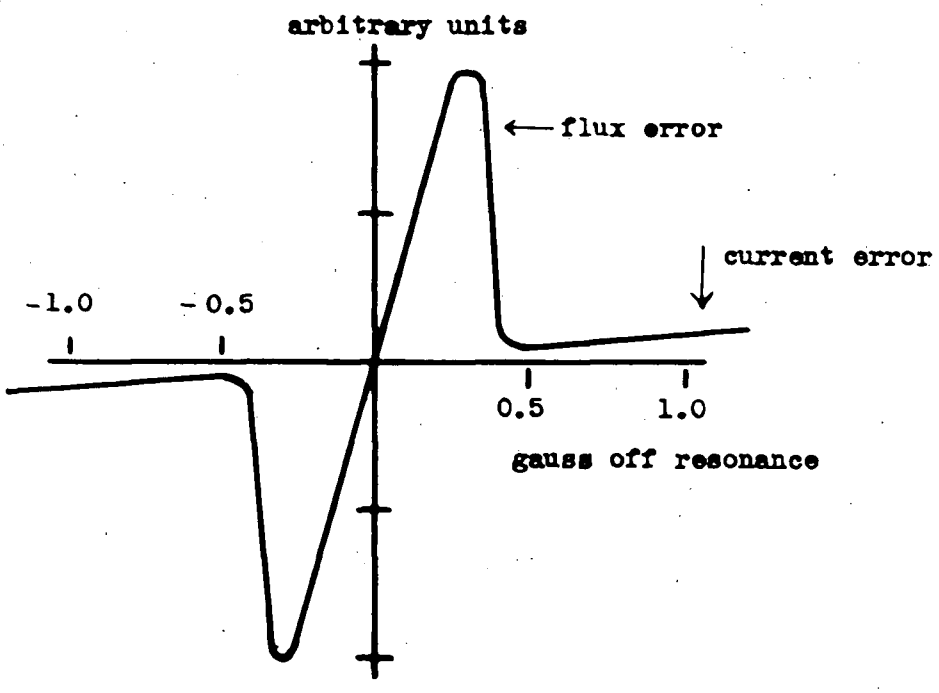

inserted between the output of the proton magnetic resonance equipment and the input to the amplifier of the current regulator apparatus. This interconnecting network gave the desired addition in the direction of flux error signal to current error signal, while keeping the undesirable coupling in the reverse direction small between the voltage across the manganin resistor and phase sensitive rectifier diodes. This may be seen in figure 11. The attenuator consisted of a 3 megohm and a 47,000 ohm resistor. This reduced the amplified proton magnetic resonance flux error signal to a few millivolts which was then added to the approximately 25 μv of error voltage derived from the magnet current. The relative magnitude and shape of the error signals is indicated in figure 12.

(h) Operation and Performance of the Flux Regulator.

The equipment was operated from the accelerator control console, by setting the oscillator in the r-f head to the proton magnetic resonance frequency pertaining to the field required for deflecting protons through 90^{o} as read from the graph figure 6 or from the equation (II.11). The magnet current was set to give a field just below the required value and increased slowly until the proton magnetic resonance signal appeared on the cathode ray tube screen mounted at the control panel. The field was held accurately at this value which defined the energy of the analyzed, accelerated proton beam. In most cases, the flux error signal was strong enough to allow one dial "frequency" control of the magnetic field over about 1 Mc/s

in 30 Mc/s, ie. about 0.2 kilogauss in 6 kilogauss, without need for altering the magnet current setting control. As a result, the current setting needed only to be changed manually at intervals.

(i) Engineering Features of the Magnet Stabilizer.

A number of safety devices and interlocks were provided to protect the operator and the magnet from the 12 kilowatts maximum of power in the circuit. A rectifier connected in the reverse direction across the magnet coils discharged them quickly and safely if the circuit was opened or the power failed. In addition, power was cut off from the magnet if the water-cooling failed, if the current regulator tubes (6AS7) drew grid current or if the cabinet door was opened to the magnet's generator's shunt field power unit (400 volts d-c at 1 ampere). An overload current relay limited the shunt field current to 1 ampere. Two re-set push-buttons placed the equipment in operation again when all faults were cleared.

The current regulator alone had six main time constants, five lagging and one leading. The longest one, 3 seconds for the magnet, was large compared to the next one, 1/20 second for the d-c generator's shunt fields. The four others, from 1/100 to 1/10,000 second were in the input and output circuits of the Brown converter d-c amplifier. Hunting did occur with a large voltage gain in the amplifier but was eliminated by reducing the gain to about 60db., leaving a phase margin[13] of about 15°. The response time of the

regulator to a step voltage input was about 1 second.

The flux regulator circuit itself had four main time constants. The longest, a 400 second lead in the Miller integrating circuit, was inserted to prevent hunting in the regulator. Two others, about 1/10 and 1/40 second were in the smoothing network following the phase sensitive rectifier. The last one, about 1/100 second was due to the relaxation time of the protons being swept through magnetic resonance by the modulation coils. With the addition of the integrating circuit, a gain of about 45 db. was allowed with good stability.

A good feature of the r-f head oscillator was its small drift of about 1 part in 10,000 over several hours. Silver ceramic condensers were used as trimmers and for coupling of the oscillator coil to the air tuning condenser. This minimized the effect of temperature changes on the frequency of oscillation. Changes in capacity of the large air condenser in series with the small ceramic coupling condenser were reduced in the ratio of their capacities, ie. about 10 to 1. All components in the oscillator circuit were rigidly mounted in a heavy brass case to reduce vibration changes of capacity. The warming up time of this oscillator as well as that of a BC221 heterodyne frequency meter was about ½ hour.

The BC221 is a calibrated, crystal-referenced, low-power oscillator fitted with an accurate vernier dial. It was made for the U.S. Signal Corps and bought as war

surplus. The fundamental tuning range, around 1 megacycle has strong harmonics up to about 40 megacycles. A chart, calibrated with the instrument allows conversion of the dial reading into frequency. An internal 1 Mc/s crystal is provided for periodic checking. After warm-up, when battery operated, the oscillator drift was found to be less than 1 part in 10,000 in several hours. Since the audio amplifier aupplied with the instrument for "zero-beat" identification was too insensitive, the outputs of this oscillator and the r-f head were coupled by means of co-axial cable to the input of a Hallicrafters SX-62 communi-cations receiver. The zero beat was detected by first tuning the receiver to one of the signals. Then by varying the other, the two signals were brought to the same fre-quency ("zero-beat") which was measured by the B.C.221. Ear-phones were usually used with the receiver as the noise level in the accelerator room was rather high.

(j) Accuracy and Stability.

The magnetic field setting was held to within a value set by the homogeneity of the field over the search coil which determined the half width of the proton resonance signal[8]. The inhomogeneity of the field over the search coil was about 1 part in 10,00 which gave rise to a proton magnetic resonance signal width of about 0.3 gauss. The relative accuracy for a field of 10,000

gauss was ± 1.5 parts in 100,000. The U.S. Signal Corps B.C.221 heterodyne frequency meter was used to measure the r-f frequency continuously to about 1 part in 10,000 so that field settings could be repeated from day to day within this accuracy. The Hallicrafter SX-62 communication receiver allowed identification and zero-beating of the proton oscillator and frequency meter. Care had to be taken not to tune to the image of the signals at twice the receiver's i-f frequency, ie. 0.9 Mc/s above the desired signal. The magnetic field regulator was checked and was able to maintain its accuracy for line voltage changes of ± 10%. For sharp drops in line voltage such as switching on the two 15 h.p. motors of the electrostatic accelerator, there was a drop in field accuracy for about one second. A variac inserted in the a-c line to the regulator equipment was used for the check against fluctuating line voltage. The regulator still functioned at voltages down to about 90 volts. On the other hand, the effect of sharp drops in line voltage was to change the magnet current more rapidly than the regulator could follow. The regulator was able to recover field control usually within a few seconds, by itself, with no manual re-adjustment needed. The good feature was perhaps due to the long time constant (about 7 minues) in the compensating network, and the shorter but inductive one in the Sola constant voltage line regulator.

4. Vacuum Deflection Box.

A large copper vacuum box, which was fitted in the one inch gap between the magnet's pole faces, joined the

lower end of the accelerating tube to the target tube. Eight ports on this box provided for entrance of the ion beam at the centre or edge of the pole face, its exit straight down, simultaneous exit of resolved mass 1 and mass 2 beams on one side or the other, and for exit of a single mass component on one side only. A ninth port allowed auxilliary pumping by a small separate oil diffusion pump and rotary backing pump. The box was provided as well with shut off valves and a liquid air trap for condensing oil and water vapors. The whole target box, which could be isolated from the accelerating tube by a large vacuum valve for quick change of targets or target assemblies, was also provided with two vacuum gauges; a Pirani gauge registering from atmospheric pressure to 10^{-3}mm. of mercury and an ionization gauge which extended the range down to 10^{-6}mm.

Two hollow lengths of thick soft iron shielded the accelerated proton beam from the fringing magnetic field at the entrance and exit ports of the magnetic box so that consistent results were obtained when the beam entrance hole was suitably defined.

III. The Spray Current Stabilizer.

After the magnetic field had been stabilized to a high order it was required that variations in the energy, E, of the beam be reduced so that a reasonable analyzed beam intensity could be maintained on a target. As the next step in the precision energy control of the accelerator

Figure 14

CATHODE FOLLOWER AS CURRENT STABILIZER

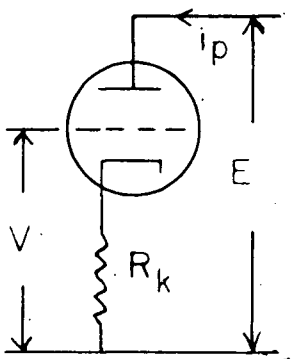

(a)

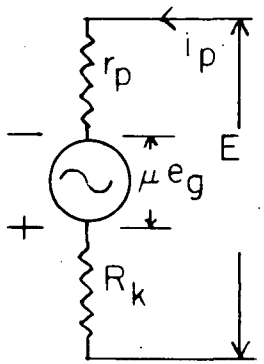

$e_g = V - i_p R_k$

(b) EQUIVALENT CIRCUIT

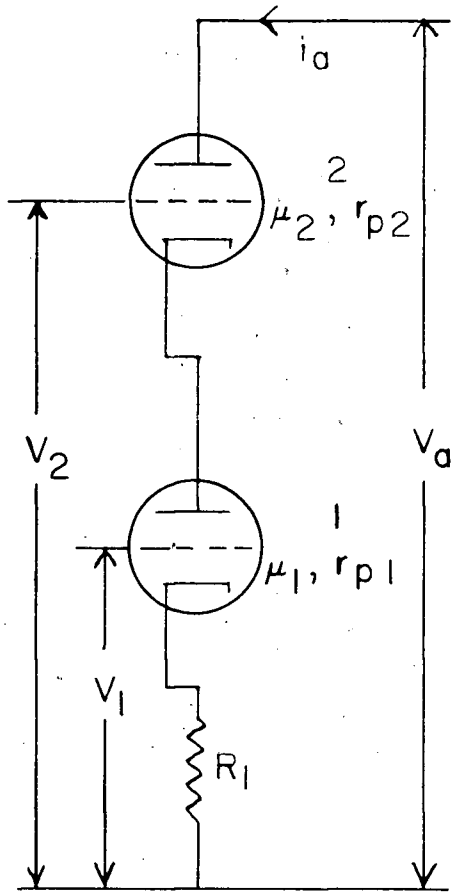

(c) WITH TRIODE, (1), AS CATHODE LOAD OF (2)

Figure 15

STABILIZING SYSTEM OF ACCELERATOR

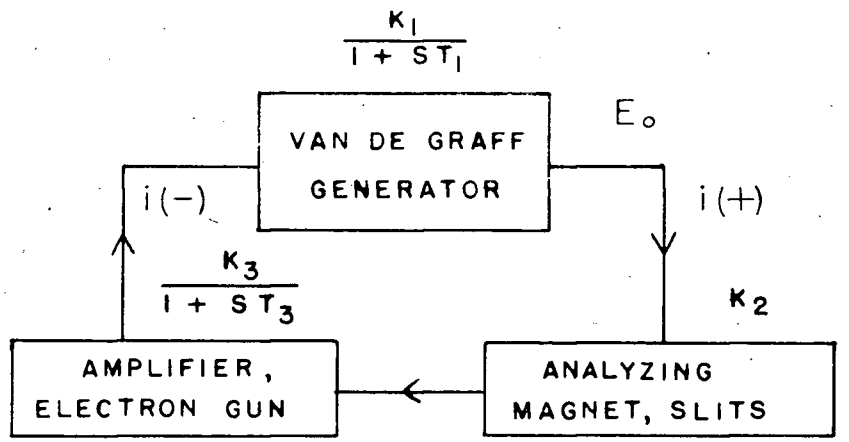

(a) BLOCK DIAGRAM

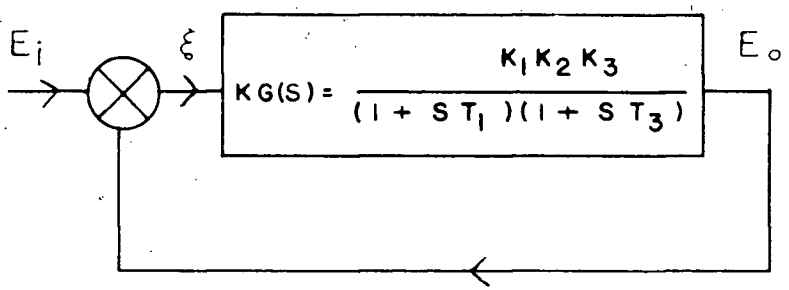

(b) EQUIVALENT BLOCK

the spray current was stabilized since the accelerating voltage, V, followed the spray current as can be seen in figure 18. For this purpose a simple adjustable current limiter was inserted in series with the high voltage spray supply. The two tube circuit, figure 13, was inserted in the high voltage lead. Large capacitive 60 cycle currents prevented it from functioning properly in the earthy lead of the spray supply. An isolation transformer insulated for 75,000 volts supplied the filaments of the two tubes while a selsyn coupled by means of a textolite rod allowed safe remote adjustment of the current setting control.

The current limiting action of the circuit is that of a cathode follower, an Eimac 15 E, having a large cathode resistance supplied by the pentode tube, the 6SJ7. With reference to figure 14 (a) and the equivalent circuit figure 14 (b), it can be seen that the total current, i_p, flowing into a cathode follower tube is given by:

$$i_p = \frac{E + \mu e_g}{R_k + r_p} = \frac{E + \mu (V - i_p R_k)}{R_k + r_p},$$

$$= \frac{E + \mu V}{R_k (1+\mu) + r_p}, \qquad \text{(III.1)}$$

where V is the grid voltage, fixed,

E is the plate voltage,

μ is amplification factor of the tube,

r_p is the internal resistance of the tube,

R_k is the cathode load resistance,

e_g is the total rise in voltage from cathode to grid.

Therefore, if $\mu \gg 1$, the cathode follower appears to

have a resistance to d-c current of the order of μR_k ohms. With reference to figure 14 (c) when R_k is replaced by an additional tube (here considered as a triode for simplicity) then the total resistance of the circuit to d-c becomes of the order of $\mu_1 \mu_2 R_1$ or exactly:

$$i_a = \frac{V_a + \mu_2 V_2}{r_{p_2} + (\mu_2 + 1)\left[r_{p_1} + (\mu_1 + 1) R_1\right]} \quad \text{(III.2)}$$

where the subscripts refer to the two tubes. When R_1 is made variable, the current i_a follows it directly.

In addition to being able to vary the equilibrium current, this circuit tends to prevent any dynamic changes of current from the set value because of the feedback from plate to grid of tube #2 (Miller effect). Consider the response of the current i_a to a sudden fluctuation ΔV_a, assuming μ_1, μ_2, r_{p_1} and r_{p_2} constant:-

$$\Delta i_a = \frac{\Delta V_a + \mu_2 \Delta V_2}{r_{p_2} + (\mu_2 + 1)\left[r_{p_1} + (\mu_1 + 1) R_1\right]} \quad \text{(III.3)}$$

But $$\Delta V_2 \approx - \frac{\Delta V_a}{2} \quad \text{(III.4)}$$

so that $\Delta i_a \approx 0$

In actual operation Δi_a is not zero but $\Delta i_a / \Delta V_a$, the dynamic impedance of the circuit, is very high, of the order of 10,000 megohms, which compared to the value of about 200 megohms for the rest of the spray circuit gives a stabilization factor of about 50 to 1. The curves, figure 18 (a) and (b), taken with a Brown chart recorder, show the spray current before and after the installation of

this stabilizer.

The spark gap in figure 13 was set at about 15,000 volts as a protection against over voltage on the 15 E tube. Thus the spray could be varied ± 7.5 kilovolts without altering the spray current appreciably, or with the spray voltage control fixed, the spray current could be adjusted remotely over a large range. This is shown by the curves in figure 13. The range of the current stabilizer was from about 100 μ amps to 300 μ amps which was sufficient to stabilize the accelerator's voltage (with a positive beam) from about 0.3 to 2.0 MeV.

IV. Stabilizer for 2 Million Volts.

1. Need for the Stabilizer.

With the installation of the spray current stabilizer, the voltage fluctuations of the accelerator with a positive beam were reduced from 4 to 6% to about 1 to 2% as shown by the curves in figure 18. These curves were taken with a Brown Electronik strip chart recorder whose input of 0 - 10 millivolt range was fed by a small resistor inserted in the generating voltmeter circuit. A vernier control consisting of a 10,000 ohm rheostat in series with the 500 kilohm cathode rheostat (figure 13) was operated by a reversing two-phase motor and remote switch at the control panel to increase the stability to about 1%. This arrangement required someone to operate the vernier control almost continuously to maintain an adequate beam current of resolved protons or deuterons on the target as the

Figure 16

STABILIZING SYSTEM OF ACCELERATOR

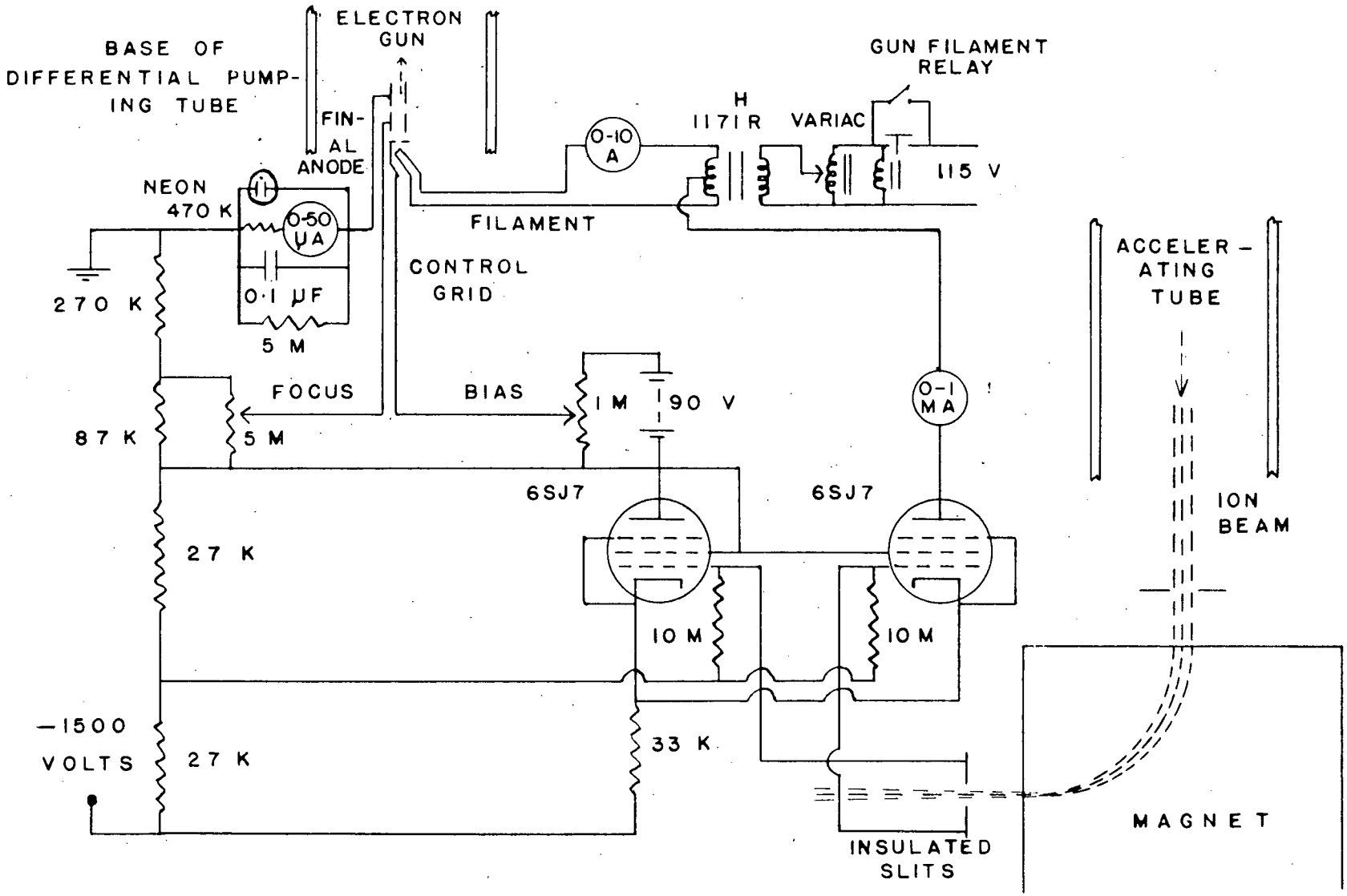

DIFFERENTIAL AMPLIFIER

accelerator's voltage varied. The variations in voltage were probably caused by the following:

(1) Non uniform charging of belt at bottom and consequent fluctuation in charge take-off at top.

(2) Changes in motor and belt speed due to line voltage fluctuation.

(3) Unequalized resistor stack current due to belt flap or beam striking the inside of the vacuum tube.

(4) Changes in ion source condition due to warm-up or voltage fluctuations.

(5) Change in lens voltages due to same causes as in (4)

(6) Ion beam defocussing by striking the first few accelerator tube sections and contributing to (3) above.

In the above (4) and (5) the voltage fluctuation in the carbon-pile regulated 400 cycle supply in the top terminal could be of the order of 2%. However rapid variations in (1) and (2) were smoothed by the top electrode which has a comparitively long time constant of about 3 seconds.

2. Modulated Reverse Electron Beam Voltage Stabilizer.[14]

The final precise voltage stabilizer used a modulated reverse electron beam controlled by an error signal obtained from the analyzed proton beam itself. A pair of insulated slit jaws ("sniffers") defining the analyzed proton beam was the source of the error signal which, after amplification, controlled the intensity of the beam emitted by the electron gun mounted at the base of the differential

Figure 17

REVERSE ELECTRON GUN

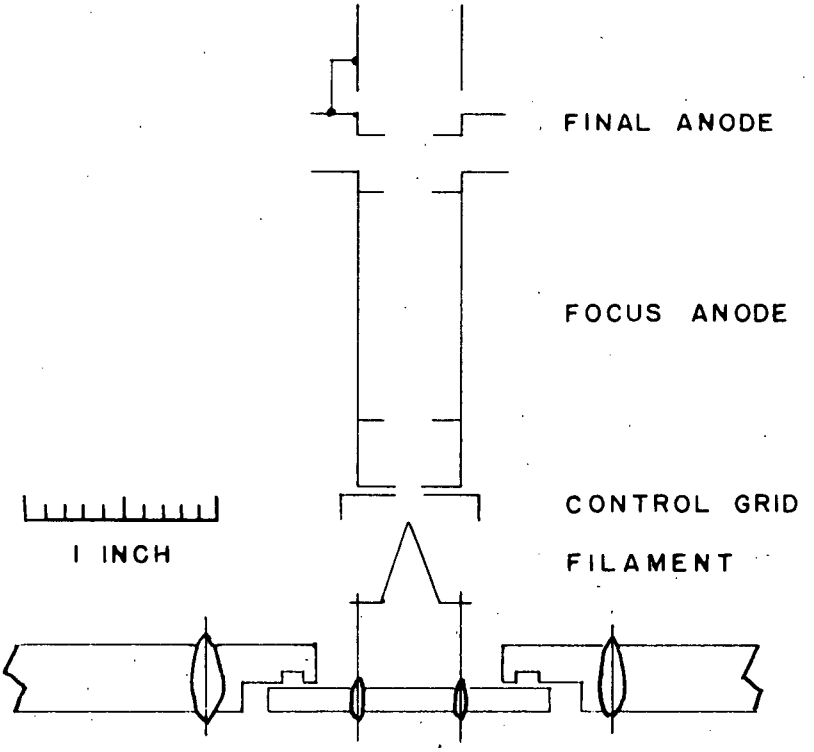

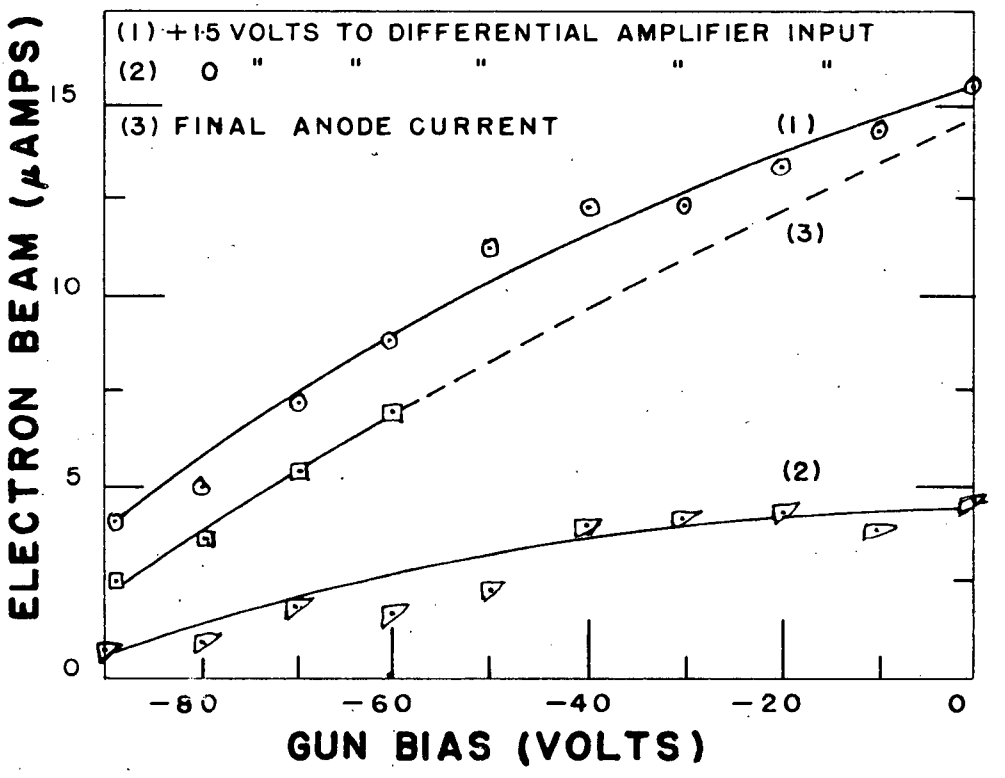

pumping tube. With reference to figure 16, if the voltage of the accelerator rises increasing the energy of the analyzed proton beam, then the bottom "sniffer" jaw receives more current since the proton beam appears to be "stiffer". (It is bent through a larger radius ρ , equation (II.3)). The amplifier converts this current difference into a voltage which reduces the bias on the electron gun's control grid so as to increase the electron emission. This increased electron emission continuing up the differential pumping tube acts as an increased load to reduce the voltage of the accelerator until the proton beam is centred between the sniffer jaws. Conversely, if the accelerator's voltage decreases, the upper sniffer jaw receives more current, the amplifier passes an error signal of opposite polarity to the electron gun to decrease its emission, decreasing the load and increasing the voltage of the accelerator until the beam is again centred between the sniffers.

(3) Theory of Operation.

The accuracy and stability of the above closed loop degenerative stabilizer depends on the gain of the system (amplification of error signal etc.) and the number and size of the time constants involved in the system[15]. Since the field of the analyzing magnet is highly stabilized, its effect on the system time constants may be neglected to a first order. A block diagram of the system, figure 15 (a), shows it to contain only two main time constants, one in the accelerator's terminal, T_1, and the other in the amplifier, T_3. T_1 is about 1.5 seconds when the accel-

erator is loaded with an ion beam, and T_3 is about 0.001 sec. (10 meg. X 100 $\mu\mu$f). T_1 was obtained by noting the time for the top terminal voltage to fall to 37% of its value when the spray was cut-off when there was no beam, and assuming that the loading was doubled when there was a beam. The "gain" K_1 of the top terminal was estimated from a plot of the top terminal voltage versus the effective spray current with a positive beam. $K_2 = \Delta i$ (sniffer beam current) μ amp/Δ V(accelerator volts), depended on the radius of the beam trajectory, the equilibrium value of the beam current intercepted by the sniffer jaws, and the separation between them. $K_3 = i(-)/i(+)$ was obtained from the performance data of the amplifier and electron gun in operation. Representative values for these are: $K_1 \approx$ 8,000 volts/μamps, $K_2 =$ 1 μ amps/1,000 volts and $K_3 \approx$ 20 μ amps/μ amps.

The block diagram may be condensed into figure 15 (b) and analyzed (see appendix 1). It can be seen that since there are only two main time constants, having a ratio of about 1,000 to 1, that the system should not oscillate or hunt[15]. Then to evaluate the steady-state error, the equations of the servo loop are written out as follows:

$$\mathcal{E} = E_i - E_o, \qquad \text{(IV.1)}$$

$$E_o = KG(S)\mathcal{E} \qquad \text{(IV.2)}$$

$$= KG(S)(E_i - E_o).$$

Thus

$$\frac{E_o}{E_i} = \frac{KG(S)}{1 \quad KG(S)} \qquad \text{(IV.3)}$$

But

$$\frac{E_o}{\mathcal{E}} = KG(S) \qquad \text{(IV.4)}$$

Dividing (IV.3) by (IV.4) gives: $\frac{\mathcal{E}}{E_i} = \frac{1}{1+K\,G(S)}$, (IV.5)

where the above symbols represent the Laplace Transforms of the quantities and $S = \sigma + j\omega$, a complex number:

$\mathcal{E}$ represents the error signal in the system,

E_i represents the constant input quantity (the energy of the analyzed positive ion beam determined primarily by the magnetic field setting),

E_o represents the regulated output quantity (the Van de Graaff accelerating voltage),

K G(S) represents the open-loop transfer function.

Now if a step function input $E_i(S) = e_i(t)/S$ is applied, the steady state error will be given by applying the "final-value theorem":[16]

$$\text{steady state error } (t \to \infty) = \lim_{S \to 0} S \left[\frac{e_i\,(t)}{S\,(1+K\,G(S))} \right]$$

$$= \frac{e_i\,(t)}{K} \,. \qquad \text{(IV.6)}$$

Since the value of $K \approx 160$, this steady state error could prove troublesome. However, because of the large time constant of T_1, $S\,T_1 \approx j\omega\,T_1$, is large compared to 1 for frequencies $f \gg \frac{1}{2\pi T_1}$, that is for $f \gg 1/10$ or $f > 1$ cycle/sec. In this case, $KG(S) \approx K/ST_1$ so that for any variations having a period less than about one second, the system behaves as if it has zero steady-state error due to this integration around the loop (appendix 1). The theoretical upper limit of accuracy of the system

(about 100eV) is less than the practical limit set by the conditions listed in chapterXVI. The above linear servo analysis holds (and is borne out by the performance of the system) so long as the total fluctuations in the accelerator's voltage are not too large. The spray current stabilizer serves to keep the fluctuations small and the range of the present reverse electron gun current is also adequate until the generator voltage approaches 2 MV, where the fluctuations at times are too large for the system to handle well.

(4) The Insulated Slits ("Sniffers").

The slit assembly, figure 19, consisted of a pair of semicircular 0.005 inch thick molybdenum plates spot welded to nickel leads. The leads were soldered to hollow kovar seals which were mounted in a vacuum tight flanged brass tube section. This was attached to the proton exit port of the magnet vacuum box. The slit width was usually set at about 1/16 inch but was used at $\frac{1}{4}$ inch spacing for some of the first resonances in N^{15}. (A more easily adjustable set of slits had been made up in a glass section but were not used in most of the experimental work because of a fracture in the glass).

A set of insulated slits mounted at the mass 2 exit port of the vacuum box was tried at first and did provide an error signal for stabilizing the proton beam when a reasonable focus of the mass 2 beam was obtained. However since it was difficult to maintain a good focus of the mass 1 and mass 2 beams together, and also because of the

small mass 2 current, this method was abandoned in favor of the proton sniffers.

(5) Differential Amplifier.

The differential amplifier consisted of two 6SJ7 pentode tubes operated with a common cathode resistor, figure 16. The input current fluctuations from the sniffer jaws were connected to two 10 megohm resistors in the control grids of the tube while the output of the amplifier was taken from the two plates and fed to the reverse electron gun control grid and cathode. A 0-1 milliampere meter in the plate circuit of the #1 tube showed the total emission current of the electron gun filament as well as indicating by its random movement that the amplifier was receiving an error signal. A conventional unregulated power supply supplied 1,500 volts to the voltage divider for the amplifier and electron gun operation.

The 6SJ7 tubes were selected for low residual grid current, and high mutual conductance and then matched in the circuit for equal plate currents. d-c coupling was needed throughout the circuit to handle slow drifts as well as rapid variations of accelerator voltage.

(6) Reverse Electron Gun.

A four-electrode electron gun was built to deliver up to 50 μ amps of electrons with about 1,500 volts for acceleration initially. The gun, taken from a 5AP1 cathode ray tube, was modified by enlarging the lens apertures and inserting a hairpin tungsten filament as cathode. When tested on a small vacuum system it produced an electron

beam of about 10 μ amps focussed to a $\frac{1}{2}$ inch spot at a distance of 37 inches. The final anode current was found to be proportional to the electon beam current so that a meter installed in the final anode lead (and therefore at earth potential) indicated the reverse electron beam current that was sent up the accelerator tube. This meter was the only part of this and the amplifier circuit that was mounted at the accelerator control panel.

The electron gun was spot welded to nickel leads which were soldered to kovar seals on a brass base plate. The filament of 0.010 inch diameter tungsten, spot-welded to nickel leads, was mounted with its two kovar seals on a separate small brass plate for ease in centering and replacement. This is shown in figure 17. The curves shown were taken on a test bench with the differential amplifier and the electron gun. The whole assembly was mounted at the base of the differential pumping tube of the accelerator. A variac in the primary of a 2,500 volt insulated filament transformer allowed adjustment of the filament current to about 7 or 8 amperes at about 2 volts. The total electron emission current amounted to about $\frac{3}{4}$ of a milliampere of which up to 50 μ amperes reached the top of the accelerator. This latter figure was calculated from the drop in accelerator voltage as a result of this emission loading the accelerator, and a curve of accelerator voltage versus spray current. When the gun was switched

on, the accelerator voltage dropped about 300 kilovolts in 1.5 MV. A one megohm potentiometer across a 90 volt battery provided a bias voltage for the electron gun grid for determining the equilibrium value of electron emission. The focus voltage was left constant at about 250 volts with respect to cathode for best operation. Representative values for the electron gun's operation on the accelerator are as follows:

Accelerator voltage	1.11×10^6 volts.
Spray current	150 μ amps.
Positive ion current	7 μ amps.
Resolved proton beam	4 μ amps.

Electron gun

Filament current	8.4 amps.
Bias setting	-50 volts.
Total emission	1,000 μ amps.
Final anode current	8 μ amps.
Electron beam current (approx.)	10 μ amps.

This reverse electron beam, accelerated by up to 2 million volts, could produce many high energy x-rays if the electrons were stopped at the top terminal by a material of high atomic number. Therefore a low atomic number metal, a plate of aluminum, was used as a stop for the electrons. In addition the top of the terminal above the aluminum plate was surrounded by about 6 inches of lead to absorb the x-rays that were gnerated there. As a result, the x-rays from the accelerator at 1.5 MV, as measured at the control panel, increased by only about 10% when the electron gun was in use.

Figure 18

SPRAY CURRENT AND ACCELERATOR VOLTAGE

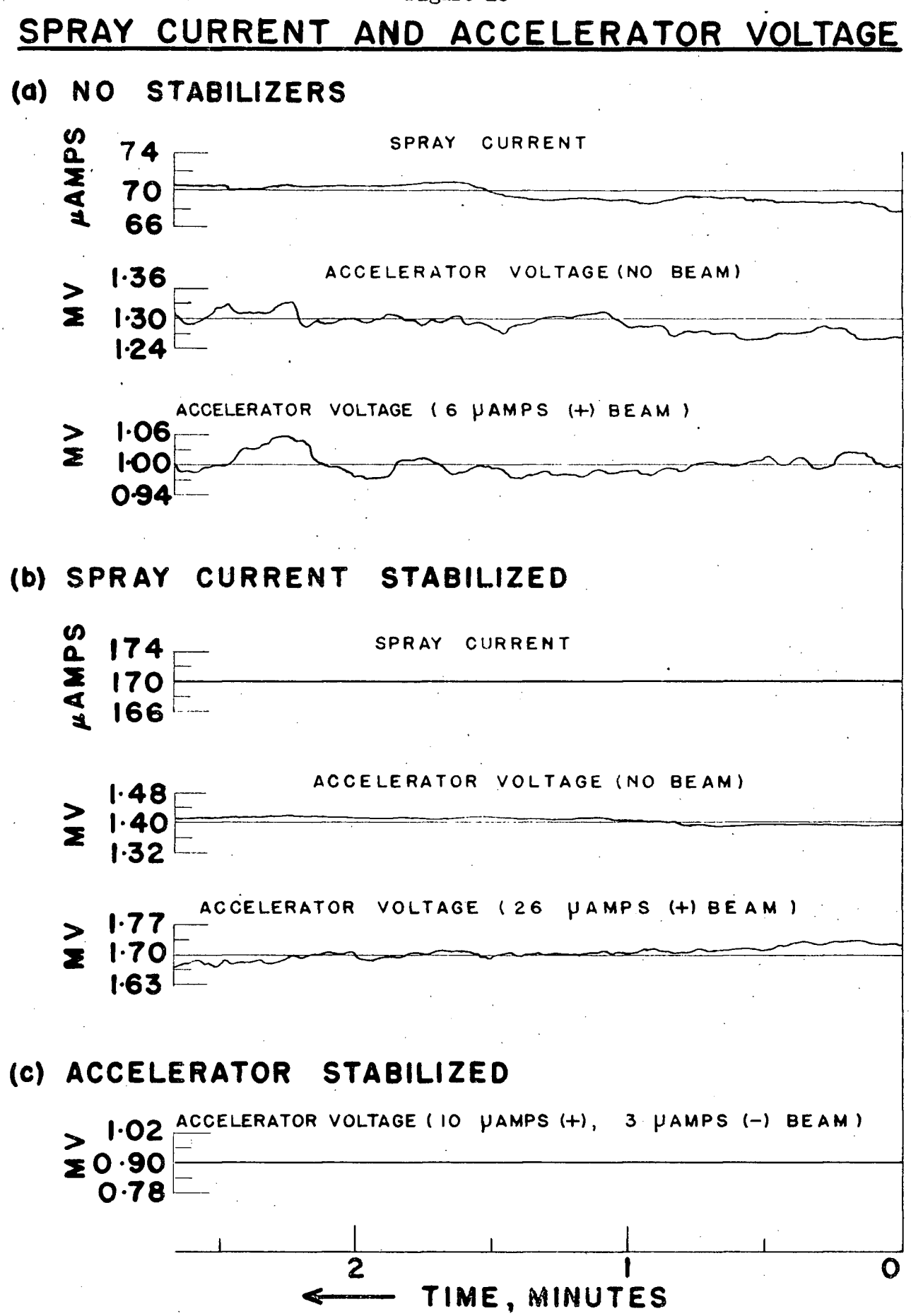

V. Voltage Stability and Control.

The University of British Columbia Van de Graaff accelerator has been in use in nuclear physics research since the summer of 1951, in various stages of stability. For example, for the production of high energy γ-rays only[2], from nuclear reactions, little voltage stability is needed provided the thickness or stopping power of the target (see part II) producing the γ rays is equal to or greater than the inhomogeneity in energy of the beam. For such experiments, the resolving magnet was not used so as to get the largest possible beam current. About one percent stability was obtained by using the resolving magnet with fairly wide slits and a manually operated vernier spray current control. There were periods, after the accelerator had been running continuously some hours, when the voltage remained within about 1 to 2% without manual readjustments. A long series of runs[17] were made with the accelerator being used as a continuously variable monoenergetic source of neutrons from the reaction $D^2(d,n)H^1$. For a part of these runs an electronic "cutter" device was used to stop the counting circuits when ever the voltage fluctuated enough to decrease the ion current to the target below a certain value. This prevented neutrons produced where the main beam hit the target box from interfering with the reaction under investigation.

The above experimental work provided a long term test also of the stability of the field of the 90^o analyzing magnet, which was to form an integral part of the precise

ion energy control system. The magnetic field stability was even sufficient when controlled by its current regulator only, with the proton magnetic resonance equipment being used for spot measurements of the field.

On addition of the precise ion energy control system using the modulated reverse electron beam the stability was brought to within about 0.1% so that more precise experimental nuclear physics research could be done. Almost no adjustments were necessary once the beam had been set and focussed. Even the initial adjustments necessary for good focussing of the beam were made very much easier since the automatic feature of the beam centering not only kept the voltage of the accelerator constant but also held the beam on the target (or quartz or molybdenum disk) during focussing. Before this time, focussing was made difficult by the interaction of the lens, probe, hydrogen gas leak and oscillator controls with the accelerator's voltage. The modulated reverse electron beam for stabilizing the accelerator's voltage was able to compensate for all the variations that were mentioned previously.

1. Placing the Stabilized Beam on the Target.

The initial adjustments of the accelerator for obtaining a stable analyzed beam were as follows:- First a vertical beam of about the desired energy was obtained and focussed approximately by letting it travel straight down through the vacuum box into a small Faraday cup. Then the magnetic field was set to the precise value for bending the protons of the desired energy, the reverse electron gun was turned on and the accelerator's voltage

adjusted until the beam "locked-on" in the horizontal direction to the target. When taking the error signal from insulated slits defining the atomic beam, care had to be taken in order that the stabilizer did not "lock" on to the mass 2 or mass 3 beams. The modulated reverse electron gun was able in most cases to maintain the beam stable for fluctuations in accelerating voltage as great as 300 KV in 1.2 MV. Small fluctuations in accelerating voltage were held automatically to within about 0.1% depending on the focussing condition and arrangment of the slits and apertures defining the beam. A spot about $\frac{1}{4}$ inch in diameter was obtained at the target, about 27 inches from the magnet, when the sniffers were about 1/16 of an inch apart.

2. <u>One-dial Adjustment</u>.

The oscillator tuning control, alone, now provided the fine accurate adjustment of the accelerator's voltage in steps as small as 250 electron volts, and as large as about 100 KeV. That is at any voltage setting from 0.34 to about 2 MV the accelerating voltage was not only homogeneous to about 1 kilovolt, but was also changed repeatedly at will in steps of about 1 kilovolt above or below any desired value. The lower limit was set by the mechanical arrangement of tuning the oscillator; the upper limit by the maximum electron gun emission. In addition, the accelerating voltage and thus the energy of the bombarding particles was obtained precisely at each step by measuring the proton magnetic resonance oscillator's frequency to-

gether with the relation obtained by combining equations (II.3) and (II.8)

$$V = \frac{e}{2mc^2}\left[\frac{\rho\omega}{\gamma_p}\right]^2 , \qquad (V.1)$$

$$V_{(MV)} = k \; f_p^{\,2}(Mc/s) , \qquad (V.2)$$

where $$k = \frac{e}{2m}\left[\frac{\rho 2\pi}{\gamma_p c}\right]^2 \frac{MV}{Mc/s^2} . \qquad (V.3)$$

k was determined experimentally as discussed in part II. The magnetic field regulator and the over all accelerator's stabilizer operated together as follow-up servo systems in response to changes in the frequency settings.

The following procedure was used to change the voltage accurately in kilovolt steps:

(1) The oscillator frequency was measured by zero-beating with the B.C.221 heterodyne frequency meter (using the Hallicrafter's communication receiver to pick up and identify both signals).

(2) The B.C.221 was increased in frequency by an amount Δf_p equivalent to the voltage step desired, from equation (V.2)

$$\Delta f_p(Mc/s) = \frac{\Delta V}{2 k f_p} \qquad (V.4)$$

or $$\Delta f_p(Mc/s) = \frac{\Delta V \; (MV)}{2\sqrt{k \; V \; (MV)}} . \qquad (V.5)$$

(3) The Hallicrafter's receiver was tuned to this new frequency, (set at C.W.), then set to receive A.M.

(4) The selsyn's remote tuning dial of the proton

magnetic resonance oscillator was adjusted carefully until a zero-beat was heard.

(5) The oscillator frequency was re-checked by zero-beating with the B.C.221 and recorded.

(6) The accelerator's voltage was determined by equation (V.2) once k had been determined.

In going over γ-ray resonances for an excitation curve, a reading of counts at the point was started after (4) since the magnet and accelerator stabilizing systems respond almost immediately. The time required to carry out (1) to (4) was about 30 seconds, while (5) which required about the same time was carried out during the taking of γ-ray counts. It was possible for one man to operate the complete accelerator and take readings for an excitation function but help of an assistant made the task somewhat easier and allowed immediate plotting of the function. For excitation functions, having resonance half-widths of the order of 1 to 15 KeV, the oscillator control was quite sufficient to vary the accelerator's voltage over them. Then as the voltage was increased by more than this amount, the current setting dial (of the Rubicon Potentiometer) of the magnet was increased a small amount, and the above procedure repeated.

The stability of the voltage was demonstrated during each experiment by the ability to repeat points taken on a resonance curve (within the statistical error of the

measurement) and to take readings between two points taken previously. This can be seen for example on the 873.5 KeV F^{19} resonance curve, figure 21, and on most of the other experimental curves that were taken. In one particular case, the resonance peak of an excitation curve was repeated on different days within a few parts in 10,000 (of the frequency measurement). All curves could be repeated on different days within a few parts in a 1,000.

VI. Homogeneity of the Beam and Energy Resolution.

Homogeneity in beam energy of about 0.1% was obtained at voltages up to 2 M.V. The best homogeneity could be obtained however only with low beam currents and consequent long times being required for a given experiment. The factors which contributed to good homogeneity with fairly good beam currents were found to be the following:-

(a) A strong well defined parallel beam entered the magnet vacuum box.

(b) The beam was centred and defined by a small aperture at the magnet vacuum box entrance port.

(c) A pair of shims at the entrance port of the vacuum box was adjusted to obtain the best focus of the resolved beam at 90° in the horizontal and vertical direction.

(d) A second pair of defining slits were placed at the 90° focus. This pair had its jaws insulated and provided the error signal for the ion energy control system.

(e) The beam was shielded magnetically with hollow soft iron cylinders from the changes in fringing field as the magnetic field was varied.

Conditions (a) and (b) were obtained with care for the calibration and fluorine excitation function experiments. However since only one set of adjustable shims was available on the magnet pole pieces some compromise had to be made in the focussing condition (c). In addition, the cylinder of soft iron at the exit port made it difficult to place the insulated slits close to the magnet box. But by careful adjustment, a focus was obtained near the insulated slits and once obtained, was held by the control system for periods as long as 4 or 5 hours at a time.

1. Beam Homogeneity.

On the assumption that the spread in energy of the beam can be represented by a Gaussian curve[18], then the experimental "half-width" of a resonance curve for a thick or semi-thick target, where $\xi > \Gamma$, is made up of

$$\Gamma_{exp}^2 = \Gamma^2 + \Delta E^2 \quad \text{(VI.1)}$$

Or for a thin target, that is one where $\xi < \Gamma$,

$$\Gamma_{exp}^2 = \Gamma^2 + \Delta E^2 + \xi^2, \quad \text{(VI.2)}$$

where: Γ_{exp} is the experimental full width at half maximum observed on the resonance curve yield of γ-rays

plotted versus energy of bombarding particle,

ΔE is the energy inhomogeneity of the beam,

Γ is the width of the resonance due to the physical nature of the nuclear process (see part III),

ε is the loss of energy of the incident particle in traversing the target, ie. the "thickness" in energy units. This will be referred to as the "stopping power" of a target, although in normal usage this would be the dE/dx of the material. Since published values of Γ obtained experimentally[20] are available in the literature, ΔE may be inferred from equation (VI.1) or with less certainty from equation (VI.2). However it is never certain that the published value of Γ represents the "natural" width because of difficulties in the calculation of ΔE. For example, the value for Γ for the 873.5 KeV resonance in F^{19} had been given as 5.2 KeV but a recent paper by Bonner and Butler[19] claimed an experimental half width of 4.3 KeV. They used a very thin LiF target (100 eV) and stated their beam energy spread was 0.08%. Since the experimental values obtained on thick and semi-thick fluorine targets in this laboratory for Γ_{exp} were always less than 5.2 KeV it was assumed that the Γ was of the order of 4.3 KeV. Therefore assuming Bonner and Butler's value for target thickness and beam homogeneity would give a value of 4.24 KeV for Γ ; then substituting this in equation (VI.1) with the Γ_{exp} of 4.7 obtained from a thick CaF_2 target, gives for the beam inhomogeneity:

$$\Delta E = 4.7^2 - 4.24^2$$

$$= 2.0 \text{ KeV}.$$

This amounted to an inhomogeneity of about ± 1.0 KeV in 873.5 KeV or ± 0.12%. This also was checked at 340.4 KeV with thin targets and was further borne out by the energy resolution obtained on the 873.5 KeV satellites and the 1355 - 1381 KeV doublet resonances.

A further check of the homogeneity was obtained by a run over the 873.5 KeV fluorine resonance at 200 - 300 eV intervals on a thin target, figure 21 . The scatter of the points at these intervals, smaller than the homogeneity of the beam, was of the order of ± 1 KeV.

2. Energy Resolution.

All the published γ-ray resonances from 0.3404 to 2.0 MeV in the proton bombardment of fluorine were observed and compared well with the good curves of Bonner et al[21] at the Rice Institute, Texas, and of Bernet et al[21a] at the University of Wisconsin. The two weak satellites of the very strong 873.5 KeV resonance were resolved as well as the 1.355 and 1.381 MeV doublet. Table 3a lists published resonance energies, cross sections and half widths for the γ-ray resonances of fluorine together with the experimental half widths obtained with the University of British Columbia Van de Graaff accelerator for comparison. The two new resonances defined during the author's work are also listed there and discussed later.

Table 3a.

Fluorine (p, $\alpha\gamma$) Resonances.[20]

Resonance Energy, E_R(MeV)	Cross section, σ_R X 10^{24} cm^2	Half Width, Γ(KeV)	U.B.C., Sept.-Nov.,1952.	
			Γ_{exp}(KeV)	ξ(KeV)*
0.3404	0.16	1.7	3.3	2.1
.486	> 0.032	< 2.0	2.4	1.6
.598	0.0071	37.	35.	1.1
.669	0.057	7.5	7.	1.0
.831	0.019	8.3	8.2	0.8
.8735	0.54	5.2	4.3	0.4
.900	0.023	4.8	4.0	1.0
.9353	0.18	8.0	8.0	1.0
1.092	> 0.013	< 1.2	3.5	0.9
1.137	0.015	4.1	4.5	0.9
1.176	0.019	~130.	broad	
1.290	0.029	19.2	28.	0.8
1.355	0.089	8.6	5.6	0.3
1.381	0.30	15.	13.5	0.3
1.62†	—	30.	—	—
1.69	—		—	—
1.84†	—		—	—
1.94	—	15.	—	—

† New resonances.

* Approximate target thickness for protons of energy E_R.

VII. Future Operation of the Accelerator.

The present arrangement of the accelerator with the above ion energy control and stabilizing system operates well in the low voltage region around 300 KV as well as up to 2 MV. However careful initial adjustment was required for good operation at 2 MV since the x-rays produced by the reverse electron gun and secondary emission in the vacuum tubes had a tendency to cause voltage breakdown and instability of a much larger order than could be handled by the automatic stabilizer. Because of the increased production of x-rays above 1.5 MV, the intensity of the reverse electron beam had been reduced, which reduced the range of voltage fluctuations over which the stabilizer could control. As a result, around 1.9 MV, occasional manual adjustment of the spray current was necessary.

By reducing the electron loading in the vacuum tubes and by installing the intermediate shield electrode, the accelerator should be capable of operation up to 3 or 4 MV. Two or three aluminum baffles with about 2 inch diameter apertures inserted in the vacuum tubes could reduce the electron loading without seriously affecting the pumping speed of the columns. If, at the same time, an overhaul of the columns allowed a better vacuum by sealing off any minute leaks it would reduce the tendency to spark from ionization of residual gas and would allow higher voltages to be maintained. The intermediate shield electrode (shown

in figure 1), has not been installed to date because of the inconvenience in lifting it each time during the initial periods of adjustment to the units in the top terminal.

If the loading from the reverse electron beam proves to be excessive above 2 MV, there are alternative devices which could be substituted as the control element in the stabilizing system. The simplest would be to use corona control[22] by means of a high voltage triode (25-50 KV). The triode's plate would be connected to a corona point facing the high voltage electrode of the accelerator while its grid would be controlled by the sniffer jaws plus amplifier. The great disadvantages of this system are the increase in corona and ionization in the insulating gas surrounding the machine and the slower response due to the lower mobility of the ions compared to that of an electron beam.

A more elegant device[23] uses an insulated "tank-liner" surrounding the machine but inside the pressure tank. A high voltage supply connected to the liner would be controlled by the error signal from the sniffers so as to vary the liner to ground potential to correct for accelerator voltage variations. This device would operate as fast as the reverse electron gun.

Since a large body of nuclear physics research was made possible by the homogeneity of the beam and energy resolution achieved with this accelerator in the energy range up to 2 MV, it was not felt that further development

should be pursued for the time being to extend the voltage limit by reducing the electron loading of the accelerator tubes.

Part II.

Voltage and Energy Calibration.

VIII. Measurement of High d-c Voltage.

1. Measuring One Million Volts.

Greatest precision is obtained by measuring the electrostatic field produced by the high voltage. For example, in a method due to Lord Kelvin, the force on an electrode in the field is balanced by a measured weight. However, the force is proportional to the square of the field strength, $\mathcal{E}$, since from Coulomb's law, F = constant X $q_1 q_2$ where q_1 and q_2, both proportional to $\mathcal{E}$, are the charge on the high potential and measuring electrodes. A linear electrostatic voltmeter, the generating voltmeter[28], described on page 46, produces a small pulsating current proportional to the field. The range of this instrument can be extrapolated within 1% from a calibration at low field strengths.

A calibrated resistor stack in oil, to reduce corona, is used on most rectifier sets. However, the voltage and temperature coefficients of the metallized or carbon resistors usually used, precludes accuracies of better than a few per cent[25a]. More costly and larger wire-wound resistors can improve this.

A less accurate but still useful method makes use of

polished spheres which are attached to the potential terminals. This sphere-gap method, relies upon measuring the distance between the spheres of known size (and at best under known conditions of humidity and temperature of the surrounding air) when spark breakdown first occurs[27]. Measurements to about 5% are possible by referring to published calibration curves although the official curves changed by 10% from 1934 to 1936.

2. The Generating Voltmeter.

A more accurate and reliable method makes use of a "generating voltmeter"[28]. This may consist of two segmented disks, one fixed and insulated, the other attached to the rotor of an electric motor. When this arrangement faces a high potential electrode so that the insulated segments are alternately exposed and shielded from the high potential, the current which flows through an external circuit connected to the insulated segments is directly proportional to the voltage of the high potential electrode. More specifically, if C is the capacity between the insulated segment and the high potential electrode and V the potential (to be measured), then if the motor rotates n times per second, the current I induced in an external circuit will be proportional to 2CVn or:

$$V = KI . \qquad \text{(VIII.1)}$$

Therefore if n is kept constant, the voltmeter may be calibrated at a low voltage and then used to measure much higher ones. The first calibration of the U.B.C. accelerator

was done by applying 50 kilovolts to the terminal and reading the small current in the external circuit. It was found that although absolute accuracy of this arrangement was within a few per cent, the relative accuracy over short and long periods was good to about 1%. A generating voltmeter as above with a pair of 6H6 diodes and d-c galvanometer provides a continuous measurement (within the above limitations) of the voltage of the U.B.C. accelerator. However for more precise measurements, it is more convenient to measure the energies of charged heavy particles that have been accelerated by the high voltage.

IX. Absolute Measurement of Energy of Heavy Charged Particles.

1. Magnetic Deflection.

This method of bending charged particles in a magnetic field in vacuum involves the accurate measurement of $H\rho$ (equation II.3). This measurement is subject to errors because of fringing field effects for which accurate corrections are difficult to obtain. The equations of motion of charged particles in a magnetic field are relativistically correct. That is, equation II.2 may be written as:

$$H\rho = \frac{mvc}{e} = \frac{(E^2 + 2m_0c^2E)^{\frac{1}{2}}}{e}, \qquad (IX.1)$$

where E, m are the relativistic kinetic energy and mass respectively of the particle and m_0 is the rest mass. For protons of energy up to 2 MV, the relativistic correction

to the momentum is less than 1 part in 1,000.

2. Electrostatic Deflection (Method of Herb, Snowdon and Sala).

This method of using an electrostatic field for bending charged particles allows for accurate corrections to be applied for the effects of fringing fields on the particles entering and leaving the deflector. The new scale for proton γ-ray resonances and proton-neutron thresholds was established with the aid of accurately made electrostatic deflectors, first by A.O. Hanson and D.L. Benedict[25] to 0.3% and more recently by R.G. Herb, S.C. Snowdon and O. Sala[26] to 0.1%.

An exact analysis of the operation of the 90° curved deflector by Warren et al[29] was applied by Herb to achieve this accuracy. The two plates were maintained at potentials up to 15,000 volts symmetrically above and below ground to minimize acceleration and deceleration effects. The potentials were obtained from stacks of 500 volt batteries, whose potentials were measured carefully and accurately with a standaed cell and potentiometer. Corrections were applied for battery drift, and leakage as well as for geometrical, electrostatic and magnetic effects in the arrangement. Then, for an ideal analyzer, considered to have an electric field determined inside by the simple equations for concentric cylinders and to have zero field outside, the relation that holds for the ideal path (where

the radius equals the geometric mean of inner and outer radius of the analyzer plates) is:

$$\tfrac{1}{2}V' = V_o \quad (1 - \chi) \frac{d}{b} , \qquad \text{(IX.2)}$$

where;

$\tfrac{1}{2}V'$ is the positive battery stack voltage (negative stack is of the same magnitude).

V_o is the voltage through which the protons have been accelerated.

d is the plate separation.

b is the arithmetic mean of inner and outer radii.

$\chi = e\ V_o / (2m_oc^2) = V_o\ (MV) / 1880.$

The entrance and exit planes of the deflector were defined by slits which also limited the extent of the electrostatic field. Corrections were also made for the effects of the finite slit widths. In the hands of R.J. Herb, this method of measuring high voltages from particle energies has proven to be one of the most accurate and reliable to date.

3. Other Methods.

Several other methods for measuring the energy of charged particles have been used, but none have exceeded the accuracy of that of Herb et al. One method however, involving the measurement of the velocity of the particles by timing[30] (where actually a frequency is measured) has given an independent confirmation of one of Herb's determinations, the $Li^7(p,n)\ Be^7$ threshold at 1.882 MeV. A secondary and less accurate method used in the early days

of particle accelerators involved the measurement of the visible range in air of the particles. Besides this, secondary determinations of energy may be made from ionization measurements in gases, heat and count of particles in a calorimeter, scintillations and even statistical scattering measurements.

X. The Importance of Accurate Energy Calibration for Nuclear Physics.

In the experimental investigation of a reaction of transmutation such as:

$$X + a \rightarrow Y + b + Q, \qquad (X.1)$$

this symbolizes a particle, a, bombarding a target nucleus, X, (assumed at rest) to produce a resultant nucleus, Y, with the emission of another particle, b. Q, "the reaction energy balance," represents the energy involved in the reaction. Two generalizations can be applied to this reaction:

(a) Conservation of momentum (linear and angular),

(b) Conservation of mass-energy.

If the reaction is endothermic (endoergic), then there exists a "threshold" value for the energy of the bombarding particle, a, such that the reaction just takes place. In this case Q is negative,

$$Q = \text{kinetic energies of } (Y + b) - \text{kinetic energy of a}, \qquad (X.2)$$

which from (a) and (b) represents the net increase in

kinetic energy in the centre of mass system of Y plus b or the net decrease of rest mass in the reaction, from Einstein's energy and mass equivalence relation:

$$\Delta E = \Delta mc^2 \qquad (X.3)$$

That is $$Q = (M_x + M_a - M_y - M_b)c^2, \qquad (X.4)$$

where the M's represent the rest masses of the respective reactants and c is the velocity of light in vacuum. Thus from an exact knowledge of the threshold of an endothermic reaction the precise Q value can be determined from only approximate mass values. Again if the kinetic energy of b is also determined, for emission in some particular direction, then both in exothermic(exoergic, positive Q values) and endothermic reactions the Q value may be fixed. In addition, from accurate Q values, accurate mass differences may be calculated from the mass-energy balance, and since one MeV corresponds to 1/931 mass unit a Q value accurate to one KeV corresponds to a mass difference accuracy of nearly one part in 10^6 which even to-day is at least as good if not better than the best precision achievable with mass spectrographs. By choosing a series of inter-related nuclear reactions it has been possible to build up an excellent set of mass values for the light elements based solely on nuclear reaction data[31].

As an example consider the following data of Taschek et al[32] for the reaction $T^3(p,n)He^3$, which is a shorthand

notation for the proton (p) bombardment of tritium (T^3) which results in the formation of helium-3 (He^3) plus a neutron (n). This may also be written as:

$$T^3 + H^1 \longrightarrow He^3 + n + Q. \qquad (X.5)$$

In addition, tritium is radioactive decaying to helium-3 plus an electron (β) plus a neutrino (μ);

$$T^3 \longrightarrow He^3 + \beta + \mu + E_\beta \ , \qquad (X.6)$$

where E_β is the maximum kinetic energy the electron ("beta-ray") carries away. If the rest mass of the neutrino is assumed to be zero[*], then by subtracting equation (X.6) from (X.5) where the symbols are taken to mean the atomic masses of the nuclei, the neutron - hydrogen mass difference may be obtained quite directly:

$$n - H^1 = (T^3 - He^3) - Q \qquad (X.6a)$$

$$= E_\beta - Q. \qquad (X.7)$$

E_β is known with an uncertainty of about one KeV. Taking Herb's value of 0.9933 KeV as the energy of the strong $Al^{27}(p, \gamma)\ Si^{28}$ resonance, Taschek determined the threshold for reaction (X.5) as 1019 ± 1 KeV. When corrected for the centre of mass motion this threshold yielded a Q value of - 763.7 ± 1 KeV for the reaction. Taking the value of E_β = 18.5 KeV for the end point of the β-ray

---

[*] S.C. Curran, J. Angus and A.L. Cockcroft, Nature, 162, p. 302 (1948) conclude from a study of the tritium β-ray spectrum that the neutrino rest mass must be less than 0.002 times the rest mass of an electron.

spectrum from the decay of tritium, then from equation (X.7)

$$n - H^1 = 782 \pm 2 \text{ KeV.} \qquad \text{(X.8)}$$

This value was 28 KeV higher than the previously accepted[33] value and approximately 20 KeV lower than the then recently determined value of Bell and Elliot[34], but was in agreement with the revised figures of Tollestrup et al[35].

From this it is clear that the fundamental mass difference between neutron and proton can be accurately deduced so long as a reliable absolute energy scale can be provided from which accurate threshold measurements may be made. In this connection it may be noted that up till 1949 an erroneous energy scale, based upon the $Li^7(p, \gamma)Be^8$ resonance at 440 KeV, had been accepted.

Historically, the above $Li^7(p, \gamma)Be^8$ resonance energy was determined by Hafstad et al[24] in 1936 with reference to the voltage of their Van de Graaff accelerator. Their accelerator had been calibrated up to 500 KeV with a potentiometer and high voltage stack of resistors. This fixed voltage point, 440 KV $\pm$ 2%, after confirmation by several other experimenters;[36] led to the adoption of a standard voltage-energy scale in nuclear physics. However as the experimental data and theoretical knowledge of nuclear physics increased, it was realized that the choice of the lithium resonance energy value as a calibration point was an unfortunate one for two reasons. The first was that the voltage scale was too low by about 1.5% due

to errors in calibration. The second was that the resonance energy value had to be corrected for the continuous yield above resonance, a factor of about 1 KeV. These errors were pointed out as a result of the different investigations in nuclear physics concerned mainly with the neutron-hydrogen mass difference. This is the fundamental quantity involved in all mass-energy determinations. The erroneous low energy scale however persisted until January 1949 when the important results of R.E. Herb, S.C. Snowdon and O. Sala established the now accepted voltage and energy scale.

While at present no satisfactory nuclear theory exists which can predict the positions of nuclear energy levels, it is important to establish the existence and accurate position of such levels from measurements of resonance maxima even if only to seek regularities in the positions of such levels by inspection. Such a phenomenological approach was useful in atomic spectra and is beginning to be of use in nuclear physics, although at present it is the order of magnitude of level separation which has significance rather than the exact energy of the "excited" states.[37]

XI. Absolute Voltage and Energy Calibration.

Calibration of the voltage and energy scale of the U.B.C. accelerator was carried out with reference to the absolute voltage determinations of Herb et al. This, rather than an independent absolute determination, was used because of the reliability of Herb's values over the past

4 years. In addition, it was felt that this calibration would be more accurate than one based on the calculation of $H\rho$ in the analyzing magnet for α-particles of known energy for the reasons given in chapter IX.

Herb, Snowdon and Sala[26] made three absolute voltage determinations based on the constants of a large electrostatic analyzer. These determinations (in absolute volts rather than international volts) stated in terms of the resonance or threshold energy of three different nuclear reactions are:

the $Li^7(p,n)Be^7$ threshold	1.882 MeV (XI.1)
an $Al^{27}(p,\gamma)Si^{28}$ resonance	0.9933 MeV
a $F^{19}(p\alpha',\gamma)O^{16}$ resonance	0.8735 MeV

The uncertainties in the measurements are given to be about 0.1%. The determinations were carried out by bombarding in turn carefully prepared thick and thin targets of materials containing the above elements and noting the yield of neutrons or γ-rays as the energy of the incident protons was varied. The author of this thesis carried out a similar procedure in the calibration of the U.B.C. accelerator with the exception that the above fixed point of 0.8735MeV was used to calibrate the magnetic analyzer.

XII. Calibration of the University of British Columbia Van de Graaff Accelerator.

A number of determinations of the fluxmeter frequency

at which the peak of the reaction in fluorine at 0.8735 MeV occurred were carried out to find an experimental value for k from equation (V.2);

$$k = \frac{V \text{ million volts}}{f_p^2 \text{ (megacycles/sec.)}^2}. \qquad \text{(XII.1)}$$

1. Preparation of Targets.

Thin and semi-thick fluorine targets were prepared in vacuum by evaporating CaF_2 on to clean polished copper backings. They were always exposed to air before they were used. Very thin targets of a few hundred angstrom units thick, were desirable to keep the experimental width of the resonance curves as small as possible for several reasons.

(1) A sharply peaked, narrow resonance curve defines the energy of the bombarding particles more closely than a broad topped, wide curve.

(2) The inhomogeneity of the proton beam and the stopping power of the target can be estimated more closely when they are small compared to the widths of the resonance curves.

(3) The natural half-widths (width of the resonance curve of half maximum) of the resonance curves can be calculated with greater reliability.

(4) The fluorine reaction gives a large yield of γ-rays so that well defined curves may be obtained from very small amounts of fluorine.

It has been calculated that 3 to 9 micrograms per $cm.^2$

SLITS AND TARGET BOX ASSEMBLY

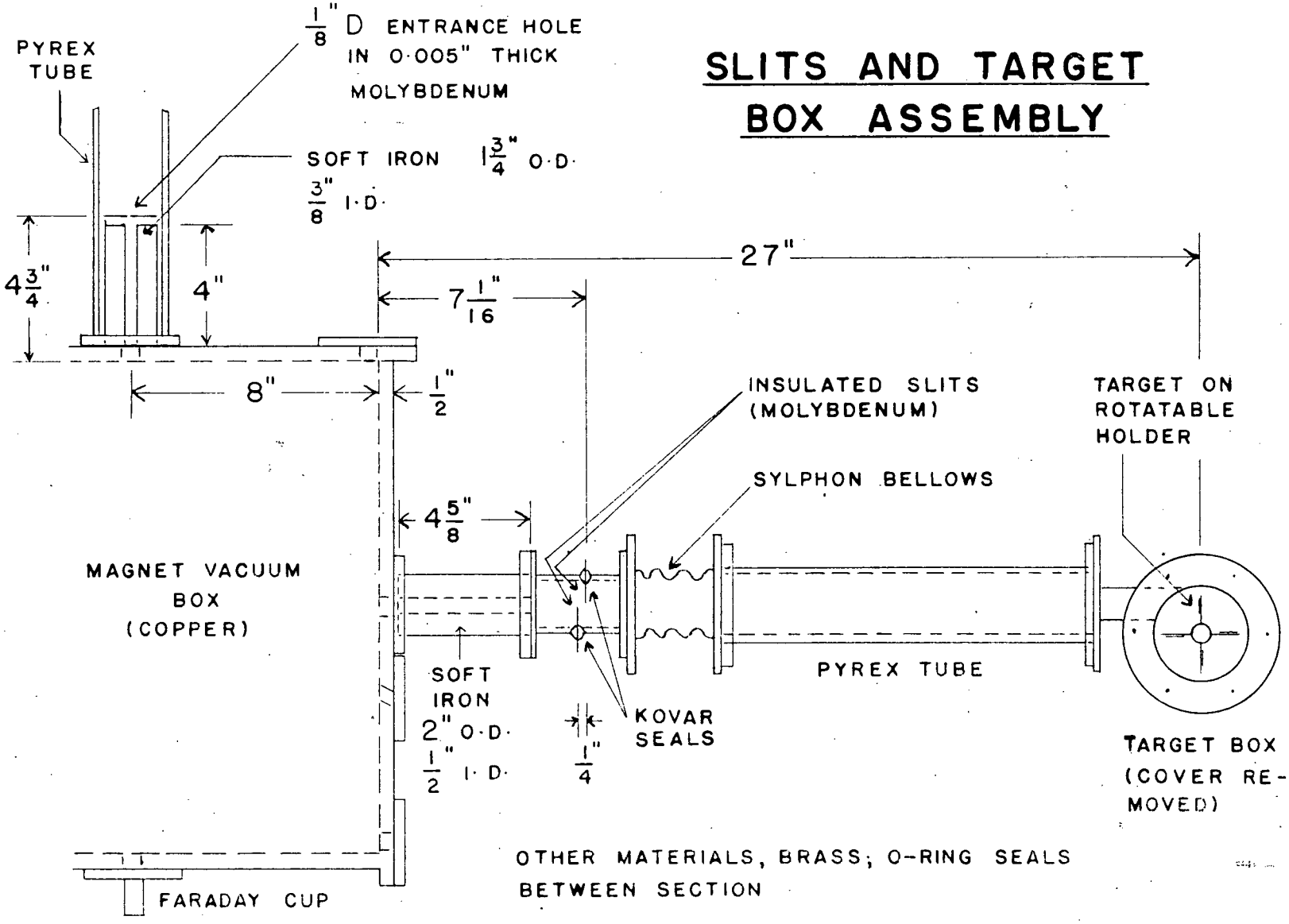

of CaF_2 have a stopping power of $\frac{1}{2}$ to 2 KeV for protons of about 1 MeV in energy. Taking the density of CaF_2, $d = 3.18$ gms./cm.^{3}, then the thickness of a layer of 10 μgms./cm.^{2} is given by: $t = 10^{-5}/3.18 = 300 \times 10^{-8}$ cm. A small amount of CaF_2 was weighed on an analytical balance and then evaporated from a hot spiral tungsten filament (in vacuum) on to a sheet of 0.005 inch copper. From the weight of the CaF_2 used, about 250 μgms., and the area of the copper, about 50 cm.^{2}, it was assumed that a film of about 1 to 2 KeV in stopping power would be formed. These calculations were found to be of the right order, when the yield of γ-rays from these targets was checked. The time taken to evaporate the thin layers was only a few minutes with a filament temperature of about 1300° C and at a pressure of 1.5×10^{-5} mm. of mercury.

Thicker targets were also prepared by using larger amounts of CaF_2 and longer times. In this case, the number of interference fringes formed on the target backing gave the order of the thickness of the layer formed. A thin polished crystal of natural fluorite was used for the thick target. A coarse mesh of nickel gauze spot welded to a nickel backing held the crystal in place and prevented the accumulation of charge on it.

2. Slits and Target Box Assembly.

The arrangement of slits and the target box used during the calibration experiments are shown in figure 19. The positive ion beam was defined by a 1/8 inch hole $4\frac{1}{4}$ inches

above the magnet box. It then passed through a 3/8 inch hole in a thick soft iron cylinder before entering the magnet box and being deflected through 90°. The resolved proton beam then emerged through a ½ inch hole in another soft iron cylinder, was defined again by a set of insulated molybdenum slits 0.085 inch apart and then proceeded to the target. In the target box were three targets plus a disk of quartz for focussing, all mounted on a paddle wheel that could be rotated through an O-ring vacuum seal. A thick glass window allowed observation of the targets during bombardment.

During the first calibration runs the target box contained the CaF_2 crystal (thick), one thin target, one semi-thick target and the quartz focussing disk. During subsequent runs, several thin targets were used so that a fresh one could be rotated into the path of the beam as soon as any oil or carbon film became visible. Runs were also made on the copper backing to evaluate the contribution of the background to the recorded counts. These runs on fluorine targets were made in September, 1952, with the targets at room temperature.

During the September runs, one spot on a fluorine target was bombarded for several hours before the build-up of an oil or carbon film on its surface amounted to about one KeV in stopping power for 873.5 KeV protons. This amount of surface contamination was easily seen although

about ¼ of this amount could be detected first by observing an upward shift in the fluxmeter frequency for the 873.5 or 340.4 KeV resonance curves. However on November 12, 1952, after a number of alterations had been made to the ion source and to the vacuum box's pumping system, it was found that a carbon film was building up very quickly (1 KeV in about 30 minutes), especially when larger proton currents (3 to 4 μ amps.) were being used. The target holder had been provided with a hollow core for water cooling or heating. Therefore steam at 100° C was passed through it to heat the targets before and during bombardment. The first result of this heating was to boil off grease and oil from the O-rings in the target box and condense it on the inside of the glass window and pyrex tube. The glass window and pyrex tube were washed and cleaned in dilute nitric acid while the disassembled target box and O-rings were baked under an infra-red lamp for several hours. It also appeared that the old targets had acquired transparent oil films of a few hundred eV in stopping power for 873.5 KeV protons, from being present in the vacuum system for over a month, with no liquid air in the trap. The O-rings although originally used dry, gave off considerable oil vapors under baking in the open air. They withstood the heating and sealed well again dry. The oil was also changed in the small diffusion and mechanical pumps attached to the vacuum box and some small leaks in the fore-vacuum connections

Figure 20

γ-RAY COUNTING EQUIPMENT BLOCK DIAGRAM

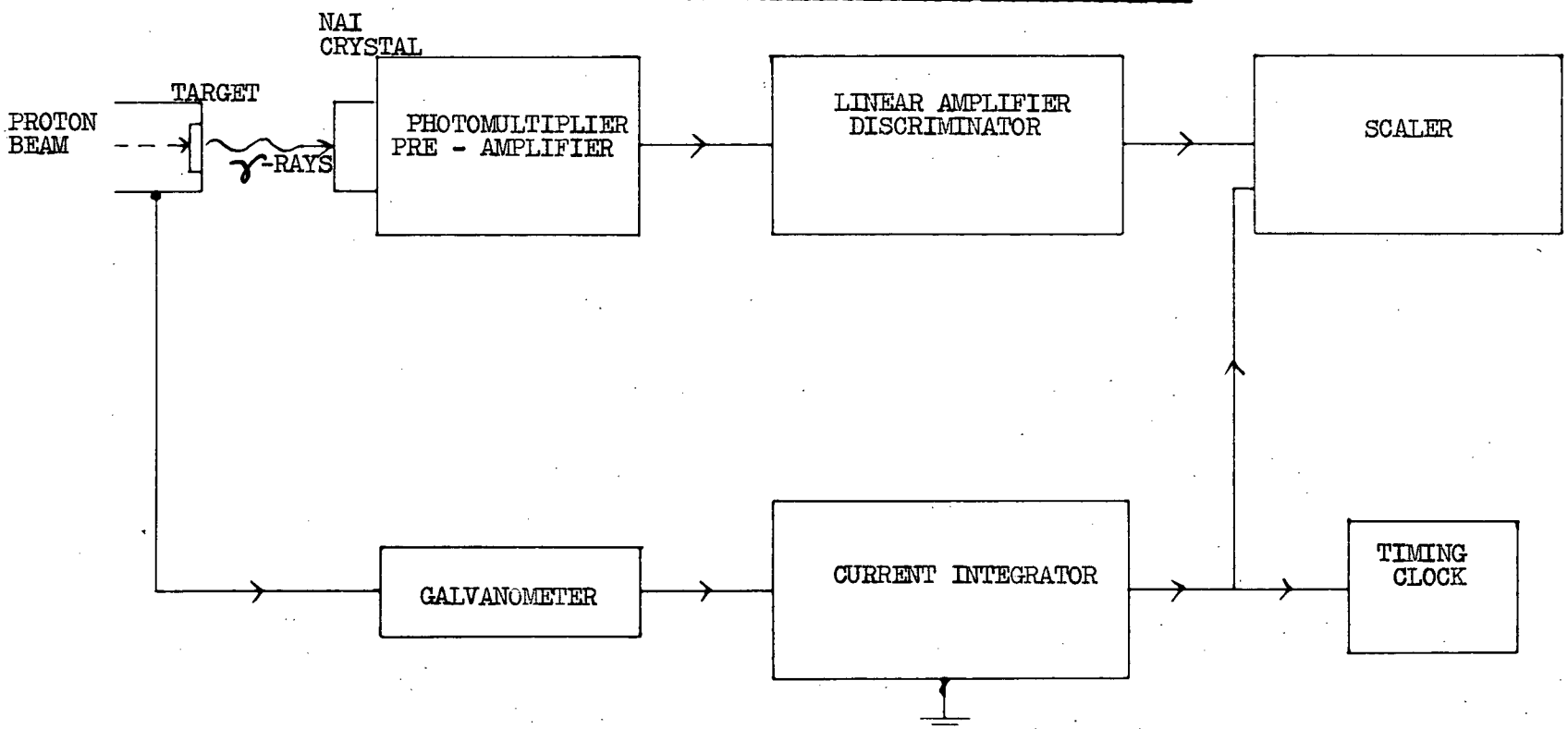

eliminated. This did not prevent the carbon or oil film from building up on the target when bombarded at room temperature, perhaps because the main vacuum column's pumping system was dirty. However, when the targets were heated to 100° C before and during bombardment, no carbon or oil film was found. For example, on Nov. 18 and 19, 1952 after 9 total hours of bombarding one spot during a 12½ hour continuous run, the spot, about 5/16 inch in diameter, appeared to be brighter after bombardment than the rest of the target.

3. Counting Equipment.

A block diagram of the γ-ray counting equipment is illustrated in figure 20. γ-rays which were intercepted at 0° with respect to the beam by a NaI crystal optically coupled to a photomultiplier tube, produced scintillations (in the crystal) which gave rise to electrical pulses in the tube. The pulses were amplified and passed on by the discriminator, if their height exceeded a certain value, to a scaler circuit where they were counted. A galvanometer and current integrator[38] connected to the target holder (which was insulated from ground) recorded the amount of charge and hence the number of protons incident on the target. An electrical timing clock, the scaler, and current integrator were controlled by one switch so that a simultaneous reading of the time, the number of counts, and the charge was taken at each bombarding energy point.

Figure 21.

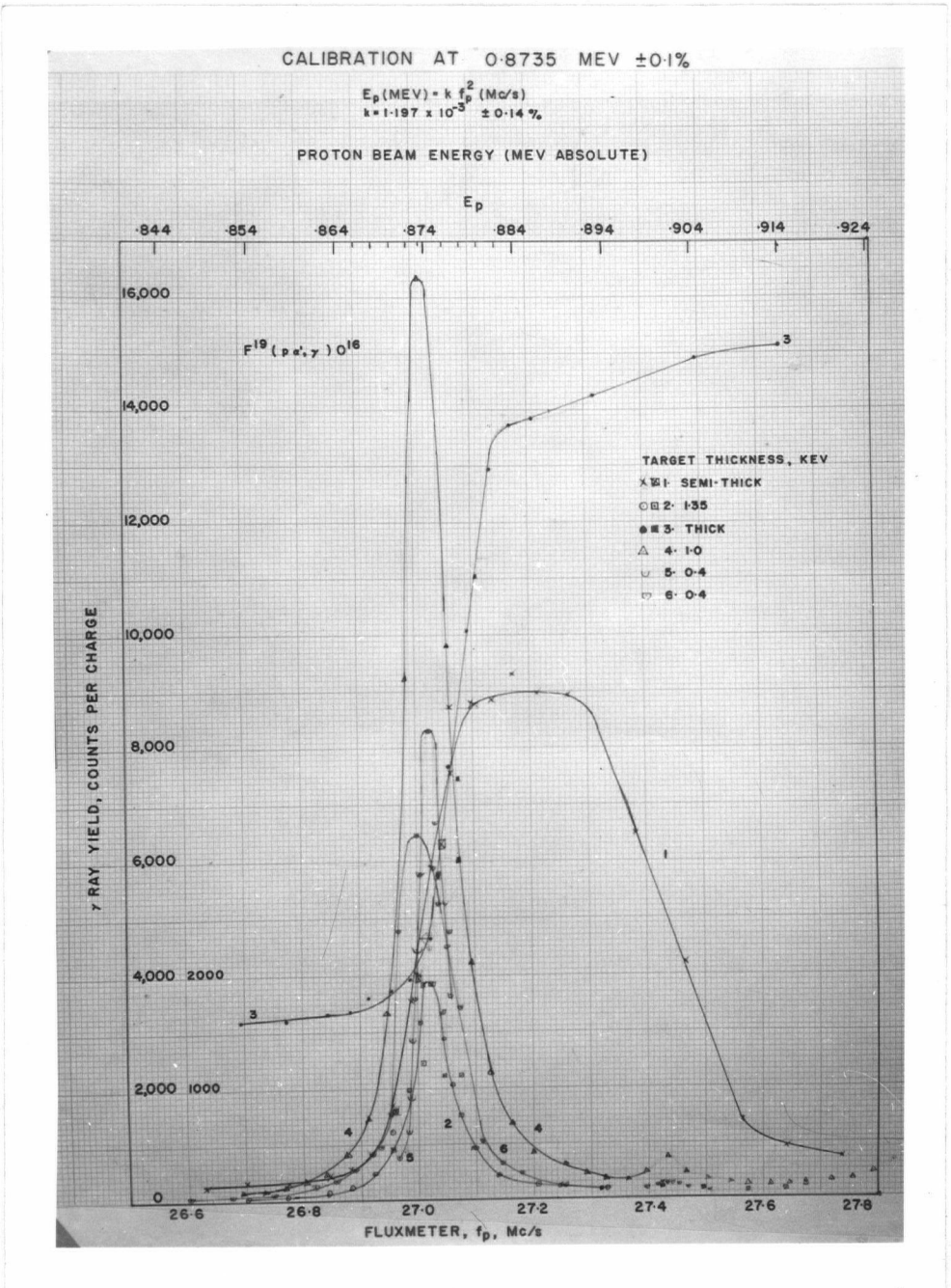
CALIBRATION AT 0·8735 MEV ±0·1%
E_p(MEV) = k f_p^2 (Mc/s)
k = 1·197 x 10^{-3} ±0·14 %
PROTON BEAM ENERGY (MEV ABSOLUTE)
E_p
·844
·854
·864
·874
·884
·894
·904
·914
·924
16,000
14,000
12,000
10,000
8,000
6,000
4,000
2000
2,000
1000
0
$F^{19}(p\alpha'\gamma)O^{16}$
TARGET THICKNESS, KEV
1· SEMI-THICK
2· 1·35
3· THICK
4· 1·0
5· 0·4
6· 0·4
γ RAY YIELD, COUNTS PER CHARGE
26·6
26·8
27·0
27·2
27·4
27·6
27·8
FLUXMETER, f_p, Mc/s

4. Checking the Counting Equipment.

A close check of the efficiency of the counting equipment was kept during all the experimental work. All the electronic equipment was operated from regulated power supplies supplied from a stabilized 115 volt a-c line source. The photomultiplier tube, an RCA 5819, was operated at a constant d-c voltage within about 0.1%. Differential and integral bias curves were taken to determine the optimum settings of the discriminator and photomultiplier. In addition, the overall counting efficiency of the equipment was checked at the beginning and at the end of each day's run. A radioactive source in a standard position was used for this test. The efficiency was found to vary by not more than a few per cent from one day to another, most of which could be attributed to voltage fluctuations in the photomultipier and discriminator circuits.

5. The Calibration Curves and Determination of k.

Seven separate runs were taken over the 873.5 KeV γ-ray resonance in fluorine during two weeks in September, 1952. Readings of the yield of γ-rays for a fixed charge of bombarding particles were recorded at intervals spaced from about 300 eV to 2 KeV. Six of the resonance curves are plotted in figure 21. The thin targets ranged from about $\frac{1}{2}$ to 1.5 KeV in stopping power while the semi-thick one was about 20 KeV. The details of the calculation of and corrections for target thickness are given below for this preliminary calibration. A discussion of the theory and reasons for these corrections is given later in part III.

Three further sets of runs were taken in November, the last using heated targets, and additional average determinations of k were made from them.

6. Calculations and Preliminary Results.

(1) The stopping power of thin target #1 was calculated first. The thin targets #1 to #4 were numbered according to the position from which they were taken in the evaporator, #1 being closest to the hot filament and #4 being furthest away. The peak of a thin target resonance curve occurs at an energy value, E, given by[18]:

$$E = E_R + \varepsilon/2 \qquad \text{(XII.1a)}$$

where E_R is resonance energy assuming an infinitely thin target, and ε is the stopping power of the target (or thickness) for protons of energy E_R. It may be shown that ε is given by dividing the area under the thin target resonance curve by the height of the step in the thick target resonance curve. The area under the thin #1 target resonance curve, from a large scale plot was 225.4 Mc/s counts. The height of the step of the thick target curve was 10,800 counts. Also from equation (V.5), 0.1545 Mc/s $\approx$ 10 KeV (assuming the correct value for k). Therefore the thickness of thin #1 target was:

$$\frac{225.4}{10{,}800} \times \frac{10}{0.1545} = 1.35 \text{ KeV} \qquad \text{(XII.2)}$$

(2) The stopping power of the other thin targets was calculated by comparing their peak yields to that of thin #1 target for the same resonance after correcting

for the amount of charge of protons and for the solid angle subtended by the counter. (Cosmic ray and copper background was negligible at the 873.5 KeV resonance, but was subtracted at the other resonances where it was appreciable). The peak yield for a target that is thin compared to the half-width of the resonance is proportional to the target thickness. For example, thin #1 target had a peak yield of 1918 counts in 165 seconds for a charge of protons of 30.8 μ c (microcoulombs) at a counter-target spacing of $8\frac{1}{2}$ inches. On the other hand, from the resonance curve of thin #2 target, the peak yield was 16,345 counts in 27 seconds for a charge of 26.6 μ c at a counter-target spacing of $2\frac{1}{4}$ inches. The solid angle for #2 was up by a factor of $(8.5/2.25)^2 = 14.27$ while the charge was down by a factor of $30.8/26.6 = 1.158$. Therefore if #2 were as thick as #1, the expected peak yield would be:

$$\frac{14.27}{1.158} \times 1918 = 23{,}635 \text{ counts}$$

or $\frac{\text{the thickness of \#2}}{\text{the thickness of \#1}} = \frac{16{,}345}{23{,}635} = \frac{0.692}{1}$.

The peak yields for the different targets were also compared at other resonances and an average was taken. The results in Table 2 give the order of the thicknesses of the targets for protons of 873.5 KeV energy. Exact values of thickness are not usually known because of non-uniformities in the layer of target material.

Table 2.

Thickness of Thin Targets.

Target #	Ratio	, thickness at 873.5 KeV
1	1.0	1.35
2	0.765	1.0
3	0.567	0.75
4	0.298	0.4

(3) Values for k in equation (XII.1) were obtained from the fluxmeter frequency readings corresponding to the peak number of counts recorded. For example, for target #1, the peak yield occurred at an energy of $873.5 + 1.35/2 = 874.18$ KeV corresponding to a frequency of 27.02 Mc/s. Therefore:

$$k = \frac{0.87418}{(27.015)^2} = 1.1974 \times 10^{-3} \text{ MeV/Mc/s}^2$$

This was repeated for the other thin targets. However, for the semi-thick and thick targets, whose resonance yield curve consists of the integral of the thin target curve, the yield corresponding to the resonance energy occurs half way up the step (see chapter XV). For example for the semi-thick target, the step height was 9,000- 300 = 8,700 counts so that half way up was $8,700/2 + 300 = 4,650$ which corresponded to a frequency of 27.003 Mc/s. Therefore:

$$k = \frac{.8735}{(27.003)^2} = 1.1979 \times 10^{-3} \text{ MeV/Mc/s}^2.$$

This was repeated for the thick target curve corrected for the extra yield above this resonances due to onset of the 900 and 935.3 KeV ones. The results are given in Table 3 for the Sept., 1952 runs.

Table 3.

Evaluation of k.

Target #	$k \times 10^3$	$(k - \bar{k}) \times 10^7$	$(k - \bar{k})^2 \times 10^{14}$
Thin			
1	1.1974	7	49
2	1.1976	9	81
4	1.1967	0	0
4	1.1985	18	324
Semi thick			
1	1.1979	12	144
2	1.1973	6	36
Thick	1.1917	50	2,500
Total	8.3771		3,134

$$\bar{k} = \frac{8.3771 \times 10^{-3}}{7} = 1.1967 \times 10^{-3}$$

$$\text{standard deviation} = \frac{3134 \times 10^{-4}}{7} = 21.2 \times 10^{-7},$$

$$\text{Probable error (p.e.)} = .674 \times 21.2 = 14 \times 10^{-7},$$

$$\%\text{ probable error} = \frac{14 \times 10^{-7} \times 100}{1.1967 \times 10^{-3}} = 0.12\%,$$

$k = 1.197 \times 10^{-3}$ MeV/Mc/s^2 0.12%(p.e.,7 measurements). (XII.3)

A check was made at the 340.4 KeV fluorine resonance which is also used as a standard by many experimenters. A resonance curve taken with target #2 was used. However, the stopping power of this target for 340.4 KeV protons is increased by a factor of about 2.06 (as taken from the slope of Bethe's most recent curve[39] for the range

of protons in air). Therefore the peak yield occurred at 340.4 + 2.06/2 = 341.33 KeV corresponding to a frequency of 16.892 Mc/s. Therefore

$$k = \frac{.34133}{(16.892)^2} = 1.1966 \times 10^{-3}$$

difference = $(1.1967 - 1.1966) \times 10^{-3} = 0.0001 \times 10^{-3}$

% difference = 1/1.1967 X 100=0.008%

This close check was very reassuring.

The calibration equation of the accelerator may be stated to an accuracy made up of the sum of the squares of the two uncertainties (since the uncertainty in the measurement of f_p is about ± 0.01%); the 0.1% for the 873.5 KeV value from Herb and the ± 0.12% for the value of k; ie. about ± 0.16%. This gives for the Sept., 1952 data,

$$V(MV) = 1.197 \times 10^{-3} f_p (Mc/s)^2 \quad 0.16\% \quad (XII.4)$$

Provided that singly charged mass 1 beams (protons) are used, the V(MV) may be replaced by E(MeV) without altering equation (XII.4). When mass 2 or 3 are used, the appropriate factor of $\sqrt{2}$ or $\sqrt{3}$ must be used.

(4) The fluxmeter frequencies at which the other resonances in fluorine should occur[20] were calculated by means of equation (XII.4) and compared to the frequency values observed experimentally. The results are given below in Table 4. The experimental frequency at which the resonance peaks occurred was corrected for the stopping power of the target for protons of that energy. For

Table 4.

Calculated and Observed Fluxmeter Frequencies for Fluorine Resonances.

E_R MeV	Experimental f_p Mc/s	Calculated f_p Mc/s	difference Mc/s	% difference in f_p
0.3404	16.866	16.863	+0.003	+0.018
.486	20.111	20.150	-0.039	-0.19
.598	22.316	22.336	-0.020	-0.09
.669	23.624	23.641	-0.017	-0.07
.831	26.418	26.349	+0.069	+0.26
.8735	Calibration	27.014		±0.08
.900	27.425	27.421	+0.004	+0.015
.900	27.429	27.421	+0.008	+0.03
.9353	27.961	27.954	+0.007	+0.025
.9353	27.948	27.954	-0.006	-0.025
1.092	30.144	30.204	-0.060	-0.20
1.137	30.840	30.821	+0.019	+0.06
1.176	Broad	31.344		
1.290	32.755	32.828	-0.073	-0.22
1.290	32.709	32.828	-0.119	-0.36
1.355	33.519	33.645	-0.126	-0.37
1.381	33.836	33.966	-0.130	-0.38
1.381	33.839	33.966	-0.137	-0.37
1.62*	36.663	———		
1.62*	36.642	———		
1.69	37.657	37.576	+0.091	+0.24
1.84*	39.139	———		

* New determination

example, the fluxmeter frequency corresponding to the experimental peak yield at the resonance energy $E_R = 340.4$ KeV was 16.892 Mc/s when thin #2 target was used. This target had a stopping power of 2.06 KeV at 340.4 KeV. Since 1.03 KeV corresponds to a shift in frequency of 0.0256 Mc/s, this amount was subtracted from the above to give the corrected experimental frequency of 16.866 Mc/s. The calculated frequency from equation (XII.4) is:

$$f_p \text{ (Mc/s)} = 28.904\sqrt{E(\text{MeV})} \pm 0.08\% \qquad \text{(XII.5)}$$

Good agreement with equation (XII.5) is shown in Table 4; seven of the eleven calculated frequencies for the resonances below about 1.2 MeV have an error less than the p.e. which should be attached to the calculated frequency, namely

$$\frac{\Delta f_p}{f_p} = \frac{\frac{1}{2}\Delta V}{V} = \frac{\Delta \rho}{\rho} = \frac{\frac{1}{2}\Delta k}{k} = \pm 0.08\% \qquad \text{(XII.6)}$$

where Δf_p, ΔV, $\Delta \rho$, Δk, are the p.e.'s or uncertainties respectively in each quantity. In these measurements the calculated frequency for the resonances above about 1.2 MeV begins to show a larger difference which was considered attributable to the effect of the fringing magnetic field on the beam. On this hypothesis at high fields, the effective radius of the path of the bent beam would be increased so that a smaller field, H, would be needed for the same $H\rho$ or momentum of the particles in the beam. The effective increase in ρ would appear to be less than 4 parts in 1,000 up to 2 MeV in proton beam energy corresponding to a magnetic field of about 10,000 gauss. Consequently, a small first order correction could be added to equation (XII.4),

of amount $\Delta V = 2\Delta f = 0.0072$ V so that for voltages above 1.2 MV, the calibration would be,

$$V(MV) \underset{\text{(above 1.2 MV)}}{=} 1.204 \times 10^{-3} f_p \ (Mc/s)^2 \pm 0.5\%(p.e). \qquad (XII.7)$$

After further checks on the 873.5 calibration curve using a mass 2 beam, this hypothesis proved to be incorrect.

7. Final Calibration and Checks in November, 1952.

The ion source focussing conditions were different from those used in the September, 1952 calibration. In the energy selector, a 0.022 inch thick molybdenum disk with a 1/8 inch aperture was added just below the original entrance aperture to the magnet, (see figure 19), and the exit slits were replaced with thicker pieces of molybdenum, 0.022 inch thick. The slit spacing was decreased to 0.067 inches.

Larger beam currents were available so that extra curves were taken using the less intense resolved mass 2 and mass 3 beams to extend the fluxmeter's, and hence the accelerator's, range of calibration. From equation (II.3),

$$H = \frac{c}{e}\sqrt{\frac{2mV}{e}}, \qquad (II.3a)$$

and from (II.8), $f_p = \frac{\gamma_p}{2\pi} H$, (II.8a)

so that the fluxmeter frequency needed to deflect through 90°a mass 2 beam at 2V was the same as that required to deflect a mass 1 beam at 4V or was twice that required for a mass 1 beam accelerated by only V. For exciting the same resonance as given by a mass 1 beam accelerated through V volts, a mass 2 beam of HH^+ needs to be accelerated

through 2V since each particle in it breaks up on impact with the target into two mass 1 particles, each having half the total kinetic energy, for the energy preventing this breakup is only a few eV. Thus, to obtain the 0.8735 MeV resonance curve with a mass 2 beam, the accelerator voltage was set to 1.747 MV and the fluxmeter frequency to 54.118 Mc/s. This fluxmeter setting was equivalent to that for a mass 1 beam at 3.494 MV. In a similar way, the fluxmeter was checked at equivalent mass 1 settings of 1.362 and 3.863 MV by obtaining the 0.3404 MeV resonance curve with mass 2 and mass 3 beams respectively.

Table 5 gives the results of the calibration runs taken over the 873.5 KeV resonance with a mass 1 beam during November 5 to 13, 1952. The average value of k from equation (XII.1) was used, as on page 66, to compute the "calculated f_p" in Table 6 for the check runs over some of the other fluorine resonances. This is repeated for tables 7 and 8 for the November 14 - 17 runs and for Tables 9 and 10 for the November 18-19 runs.

Close agreement, within $\pm$ 0.1%, is shown between the three k values from the 873.5 KeV calibration runs taken in November although they are all about 0.4% lower than the September, 1952 value for k. The mass 2 checks on the 873.5 KeV resonance show that the fluxmeter frequency reads 0.4% high at 54.1 Mc/s. This is confirmed by the checks on the 340.4 KeV resonance with mass 2 and mass 3 beams. The calibration equation of the accelerator, from the November

Table 5.

Re-determination of k, Nov. 5-13, 1952.

Thin target #4, ε = 0.4 KeV at 873.5 KeV.

Date	Time	($k \times 10^3$)	$(k - \bar{k}) \times 10^7$	$(k - \bar{k}) \times 10^{14}$
5	4:00p.m.	1.1882	− 24	576
5	8:00p.m.	1.1904	− 2	4
7	11:00p.m.	1.1886	− 20	400
7	11:30p.m.	1.1907	+ 1	1
13	9:45p.m.	1.1931	+25	625
13	10:30p.m.	1.1927	+ 21	441
	Total	7.1437		2047

$k = 1.191 \times 10^{-3}$ MV/Mc/s^2 ± 0.1%,

f_p (Mc/s) = $28.980 \sqrt{V(MV)}$ ± 0.07%.

Table 6.

Calculated and Observed Fluxmeter Frequencies for Fluorine Resonances, Nov. 5-13, 1952.

Thin target #4.

Date	Time	Beam Mass	E_R(MeV)	Exp. f_p Mc/s	Calc. f_p Mc/s	% Diff in f_p
5	5:00p.m.	1	0.900	27.535	27.493	+0.14
5	8:45p.m.	1	0.900	27.447	27.493	−0.17
7	9:00p.m.	1	1.355	33.649	33.736	−0.26
7	9:15p.m.	1	1.381	33.975	34.056	−0.24
13	10:30a.m.	1	0.3404	16.937	16.908	+0.17
13	10:40a.m.	1	0.3404	16.941	16.908	+0.20
13	12:30p.m.	3	0.3404	51.120	50.723	+0.68
13	1:30p.m.	3	0.3404	50.930	50.723	+0.41
13	1:40p.m.	3	0.3404	50.996	50.723	+0.54
13	10:00p.m.	1	0.9353	27.998	28.027	−0.10

Table 7.

Re-determination of k, Nov. 14-17, 1952.

Thin target #6, ξ = 1.0 KeV at 873.5 KeV.

Date	Time	k X 10^3	(k - $\bar{k}$) X 10^7	(k - $\bar{k}$) X 10^{14}
14	10:45p.m.	1.1946	+15	225
15	9:45p.m.	1.1941	+10	100
17	4:00p.m.	1.1925*	- 6	36
17	4:30p.m.	1.1932*	+ 1	1
17	5:00p.m.	1.1929*	- 2	4
18	1:45a.m.	1.1920*	-11	121
18	2:00a.m.	1.1925*	- 6	36
	Total	8.3518		523

* Target heated to 100° C.

k = 1.193 X 10^{-3} MV/Mc/s^2 ± 0.05%,

f_p = 28.952 $\sqrt{V(MV)}$ ± 0.06%.

Table 8.

Calculated and Observed Fluxmeter Frequencies for Fluorine Resonances, Nov. 14-17, 1952.

Thin target #6.

Date	Time	Beam Mass	E_R(MeV)	Exp. f_p Mc/s	Calc. f_p Mc/s	% Diff. in f_p
14	2:30p.m.	2	0.3404	33.879	33.783	+0.28
14	6:00p.m.	3	0.3404	50.919	50.674	+0.69
17	2:00p.m.	1	0.3404	16.900	16.892	+0.05
17	2:10p.m.	1	0.3404	16.927	16.892	+0.21
17	6:00p.m.	2	0.8735	54.387*	54.118	+0.48
17	9:00p.m.	1	1.69	37.746*	37.638	+0.29
17	9:20p.m.	1	1.69	37.756*	37.638	+0.31
17	10:11p.m.	1	1.69	37.676*	37.638	+0.10
17	10:25p.m.	1	1.69	37.729*	37.638	+0.24
18	12:10a.m.	1	1.69	37.699*	37.638	+0.16
18	12:30a.m.	1	1.69	37.756*	37.638	+0.31

* Target heated to 100° C.

Table 9.

Re-determination of k, Nov. 18-19, 1952.

Thin target #7, ξ = 1.5 KeV at 873.5 KeV.

Date	Time	k X 10^3	$(k - \bar{k})$ X 10^7	$(k - \bar{k})$ X 10^{14}
18	6:30p.m.	1.1925	0	0
18	9:30p.m.	1.1930	+ 5	25
18	9:45p.m.	1.1945 *	+20	400
19	5:45a.m.	1.1904	-21	441
19	5:55a.m.	1.1919	- 6	36
	Total	5.9623		902

All targets heated to 100° C, only one spot bombarded.

* semi-thick target #3, $\xi \approx$ 20 KeV.

$k = 1.192 \times 10^{-3}$ MV/Mc/s^2 ± 0.1%,
f_p (Mc/s) = $28.958 \sqrt{V(MV)}$ ± 0.12%.

Table 10.

Calculated and Observed Fluxmeter Frequencies for Fluorine Resonances, Nov. 18-19, 1952,

Thin target #7.

Date	Time	Beam Mass	E_R(MeV)	Exp. f_p Mc/s	Calc. f_p Mc/s	% Diff in f_p
18	10:45p.m.	1	1.381	33.946	34.030	-0.26
18	12:00p.m.	1	1.69	37.724	37.645	+0.21
19	1:40a.m.	2	0.8735	54.342	54.129	+0.42
19	3:45a.m.	1	1.94	40.391	40.336	+0.12
19	3:45a.m.	1	1.94	40.419	40.336	+0.21

All targets heated to 100° C, same spot used as for data in Table 9.

Figure X

GENERATING VOLTMETER CALIBRATION

SEPTEMBER, 195

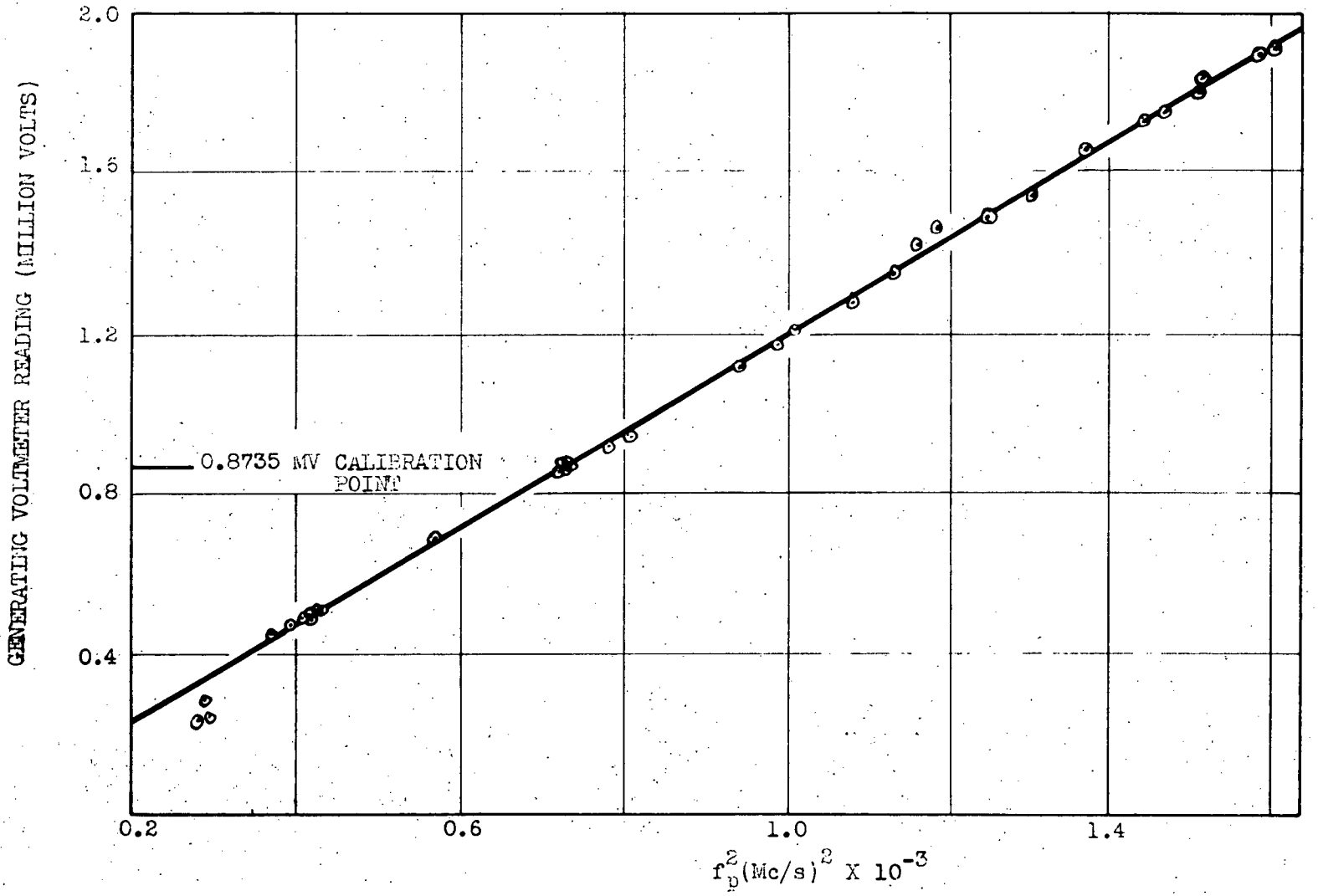

data is therefore,

$$V(MV) = 1.192 \times 10^{-3} f_p^2 \pm 0.1\%, \quad \text{(up to 1.0 MV)} \qquad \text{(XII.8)}$$

and adding a first order correction,

$$V(MV) = 1.184 \times 10^{-3} f_p^2 \pm 0.5\%. \quad \text{(from 1.0 to 3.5 MV)} \qquad \text{(XII.9)}$$

8. Calibration of the Generating Voltmeter.

Figure 22 shows the linearity of the generating voltmeter readings plotted against the square of the fluxmeter frequency for the September, 1952 data after calibration at 873.5 KeV. A similar line was obtained for the November data. The generating voltmeter is therefore reliable within the reading error of its meter, about 5 KeV in 873.5 KeV or 0.6%, and rather better using a Brown recorder with a 10 inch long scale to observe the current.

XIII. Summary of Results on Calibration.

1. Reproducibility and Absolute Calibration.

The short time reproducibility of the accelerator voltage is very good to within 0.2%, from the data on the 873.5 KeV resonance, over a period of hours to several days. The absolute voltage calibration from the November data is good to about the same order of accuracy over several weeks. However, over the two month period from Sept. to Nov. 1952, it was only good to 0.4%. The reason for this was partly due to the changes in the focussing conditions in the magnet box, and at the ion source. Either this or perhaps electrostatic charging of parts

of the accelerating tube, may produce small changes in the angle at which the beam enters the magnet box. A change in the entrance angle of only a few minutes of arc would cause the beam to describe a slightly shorter or longer path in the magnetic field and therefore require a smaller or larger magnetic field, than in the case of vertical incidence, to deflect a beam of the same energy through the exit slit. The resulting small change in fluxmeter frequency would give a small error in the voltage calibration. Sparks in the accelerator may give a similar result.

Therefore, for most accurate work, the voltage or energy scale of the accelerator should be calibrated within a few hours before and after, or if possible, during an experiment. Alternatively, with more difficulty, better collimation of the beam could be introduced.

The energy resolution expected from the exit slit spacing of 0.067 inches for a beam radius of 8.8 inches is:

$$\frac{\Delta E}{E} \approx \frac{2\,\Delta \ell}{\ell} \approx \frac{2 \times 0.067}{8.8} \approx 0.016, \text{ or } \pm 0.008, \qquad \text{(XII.1)}$$

which is 8 times larger than the reproducibility actually achieved. A similar result was also found by Bennet et al[21] who also used a reverse electron gun stabilizing system. One great advantage of the U.B.C. ion energy selector is the reproducibility and precise measurement of a magnetic field setting independent of any magnetic hysteresis effects. Points taken in any order over a resonance could be fitted to a smooth curve.

2. Possible Sources of Error in Absolute Energy Measurements.

In these calibration the positive ion beam was centred at and defined by the small entrance aperture at the magnet box and focussed carefully on the target. It was believed that the 90° focus of the beam occurred just inside of the magnet box since a spot size of about 5/16 inches was produced by the beam 34 inches from this point after passing through the 0.067 inch slit 7 inches from this point. It was found, however, that the stabilizing system could hold a poorly focussed beam on the target, at times, but at slightly different fluxmeter setting than that for the properly focussed one for the same point on a resonance. Again the fluxmeter r-f head measured the magnetic field over an area of about 1 cm^2 at one upper corner of the gap between the pole faces. An average field along the path of the deflected ion beam was then inferred from this. Errors up to a few parts in a thousand in frequency (or magnetic field) might occur if the ratio of these two fields changed at high magnetic fields. From previous work on the magnet[3] the author had found that the field strength over the pole face of the magnet at 10,000 gauss varied by as much as 40 gauss in 10,000 gauss up to an inch from the pole face edges. A further check on this at different field strengths would seem advisable if an increase in the accuracy of the beam energy measurements is needed.

Part III.

Determination of Some Nuclear Excitation Functions.

XIV. Resonant Reactions[37]

In many cases when a nucleus is bombarded by a nucleon such as a proton, neutron or alpha particle, a compound nucleus having discrete energy levels, E_R, is formed. We may properly speak of the existence of this intermediate or compound nucleus only if it has a lifetime greater than the characteristic nuclear time (time for a nucleon to travel across the nucleus, about 10^{-21} seconds). An average lifetime of such a compound nuclear state may be deduced from the energy level width, δE, from Heisenberg's uncertainty relation; e.g. for $\delta E = 4$ KeV,

$$\delta t \approx \frac{h}{\delta E} \approx \frac{6.6 \times 10^{-27}}{4{,}000 \times 1.6 \times 10^{-12}} \approx 10^{-18} \text{ sec.,} \qquad \text{(XIV.1)}$$

which is small compared to the above. This compound nucleus may lose its surplus energy by decaying to the ground state via the emission of γ-rays or, if energetically possible, by particle emission to the ground or an excited state of a residual nucleus. The residue nucleus, if left in an excited state, will also decay be the emssion of a γ-ray. When the energy levels of the compound nucleus are widely

separated, the reaction yield of particles or γ-rays exhibits strong resonances as the energy of the incident particle is varied corresponding to the formation of the compound nucleus in one of its possible excited states.

In such resonant reactions we wish to detect and measure accurately the maxima in the excitation function since this gives directly the location in energy and number of the excited states of the compound nucleus. The "level width", which is related to the probability of decay of the compound nucleus, may also be ascertained if the natural shape of the resonance can be measured. Further arguments, based for example on the angular distribution of the emitted particles or quanta, make it possible in some cases to assign an angular momentum quantum number and a parity to the stationary state.

In this way it is hoped to build up a detailed picture of the energy levels of at least the lighter nuclei, from which in the present poor state of our knowledge regarding nuclear forces, we may at least hope to select nuclear models which yield level schemes in accord with the experimental data. This in itself will be a major advance towards a proper understanding of inter-nuclear forces.

XV. The Breit-Wigner One-Level Dispersion Formula.

1. Reaction Cross Section and Yield.[40]

Consider a beam of charged particles of N per second and cross sectional area "a" cm^2 striking a target

of thickness t cm. containing ν nuclei per cm^3. If we assume no overlapping of nuclei then the number of nuclei n, in the path of the beam is given by,

$$n = \nu a\, t. \qquad (XV.1)$$

We define the cross section for a reaction, σ, in terms of the above and the yield, Y, in disintegrations of the type under consideration per second, by the equation:

$$Y = N \frac{n\sigma}{a} = N \nu t\, \sigma, \qquad (XV.2)$$

where σ has the dimensions of area (cm^2). σ may be interpreted as the effective area that the target nucleus presents to the incident particles. In other words, σ is proportional to the probability of occurrence of the reaction. Representative values for σ for (p, γ) reactions are of the order of 10^{-24} cm^2, a convenient unit termed one "barn". It is found from experiment, that σ sometimes varies with the energy of the bombarding particles in a characteristic resonance way. This variation of σ over a γ-ray resonance may be simply described by a one-level "dispersion formula" as proposed by Breit and Wigner, provided that the resonance is well defined and well separated in energy from other resonances. In the case of a simple (p, γ) resonant reaction, the dispersion formula gives:

$$\sigma(p, \gamma) = g \pi \lambda\!\!\!^{-2}_{p} \frac{\Gamma_p \Gamma_{rad}}{(E - E_R)^2 + \frac{1}{4}\Gamma^2}, \qquad (XV.3)$$

where: g is a statistical weighting factor determined by the spins of the nuclei involved,

$\lambda\!\!\!^{-}_{p} = \lambda_p / 2\pi$ where λ is the De Broglie wavelength of the incident particle in centre of mass coordinates,

Γ_p is the particle width (at resonance energy E_R),

ie. $\Gamma_p/\hbar$ is a measure of the probability of decay of the compound nucleus via re-emission of a proton of the same energy. Included in this term is the effect of Coulomb and Centrifugal barriers as it may be written as:

$$\Gamma_p^{Res} = \frac{(2\ R\ B)}{(\lambda)} \gamma_p^{Res},$$

where R is the radius of the nucleus,

B is the penetration factor,

Γ_p^{Res} is the reduced width, a constant set by the particular nucleus,

Γ_{rad} is the "reaction" width, ie. in this case a measure of the probability of decay via γ-radiation,

Γ is the total level width or resonance width, here just $\Gamma_p + \Gamma_{rad}$.

E is the energy of the bombarding particle,

E_R is the energy of the bombarding particle at resonance.

Γ is related to the lifetime, τ, of the particular state of the compound nucleus by the uncertainty relation of Heisenberg; $\Gamma\ \tau \approx h/2\pi$. Since the probability of decay of this state, $P = 1/\tau$, then $\Gamma = \hbar P$.

In general over a sharp resonance these widths will not change significantly from their value at resonance, so that the variation in σ over a resonance is settled by the resonance or dispersion form of the denominator.

If the total level width exceeds the experimental energy resolution, ΔE, then E_R and Γ can be obtained directly and the absolute yield of γ-radiation at resonance

provides a measure of σ_R (the value of σ at the resonance energy) provided the number of nuclei/cm^3 in the target is known and the yield is measured over a sufficient range of angles to estimate the total σ_R. Γ_{rad} is unlikely to exceed a few eV so that the total width will only exceed the experimental resolution (about 1 KeV) if Γ_p is large enough (about 1 KeV).

(a) Under the afore mentioned circumstances where $\Gamma_p > \Delta E$ resolvable,

$$\sigma = g\pi\lambda^2 \frac{\Gamma_{rad}\Gamma}{(E - E_R)^2 + \frac{1}{4}\Gamma^2}. \qquad (XV.5)$$

At resonance,

$$\sigma_R = g\pi\lambda^2 4\Gamma_{rad}/\Gamma \quad , \qquad (XV.6)$$

so that

$$\sigma = \sigma_R \frac{\frac{1}{4}\Gamma^2}{(E - E_R)^2 + \frac{1}{4}\Gamma^2}. \qquad (XV.7)$$

Hence measurements of the shape of the resonance curve, E_R, and σ_R give a value of $g\Gamma_{rad}$.

(b) When $\Gamma \ll \Delta E$, then only the cross section averaged over the level can be measured, and this is usually done by using a thick target and a bombarding energy, E, greater than E_R by an amount at least equal to the resolution of the beam. Assuming no higher resonance is involved, the yield in this case can be found by integration of the cross section over the resonance.

2. Application of the Dispersion Formula to Show the Peak Yield For a Thin Target Resonance Curve Occurs at $E = E_R + \varepsilon/2$.

For an infinitely thin target, ie. where the

loss of energy in the target, $\xi \ll \Gamma$, equation (XV.2) gives the yield of γ-rays directly. However, when the resonance width Γ, and the loss of energy ξ in a thin target are comparable, the yield of γ-rays is obtained by integration of the Breit-Wigner formula over the resonance energy range:

$$y = \int_{E-\xi}^{E} \frac{\sigma \, dE}{\epsilon}, \qquad \text{(XV.8)}$$

where y is the yield per incident particle, ϵ is the stopping cross section per disintegrable nucleus in the target. Now $\xi = \sqrt{t}\,\epsilon$, if ξ and ϵ do not vary over the resonance. Substituting for σ from (XV.7) and integrating gives:

$$y(\xi) = \frac{\sigma_R \Gamma}{2\epsilon} \left(\tan^{-1} \frac{E-E_R}{\Gamma/2} - \tan^{-1} \frac{E-E_R-\xi}{\Gamma/2} \right). \qquad \text{(XIV.9)}$$

To find the maximum yield as a function of the energy, of the bombarding particle for a fixed target thickness, ξ, (XIV.9) may be differentiated with respect to E and equated to zero. This shows that the peak yield occurs when:

$$E = E_R + \frac{\xi}{2}, \qquad \text{(XV.10)}$$

and by substituting this in (XV.9), this peak yield is given by:

$$y_{max}(\xi) = \frac{\sigma_R \Gamma}{\epsilon} \tan^{-1} \frac{\xi}{\Gamma}. \qquad \text{(XV.11)}$$

3. Relative Yield of Thick and Thin Targets.

Equation (XV.11) may now be compared to the peak yield from a thick target, ie. one where $\xi \gg \Gamma$. This is given by considering equation (XV.9) in the limit as tends to infinity:

$$y_{max}(\infty) = \frac{\sigma_R \Gamma \pi}{2\epsilon}. \qquad \text{(XV.12)}$$

Dividing (XV.11) by (XV.12) gives,

$$\frac{y_{max}(\xi)}{y_{max}(\infty)} = \frac{2}{\pi} \tan^{-1} \frac{\xi}{\Gamma}, \qquad \text{(XV.13)}$$

which shows the relative peak thin target yield compared to that from a thick target.

Now the area $A(\xi)$, under a thin target resonance curve is given by the integral of the yield over the resonance:

$$A(\xi) = \int_{\text{Resonance}} y(\xi)\,dE = \frac{\pi}{2} \frac{\xi \sigma_R \Gamma}{\epsilon} = \xi\, y_{max}(\infty), \qquad \text{(XV.14)}$$

from equations (XV.() and (XV.11), which shows that it is only proportional to the energy loss in the target and the thick target yield step. It may also be shown that this area is independent of the homogeneity of the beam and the nature of the thin target yield curve.[21a]

The yield for a thick target curve as a function of E is given by equation (XV.9) with $\xi \gg \Gamma$:

$$y_{thick} = \frac{\sigma_R \Gamma}{2\epsilon} \left[\frac{\pi}{2} + \tan^{-1} \frac{E - E_R}{\Gamma/2} \right] \qquad \text{(XV.15)}$$

4. <u>(p, $\alpha\gamma$) Resonant Reactions</u>.

A few light nuclei show discrete resonance levels for (p, α) reactions. Thus in $F^{19}(p, \alpha\gamma)O^{16}$, sharp levels are found corresponding to maxima in the yield of low energy α-particles, as O^{16} is produced in a state with excitation energy of 6 to 7 MeV. Thus these alpha resonances may be investigated by measuring the γ-ray yield. The emission of more energetic α-particles corresponding to formation of O^{16} in the ground state is not possible for these states of the compound nucleus Ne^{20}.

owing to symmetry properties. The Breit-Wigner formula can also be applied to these resonant reactions; in this case, Γ_{rad} must be replaced by Γ_{α} .

XVI. Limits of Energy Resolution.

1. Doppler Limit to Energy Resolution.[41]

The parameters E_R, Γ and σ_R may be evaluated to a precision determined by the experimental definition of the bombarding energy, E. However, the amount of energy that is available for excitation of the compound nucleus must be calculated in the centre-of-mass system of the compound nucleus. Due to the thermal motion of the target nuclei, the effective energy of the incident protons, will be spread out (Doppler broadening of level) over a range of energies having the gaussian distribution:

$$N(E)dE = \frac{1}{2\pi D} e^{\frac{-(E_o-E)^2}{2D^2}} dE, \qquad \text{(XVI.1)}$$

where $D = \sqrt{\frac{2m}{M} E_o kT}$,

$\frac{m}{M}$ is the ratio of the mass of the proton to the mass of the target nucleus,

T is the absolute temperature,

k is Boltzmann's constant.

For the energies and the targets considered here, this amounts to an uncertainity in E of the order of 100 eV.

2. Practical Limits to Energy Resolution.

Evaluation of the parameters of $(p, \alpha\gamma)$ resonant

reactions requires a source of bombarding particles easily variable and homogeneous in energy and of sufficient intensity for accurate measurements to be taken in a reasonable time. In addition, thin targets are needed for identification and resolution of the resonances, especially when the curves are narrow and closely spaced. The main factors which decrease the definition in the energy, E, of the proton beam are:

(1.) Variations in the energy of the ions emerging from the ion source and focussing lenses,

(2.) Loss of energy of the ions by collisions with gas molecules in the accelerator colums,

(3.) Voltage fluctuations in the accelerator due to corona, sparks and belt rubbing,

(4.) Deterioration of target with time due to bombardment and formation of oil and carbon films,

(5.) Uncertain variations in target thickness.

On the other hand, the homogeneity of the beam may be improved by using narrow slits on the analyzer to define the energy and by using very thin targets (so that the energy loss in all parts of the target is small). In the U.B.C. accelerator, the r-f ion source keeps the variations in (1.) of the order of 100 eV or less. With a vacuum of 2×10^{-6} mm. (good for the size of the accelerator tubes, about 20 feet long by about 8 inches in diameter), the mean free path of the protons is of the order of 20 feet so that factor (2.) is small. Voltage fluctuations are

Figure 26

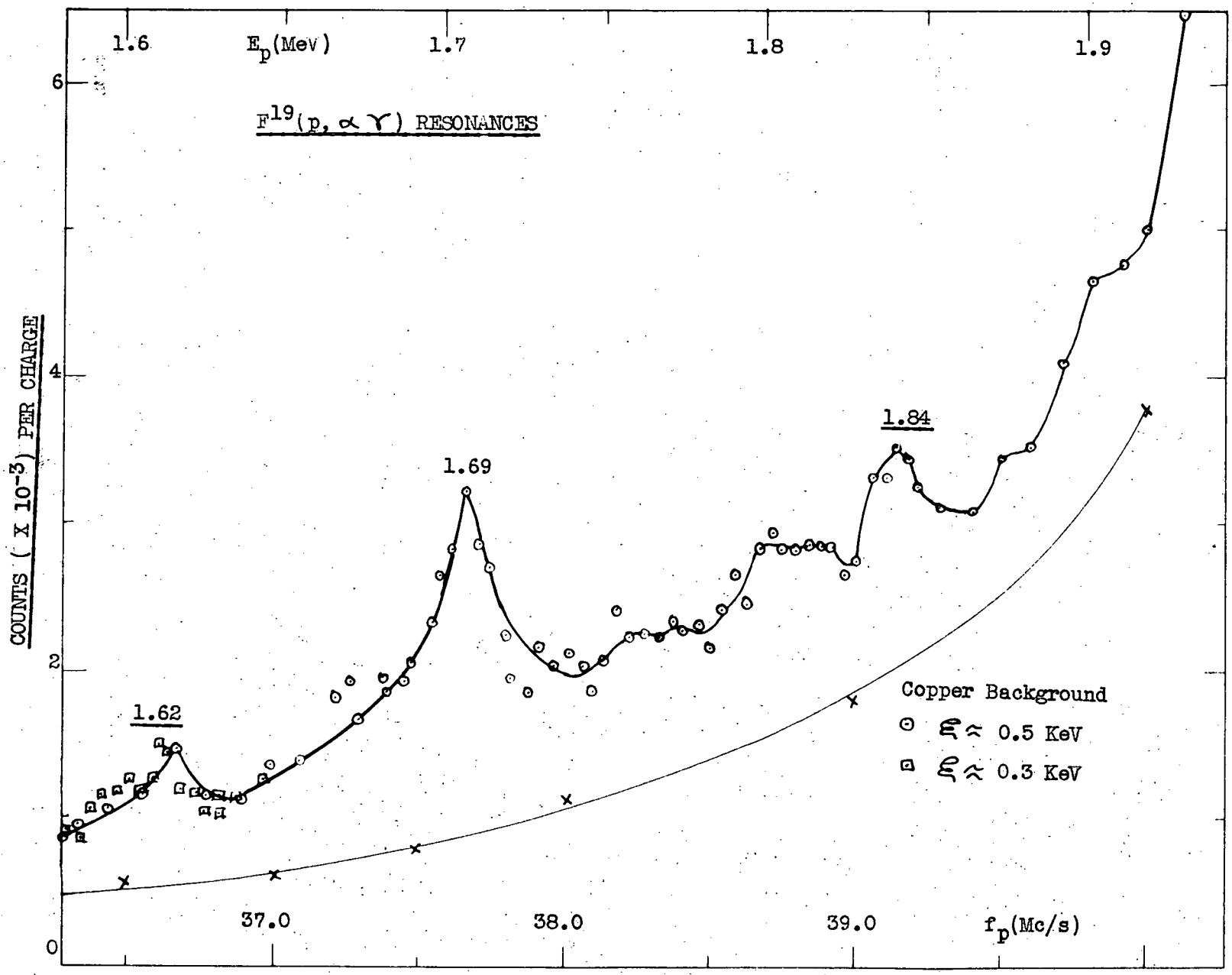
1.6
E_p(Mev)
1.7
1.8
1.9
$F^{19}(p, \alpha\gamma)$ RESONANCES
COUNTS (X 10^{-3}) PER CHARGE
6
4
2
0
1.62
1.69
1.84
Copper Background
$\xi \approx$ 0.5 KeV
$\xi \approx$ 0.3 KeV
37.0
38.0
39.0
f_p(Mc/s)

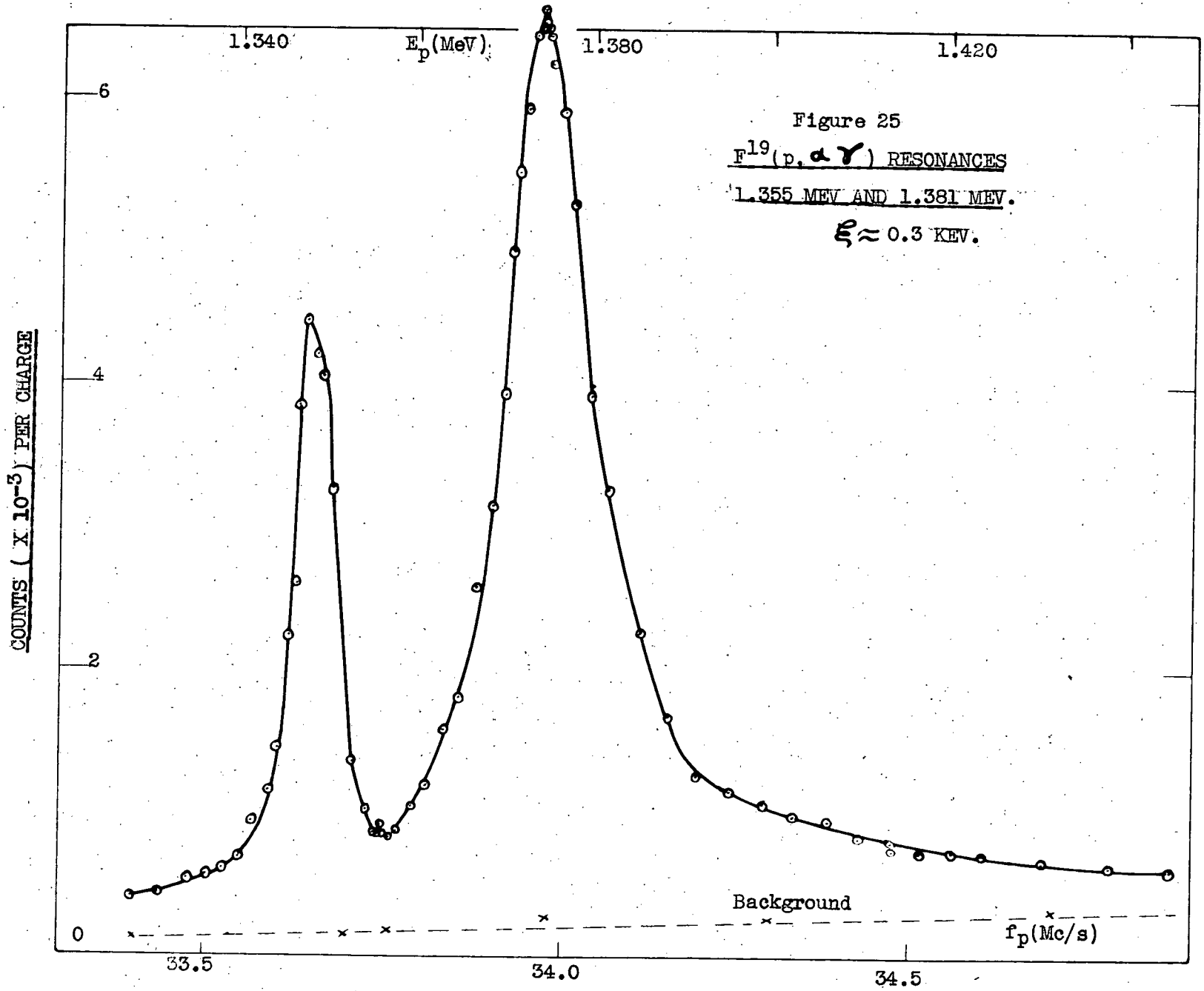

Figure 25

$F^{19}(p,\alpha\gamma)$ RESONANCES

1.355 MEV AND 1.381 MEV.

$\xi \approx$ 0.3 KEV.

Figure 24

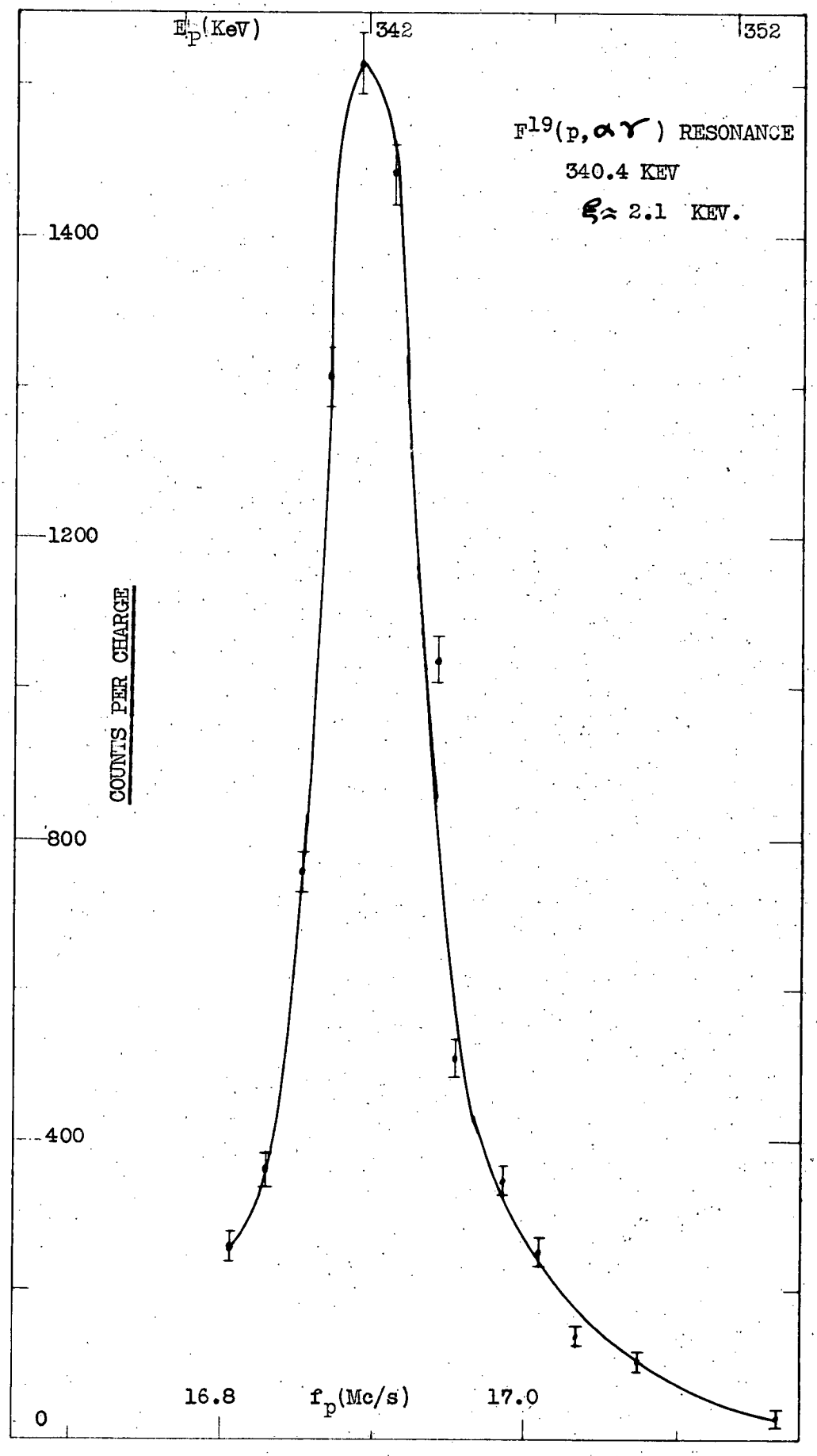
E_p(KeV)
342
352
$F^{19}(p,\alpha\gamma)$ RESONANCE
340.4 KEV
$\xi \approx$ 2.1 KEV.
1400
1200
800
400
0
COUNTS PER CHARGE
16.8
f_p(Mc/s)
17.0

kept small by the ion energy control system which has a theoretical upper limit of about 100 eV. Target deterioration is minimized by keeping the intensity of the beam as high as possible so that the time required for a run over a resonance is as small as possible. The other considerations of using narrow slits and thin targets reduce the yield of γ-rays per second so that longer times are required to obtain sufficient counts for good statistical accuracy. A compromise between maximum homogeneity and low intensities of beam must be made. However due to the method of ion energy control adopted at U.B.C., good homogeneity is obtained with up to $4\frac{1}{2}$ μ amperes of resolved protons.

XVII. The Proton Bombardment of Fluorine.

1. γ-ray Excitation Function.

The γ-ray excitation function from the proton bombardment of fluorine is shown in figure 23. The γ-rays of 6 and 7 MeV energy are produced in the reaction:

$$F^{19} + H^{1} \longrightarrow Ne^{20*} \longrightarrow O^{16*} + He^{4}$$
$$\downarrow$$
$$O^{16} + \gamma \quad . \qquad \text{(XVII.1)}$$

Proton capture radiation has been observed at the 669 KeV resonance[42], but was ignored in this work because of its extremely low intensity. The experimental counting arrangement was the same as in part II, section XII. All the published resonances[20] between 0.340 and 2.0 MeV were observed as well as two new resonances at 1.62 and 1.84 MeV.

Figure 23.

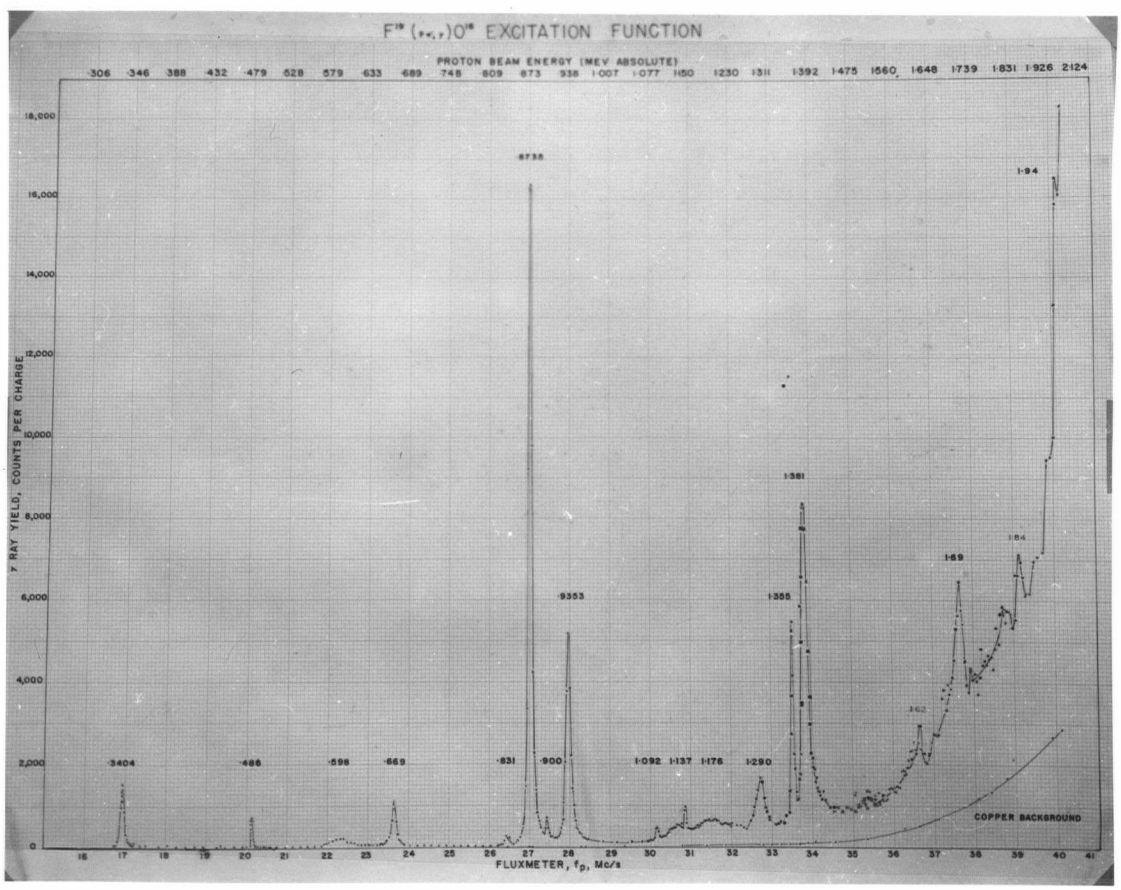
F¹⁹ (p,γ)O¹⁶ EXCITATION FUNCTION
PROTON BEAM ENERGY (MEV ABSOLUTE)
·306 ·346 ·388 ·432 ·479 ·528 ·579 ·633 ·689 ·748 ·809 ·873 ·938 1·007 1·077 1·150 1·230 1·311 1·392 1·475 1·560 1·648 1·739 1·831 1·926 2·124
γ RAY YIELD, COUNTS PER CHARGE
FLUXMETER, fp, Mc/s
·8735
·9353
1·381
1·358
1·94
1·69
1·84
1·62
·3404
·486
·598
·669
·831
·900
1·092
1·137
1·176
1·290
COPPER BACKGROUND

Figure 27

$F^{19}(p,\alpha\gamma)$ 1.84 MEV RESONANCE

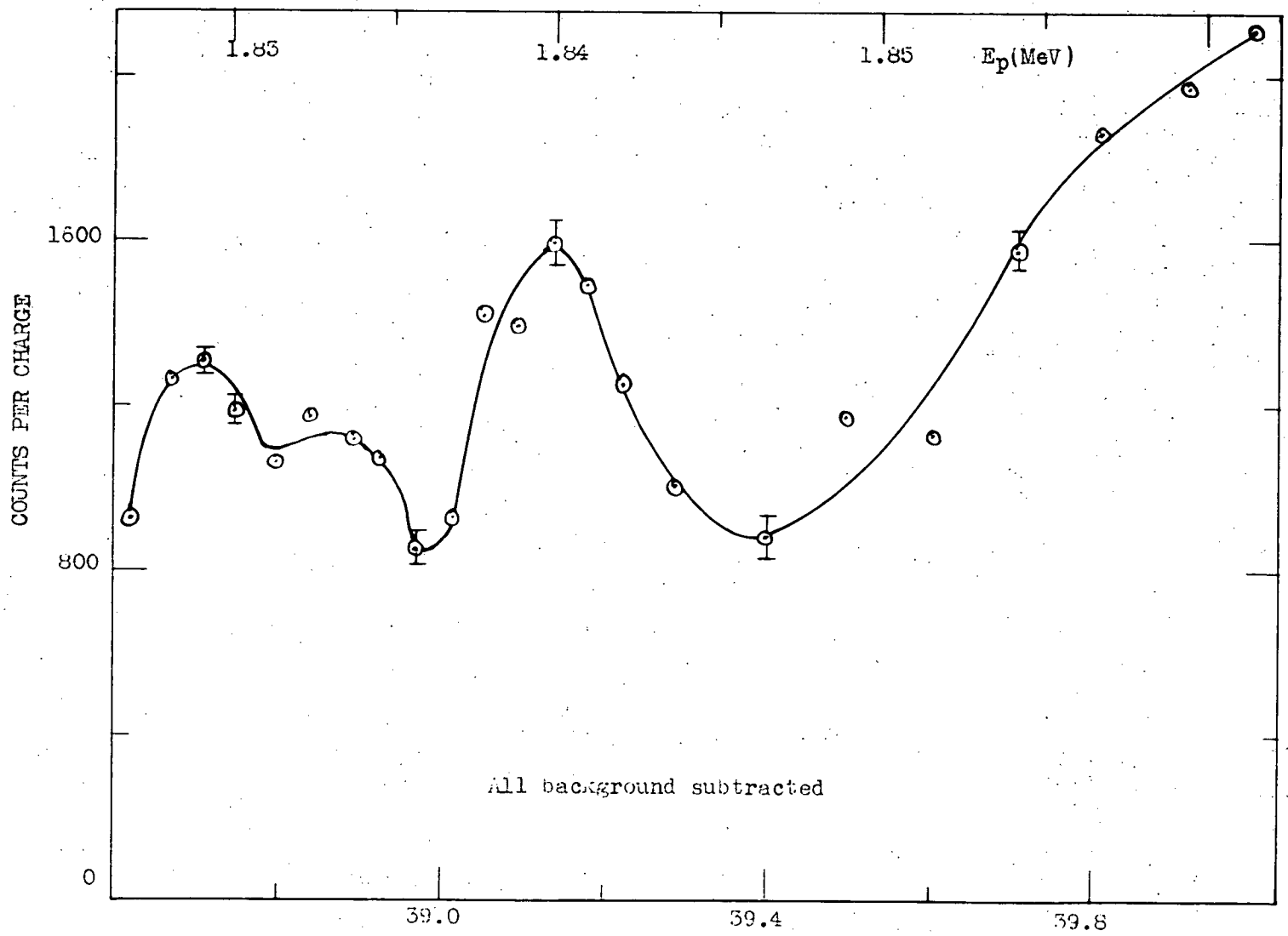

Figure 28

$F^{19}(p,\alpha\gamma)$ RESONANCE WITH MASS 2 BEAM

SEPT. 1952, ξ = 1.5 KEV

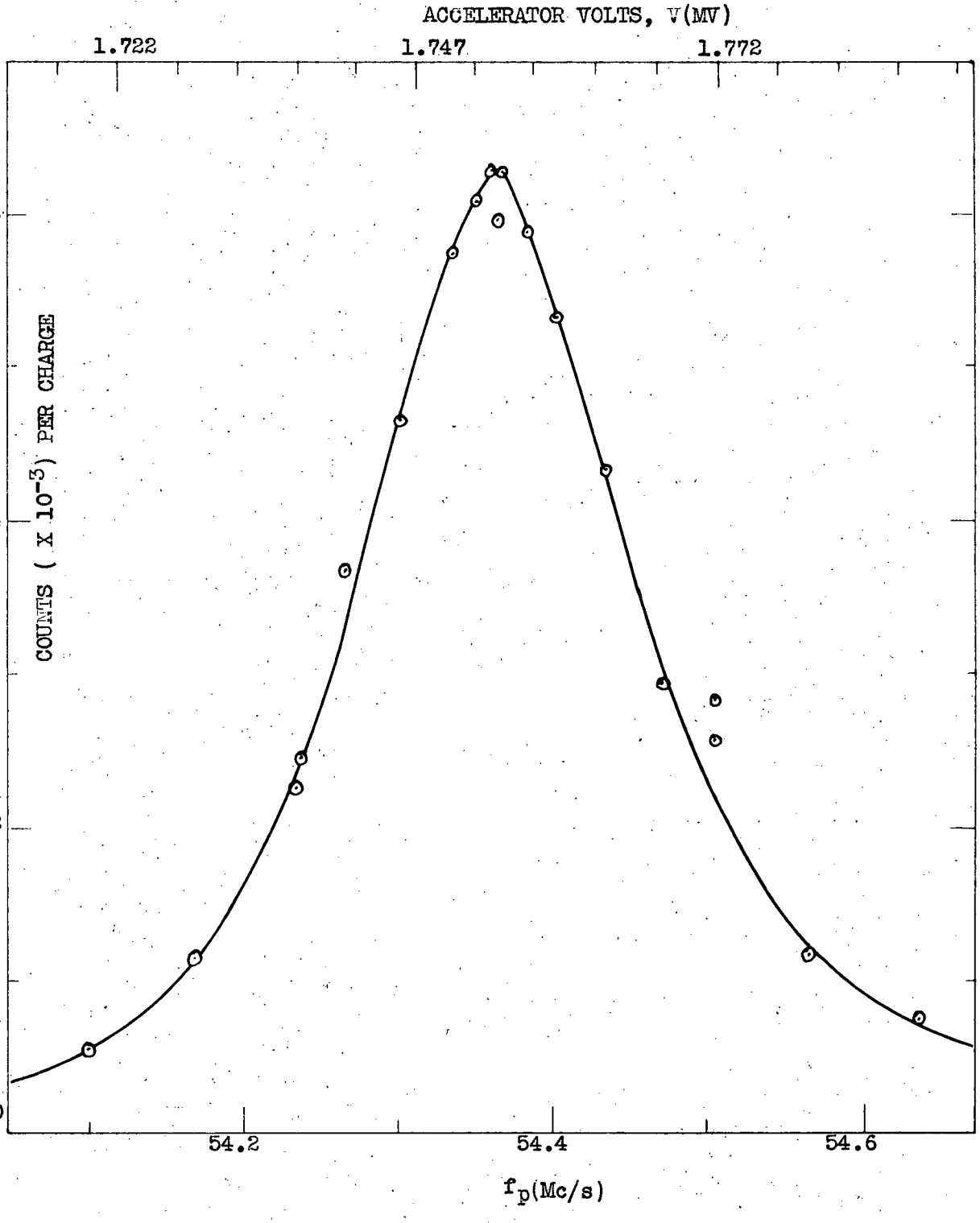

Figure 29

$F^{19}(p,\alpha\gamma)$ RESONANCE, 873.5 KEV CALIBRATION, NOV., 1952

THIN TARGET, ξ = 1.5 KEV, TARGETS HEATED TO 100° C

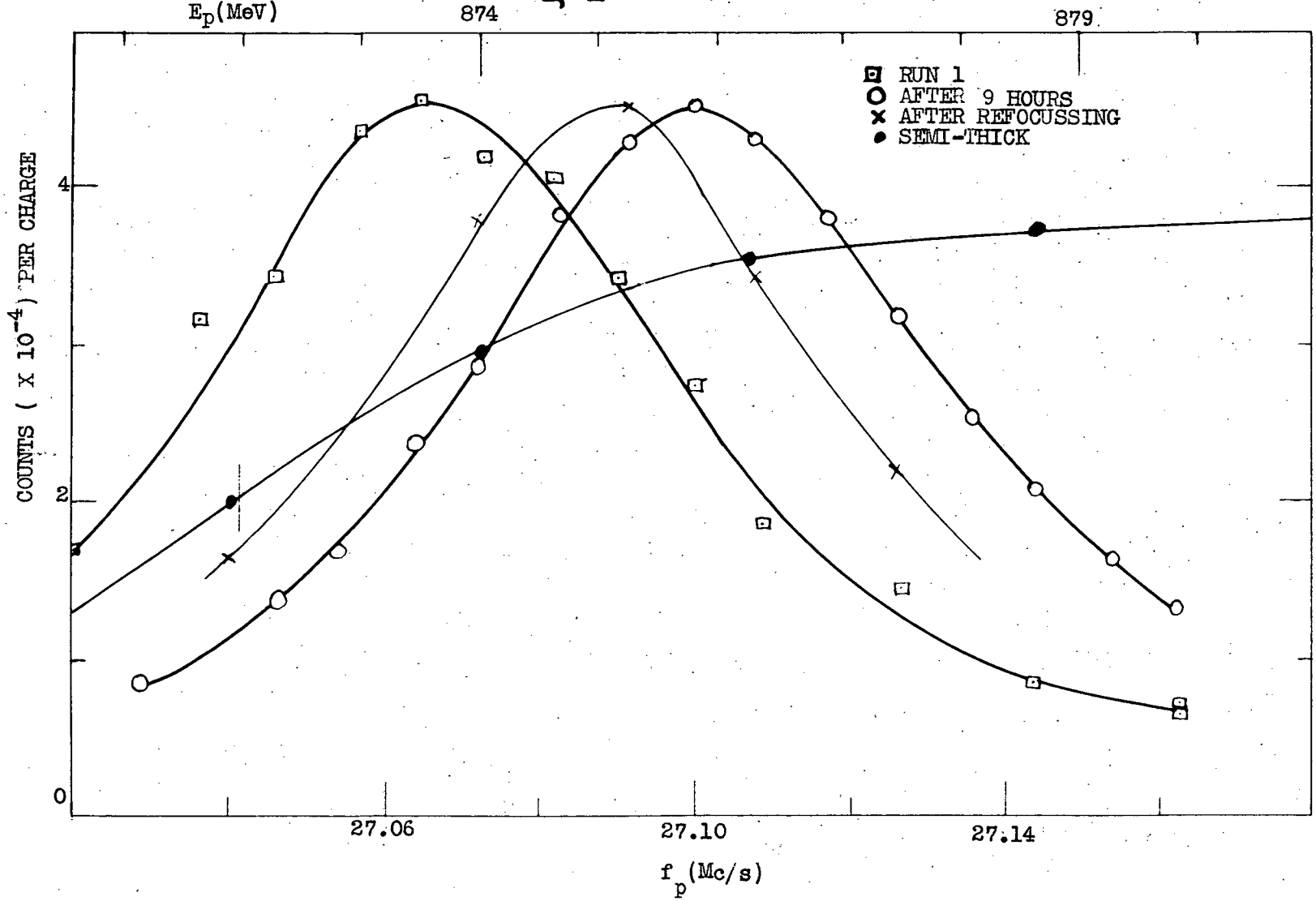

These are listed in Tables 3a, 5, 7 and 9.

The curves that make up figure 23 were normalized at the 0.8735 MeV resonance by correcting the yield for target thickness, charge collected and counter-target spacing. The cosmic ray background, about 1/5 count/sec. was negligible and was not subtracted. A charge dependent background from the copper target backing above 1 MeV was also not subtracted but is plotted beneath the fluorine excitation function.

Some of the resonance curves are plotted on a larger scale in figures 24 to 29. The widths of the resonances shown, and listed in Table 3a, are equal to or less than the widths of the best previous work.[21] A further check of the overall resolution of the present experimental work is the peak to trough ratio of the 1.355-1.381 MeV doublet. After subtracting the copper background, this ratio is about 10:1, to be compared with about 8:1 obtained by Bennet et al[21] and 5:1 obtained by Bernet et al.[21a]

2. <u>New Resonances at 1.62 and 1.84 MeV</u>.

During the course of this investigation two new resonances were observed at approximately 1.62 and 1.84 MeV. Two separate runs were made over the 1.62 MeV resonance with different targets as shown in figure 26, and the 1.84 MeV resonance shown there as well, is plotted

Figure 30

N^{15} (p, $\alpha\gamma$)

898 KEV RESONANCE

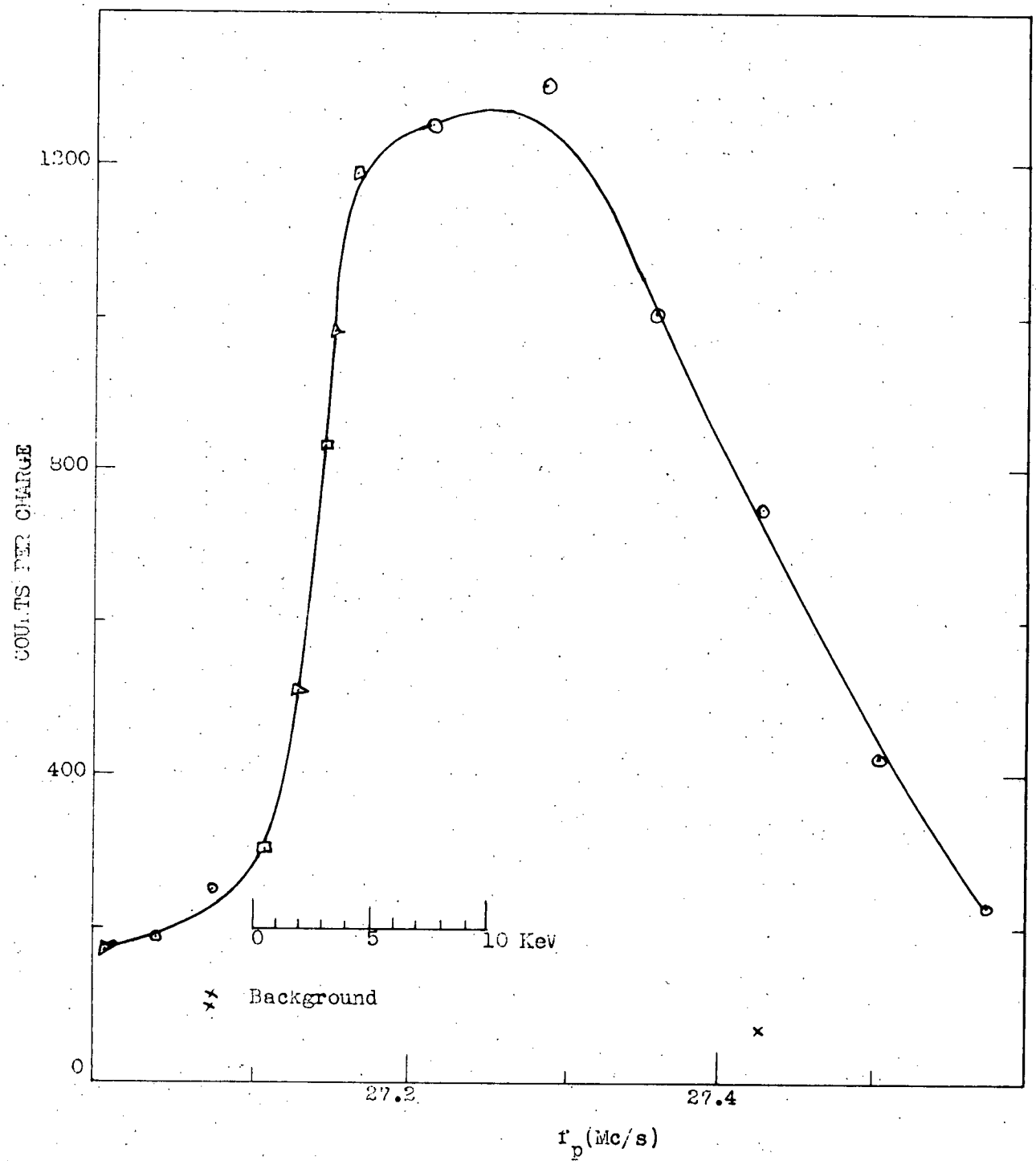

Figure 31

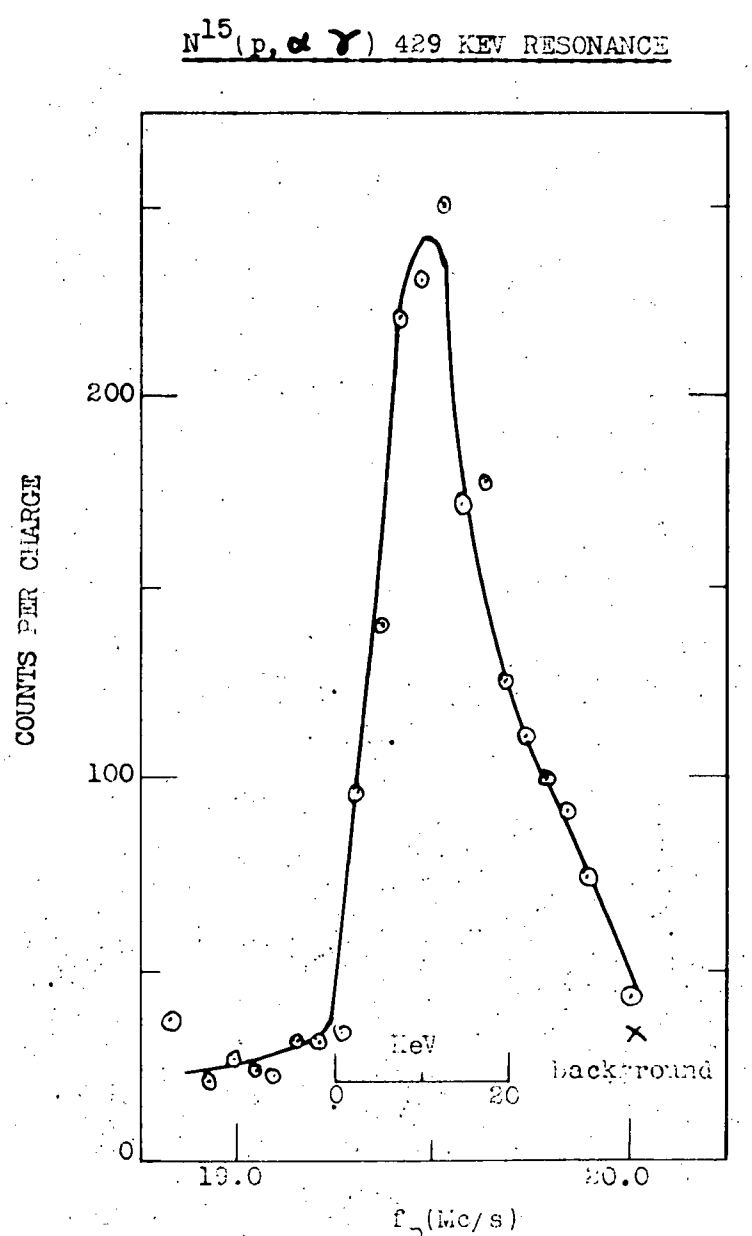
$N^{15}(p, \alpha\gamma)$ 429 KEV RESONANCE
COUNTS PER CHARGE
200
100
0
keV
0
20
background
19.0
20.0
f_p(Mc/s)

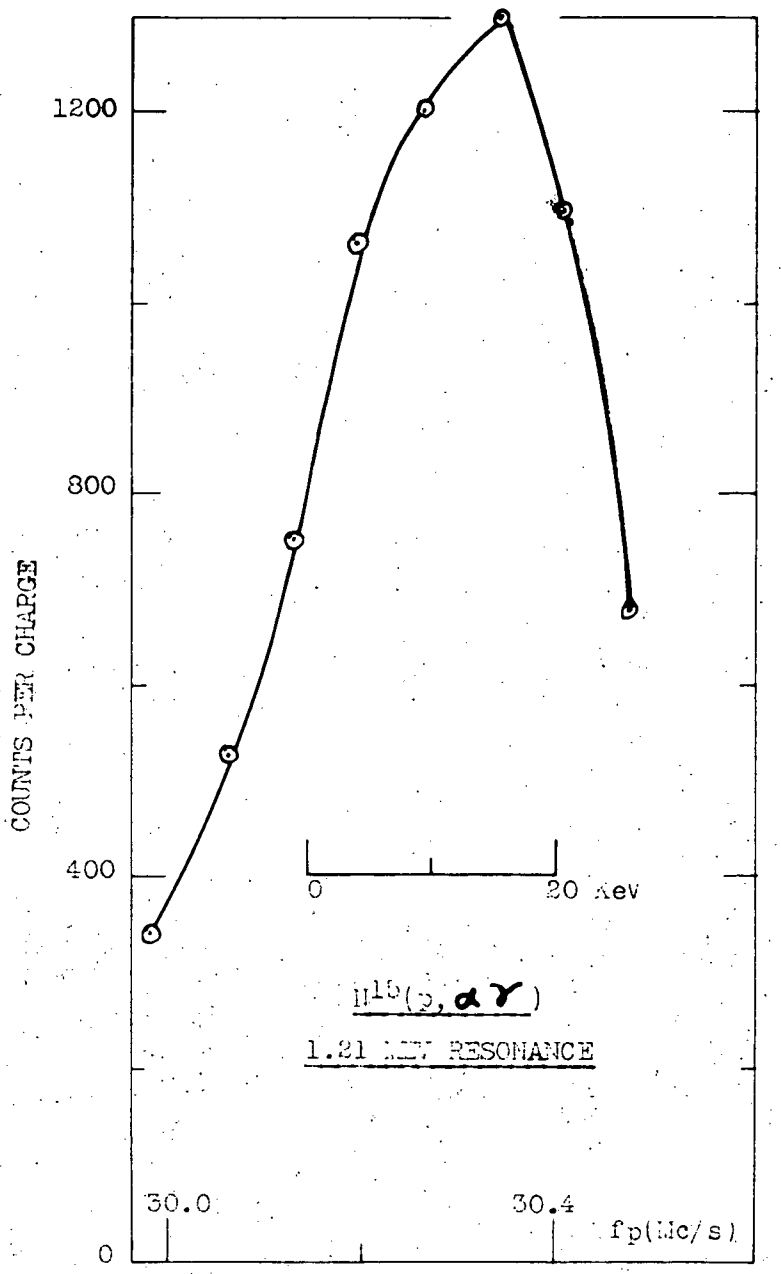
1200
800
400
0
COUNTS PER CHARGE
0
20 Kev
$N^{15}(p, \alpha\gamma)$
1.21 KEV RESONANCE
30.0
30.4
fp(Mc/s)

again in figure 27 with the copper and cosmic ray background subtracted. These energy values were assigned with reference to the preliminary calibration of the accelerator. However, with reference to the final calibration, these energy values should be altered to 1.60 MeV 1% and 1.82 MeV 1%.

XVIII. The Proton Bombardment of N^{15}.

The γ-ray resonances resulting from the proton bombardment of N^{15} are shown in figures 30 and 31. The γ-rays of $4\frac{1}{2}$ MeV energy come from a reaction[43] that is analogous to the fluorine one:

$$N^{15} + H^1 \longrightarrow O^{16*} \longrightarrow C^{12*} + He^4$$
$$\downarrow$$
$$C^{12} + \gamma. \qquad \text{(XVIII.1)}$$

Proton capture radiation also occurs at 1.05 MeV but its intensity is weak compared to the $4\frac{1}{2}$ MeV γ-rays.

Semi thick targets of KNO_3, enriched to 60% with N^{15} were evaporated onto silver backings in vacuum. During the experiments, the targets were cooled to about -70° C with a mixture of solid CO_2 and ether to prevent loss of the nitrogen. Yield from this reaction is small compared to that from fluorine which had to be eliminated as a contaminant from the beam stop on the target box. Since large beam currents were needed, no attempt was made to define the beam at the magnet box in order to check the resonance energy values. No resonances were observed above 1.2 MeV because of the rapidly rising background observed from all target backing materials tested. These included copper, silver, platinum, tantalum and tungsten.

Of these possible target materials, tungsten offers more promise in extending the $N^{15}(p, \alpha\gamma)$ reaction to 2 MeV since its background yield was the least. However, in sheet form it is very difficult to cut or machine.

The angular distribution of these N^{15} gamma rays has been investigated in this laboratory[44] using the stabilized beam to achieve constant operating conditions over long periods of time.

Appendix 1.

The Laplace Transformation Method of Analysis.

The differential equations of the components of the system are written out, the Laplace transforms are taken and then solved usually for the output quantity in terms of the input. The inverse Laplace transform then gives the output quantity as a function of time for the particular input conditions. However, information about stability, and transient response of the systems may be obtained by analyzing the Laplace transform without the need of finding its inverse. To further simplify the analysis, it is conventional to introduce a certain concept, a "transfer function", defined so that the Laplace transforms of the separate units of the system may be written down by inspection. For example, consider a simple r-c network, where the condenser is intially uncharged. Let the Laplace transforms of the current i(t), the input voltage, $e_i(t)$, and the output voltage $e_o(t)$, be denoted by I(S), $L\left[i(t)\right] = I(S)$, $L\left[e_i(t)\right] = E_i(S)$ and $L\left[e_o(t)\right] = E_o(S)$ respectively:

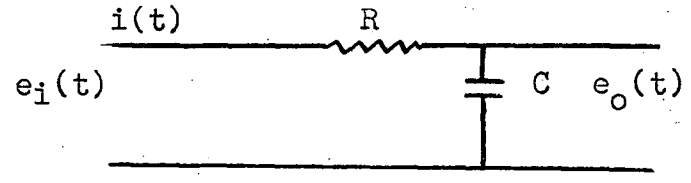

The differential equation of this circuit is:

$$Ri(t) + \frac{1}{C}\int i(t)dt = e_i(t), \qquad (1.1)$$

$$e_o(t) = \frac{1}{C}\int i(t)dt. \qquad (1.2)$$

Taking the Laplace transformation of these two equations:

$$\left(R + \frac{1}{SC}\right)I(S) = E_i(S), \tag{1.3}$$

$$E_o(S) = \frac{1}{SC} I(S). \tag{1.4}$$

From (1.3), $$I(S) = \frac{E_i(S)}{R + \frac{1}{SC}} \tag{1.5}$$

and from (1.4) and (1.3),

$$E_o(S) = \frac{1}{SC}\left[\frac{E_i(S)SC}{1 + SRC}\right], \tag{1.6}$$

or $$E_o(S) = \frac{1}{1+SRC} E_i(S).$$

The "transfer function", KG(S) of the network is defined by the equation:

$$E_o(S) = KG(S)E_i(S). \tag{1.7}$$

In this case, $K = 1$ and $G(S) = 1/(1+SRC)$.

The "time constant" of the network is $T = RC$.

Further, this network may be replaced by an equivalent box containing this transfer function:

Recognitions of the behaviour of this transfer function from experience, or tables, under general input conditions allows prediction of the behaviour of the network without carrying the solution any further. Since this transfer function could be obtained using the usual impedance concept from a-c circuit theory it can be seen that practically,

if S is specialized to $S = j\omega$, the steady-state response of the network is obtained. It must be remembered however, that while the impedance concept of a-c theory applies directly only where sinusoidal voltages and currents are concerned that the Laplace transformation method is valid for any type of voltage or current waveforms.

Two transfer function "boxes" in cascade may be represented by multiplying their transfer functions together, provided that the input of the second does not load the output of the first. If it does, then the circuit must be analyzed as a whole.

The open-loop transfer function for the accelerator's stabilizer, ie. the Laplace transform of the ratio of the output to the input error signal is given by:

$$KG(S) = \frac{K_1 K_2 K_3}{(1+ST_1)(1+ST_3)}, \qquad (1.8)$$

where $S \approx j\omega = j 2\pi f$.

For all frequencies, $j\omega T_1 \gg j\omega T_3$, so that when $\omega T_1 > 1$, ωT_3 is negligible compared to 1. In addition $K = K_1 K_2 K_3$ is $\gg 1$. Thus for any variations having a period less than about 1 second,

$$\frac{1}{1 + KG(S)} \approx \frac{ST_1}{K}. \qquad (1.9)$$

Under these condition with a step input function,

$E_i(S) = \frac{e_i(t)}{S}$, the steady-state error becomes:

$$\begin{array}{l} \text{steady-state error } (t \to \infty) \\ f > 1 \\ K \gg 1 \\ T_1 \gg T_3 \end{array} = \lim_{S \to 0} S\left[\frac{ST_1}{K}\right]\frac{e_i(t)}{S}$$

$$= 0$$

REFERENCES.

1. The Physical Society; "Reports on Progress in Physics", vol. XI (1946-47) page 1, London, 1948.

2. S.B. Woods; "A Search for the Photodisintegration of Neon with the U.B.C. Van de Graaff Generator", Ph.D. Thesis, unpublished, U.B.C., 1952.

3. D.A. Aaronson; "Design, Construction and Stabilization of a Large Electromagnet", M.A. Thesis, unpublished, U.B.C., 1950.

4. J.B. Warren; "High Voltage Electrostatic Generators and Their Application to the Production of Energetic Electron, Ion and Neutron Beams", Document L P - 17, page 28, National Research Council of Canada, Chalk River, 1946.

5. D.H. Halliday; "Introductory Nuclear Physics", pages 496,497, and 512, J. Wiley and Sons, N.Y., 1950.

6. H.A. Thomas, R.L. Driscol and J.A. Hipple; P.R., 78, 787 (1950).

7. G.E. Pake; Am. Jour. of Phys., 18, 438 and 473 (1950).

8. N. Bloembergen, E.M. Purcell, and R.V. Pound, P.R., 73, 679 (1948).

9. M.E. Packard, R. S. I., 19, 435(1948).

10. T.L. Collins; "Measurement of Nuclear Magnetic Moments", Ph.D. Thesis, unpublished, U.B.C., 1950.

11. W.A. Elmore and M.L. Sands; "Electronics, Experimental Techniques", vol. I, McGraw Hill, 1949.

12. B. Chance; "Waveforms", M.I.T. Radiation Lab. Series, vol.19, McGraw Hill, 1949.

13. I.A. Greenwood, J.V. Holdam, D. Macrae Jr.; "Electronic Instruments", M.I.T. Radiation Lab. Series, vol. 21, chapter X, page 290, McGraw Hill, 1948.

14. S.J. Bame Jr. and L.M. Bagget, R.S.I.,20, 839 (1949).

15. H. Chestnut and R.W. Mayer, "Servomechanisms and Regulating System Design", vol. I, chapter 6, John Wiley, 1951.

16. M.F. Gardner, J.L. Barnes, "Transients in Linear Systems", vol.I, page 265, John Wiley, 1942.

17. F.C. Flack,"Private Communication", U.B.C., 1952.

18. W.A. Fowler, C.C. Lauritsen, and T. Lauritsen, Rev. Mod. Phys., 20, 236 (1948).

19. T.W. Bonner and J.W. Butler, P.R., 83, 1091 (1951).

20. W.F. Hornyak, T. Lauritsen, P. Morrison, and W.A. Fowler; Rev. Mod. Phys., 22, 291 (1950), page 356.

21. T.W. Bonner and J.E. Evans, P.R., 73, 666 (1948). See also W.E. Bennet, T.W. Bonner, C.E. Mandeville and B.E. Watt, P.R., 70, 882 (1946).

21a. E.J. Bernet, R.G. Herb and D.B. Parkinson, P.R., 54, 398 (1938).

22. R.O. Haxby, W.E. Shoupp, W.E. Stephens, and W.H. Wells, P.R.,58, 1035, (1940).

23. W.C. Miller, B. Waldman, J.C. Noyes, J.E. Van Hoomissen, P.R., 77, 758(A), (1950).

24. L.R. Hafstad, N.P. Heydenberg, and M.A. Tuve, P.R., 50, 504 (1936).

25. A.O. Hanson, D.L. Benedict, P.R., 65, 33(1944). See also A.O. Hanson, R.S.I., 15, 57 (1944).

26. R.G. Herb, S.C. Snowdon, and O. Sala, P.R., 75, 246(1949).

27. J.B. Hoag, "Electron and Nuclear Physics", p. 461, D. Van Nostrand, 2nd edition, 1938.

28. D.B. Parkinson, R.J. Herb, E.J. Bernet, J.L. McKibben, P.R., 53, 642(1938).

29. R.E. Warren, J.L. Powell, and R.G. Herb, Rev. Sci. Inst., 18, 559 (1947).

30. W.E. Shoupp, B. Jennings, W. Jones and M. Garbundy, P.R., 75, 336(A) (1949).

31. C.W. Li, W. Whaling, W.A. Fowler, and C.C. Lauritsen, P.R., 76, 325(1949).

32. R.F. Taschek, H.V. Argo., A. Hemmendinger, G.A. Jarvie, P.R., 76, 325 (1949).

33. K.T. Bainbridge; "Isotopic Weights of the Fundamental Isotopes", National Research Council (U.S.A.), June 1948, p.4.

34. R. Bell and L. Elliot, P.R., 74, 1552 (1948).

35. A.V. Tollestrup, F.A. Jenkins, W.A. Fowler and C.C. Lauritsen, P.R., 75, 1947(L) (1949)

36. R. Tangen, Kgl. Norske Vid. Sels. Skrifter,(1946) N.R.I., and D.B. Parkinson et al, loc. cit.

37. S. Devons, "Excited States of Nuclei", p.53, Cambridge University Press, 1949.

38. M. Edwards; "The Design and Operation of a Current Integrator", M.A. Thesis, unpublished, U.B.C., 1951.

39. H.A. Bethe, Rev. Mod. Phys.,21, 213 (1950).

40. H.A. Bethe, Rev. Mod, Phys., 9, 69 (1937).

41. S. Devons, Op cit, p.60.

42. S. Devons and M. Hine, Proc. Roy. Soc., 199A, 56(1949).

43. A. Schardt, W.A. Fowler, and C.C. Lauritsen, P.R., 86, 527 (1952).

44. C.A. Barnes, D.B. James and G.C. Neilson, Canad. J. Phys. 30, 717 (1952).